

---

Electronic Theses and Dissertations, 2004-2019

---

2015

## Damage Detection Methodologies For Structural Health Monitoring of Thin-Walled Pressure Vessels

Arturo Modesto  
*University of Central Florida*

 Part of the [Civil Engineering Commons](#), [Geotechnical Engineering Commons](#), and the [Structural Engineering Commons](#)

Find similar works at: <https://stars.library.ucf.edu/etd>

University of Central Florida Libraries <http://library.ucf.edu>

This Masters Thesis (Open Access) is brought to you for free and open access by STARS. It has been accepted for inclusion in Electronic Theses and Dissertations, 2004-2019 by an authorized administrator of STARS. For more information, please contact [STARS@ucf.edu](mailto:STARS@ucf.edu).

---

### STARS Citation

Modesto, Arturo, "Damage Detection Methodologies For Structural Health Monitoring of Thin-Walled Pressure Vessels" (2015). *Electronic Theses and Dissertations, 2004-2019*. 1389.

<https://stars.library.ucf.edu/etd/1389>

INVESTIGATION OF DAMAGE DETECTION METHODOLOGIES FOR STRUCTURAL  
HEALTH MONITORING OF THIN-WALLED PRESSURE VESSELS

by

ARTURO MODESTO  
B.S.C.E. University of Central Florida, 2012

A thesis submitted in partial fulfillment of the requirements  
for the degree of Master of Science  
in the Department of Civil, Environmental, and Construction Engineering  
in the College of Engineering and Computer Sciences  
at the University of Central Florida  
Orlando, Florida

Fall Term  
2015

Major Professor: Necati Catbas

© 2015 Arturo Modesto

## ABSTRACT

There is a need in exploring structural health monitoring technologies for the composite structures particularly aged Composite Overwrapped Pressure Vessels (COPVs) for the current and future implementation of COPVs for space missions. In this study, the research was conducted in collaboration with NASA Kennedy Space Center and also NASA Marshall Space and Flight Center engineers. COPVs have been used to store inert gases like helium (for propulsion) and nitrogen (for life support) under varying degrees of pressure onboard the orbiter since the beginning of the Space Shuttle Program. After the Columbia accident, the COPVs were re-examined and different studies (e.g. Laser profilometry inspection, NDE utilizing Raman Spectroscopy) have been conducted and can be found in the literature. To explore some of the unique in-house developed hardware and algorithms for monitoring COPVs, this project is carried out with the following general objectives:

- 1) Investigate the obtaining indices/features related to the performance and/or condition of pressure vessels
- 2) Explore different sensing technologies and Structural Health Monitoring (SHM) systems
- 3) Explore different types of data analysis methodologies to detect damage with particular emphasis on statistical analysis, cross-correlation analysis and Auto Regressive model with eXogeneous input (ARX) models
- 4) Compare differences in various types of pressure vessels

First an introduction to theoretical pressure vessels, which are used to compare to actual test specimens, is presented. Next, a background review of the test specimens including their applications and importance is discussed. Subsequently, a review of related SHM applications to this study is presented. The theoretical background of the data analysis methodologies used to detect damage in this study are provided and these methodologies are applied in the laboratory using Composite Overwrapped Pressure Vessels (COPVs) to determine the effectiveness of these techniques. Next another study on the Air Force Research Laboratory (AFRL) Tank that is carried out in collaboration with NASA KSC and NASA MSFC is presented with preliminary results. Finally the results and interpretations of both studies are summarized and discussed.

## ACKNOWLEDGMENTS

I would first like to thank my advisor Dr. F. Necati Catbas for his guidance and assistance throughout my time at UCF. He introduced me to research as an undergraduate student and encouraged me to continue my studies as a master's student. He has provided with all the tools and resources to be a successful student and therefore I will always be grateful.

This study is made possible through the support of the NASA Florida Space Grant Consortium, I would like to acknowledge Dr. Jaydeep Mukherjee for his support to the research. The guidance, suggestions and feedback of several NASA engineers have to be acknowledged. Mr. Rudy Werlink from NASA Kennedy Space Center (KSC) has been very generous with his time and sharing his technical expertise in developing the problem statement and the direction of the research. Dr. Curtis Banks from NASA Marshall Space and Flight Center provided valuable input on fiber optic sensing, shared his expertise and data for the project. Dr. Ravi Margasahayam from NASA KSC also supported the project idea at the proposal stage and provided his input for general research directions.

I would also like to thank Dr. Ricardo Zaurin and Dr. Manoj Chopra for serving on my committee and providing great feedback for improving the thesis manuscript. I had the pleasure of working with Dr. Zaurin as a teacher's assistance and taking multiple classes with him. He has taught me so much within and outside the classroom. Many thanks to him especially in teaching me about sensor technology and the LabView software which were implemented in this study.

I would like to thank everyone at my company AW Solutions for their patience and support though my thesis process. It was incredibly difficult to work full time as an engineer and work on my masters at the same time. A special thanks to Alan and Emmanuel for their advice and flexibility throughout the entire process.

I would like to thank all the current and former members of our research team and visiting faculty for their contributions and assistance, especially Ozan, Luca, Hugo, Tung, Shuhei, Evan, Daniela, and Erin. Many thanks to Dr. Masoud Malekzadeh for his knowledge, support and contributions to the fiber optic system as well as mentoring me through the duration of my thesis.

Finally, I would like to express my gratitude towards my friends and family for their support and encouragement throughout my entire academic and professional career. I've been blessed with so many good friends and would especially like to thank Ky, Jordan, Aaron, Isaac, Nick, Sean, Pitt, Logan, Amanda, Lo, Bird, Mehdi, MB, Ganesh, Liuliu, Alisha, Leo, Julien and Tyler. My entire family has been incredibly supportive throughout my whole life and I would like to give extra thanks to my aunts Elba and Lisa; my cousins Frank and Chris; my grandfathers Arturo and Jorge (which I named after); my sisters Ashley and Amanda; and finally my dear mother Amy, she has been unbelievably supportive and my number one cheerleader my entire life. I know I mentioned so many people in this acknowledgments but I am truly grateful for all their support and appreciate all the help they've given me.

# TABLE OF CONTENTS

LIST OF FIGURES .....	xi
LIST OF TABLES .....	xvi
CHAPTER 1: INTRODUCTION .....	1
1.1 Structural Health Monitoring (SHM).....	1
1.2 SHM Applications .....	1
1.3 Objectives and Scope .....	3
1.4 Organization of the Thesis .....	4
CHAPTER 2: MECHANICS OF PRESSURE VESSELS AND RELATED SHM APPLICATIONS .....	7
2.1 Mechanics of Pressure Vessels .....	7
2.1.1 Hoop Stress .....	8
2.1.2 Axial Stress .....	9
2.1.3 General Comments.....	11
2.2 Pressure Vessel Applications and Test Specimens .....	11
2.2.1 Composite Overwrapped Pressure Vessel (COPV).....	12
2.2.2 Air Force Research Laboratory (AFRL) Tank.....	14

2.3 Related Work .....	16
CHAPTER 3: DATA ANALYSIS TECHNIQUES FOR DAMAGE DETECTION .....	19
3.1 Cross-Correlation Analysis.....	19
3.2 Time Series Modeling.....	20
3.2.1 Formulations of Time Series Modeling.....	21
3.2.2 Time Series Modeling for Structural Dynamics .....	24
3.2.3 Damage Feature (DF) .....	26
CHAPTER 4: TESTING AND MONITORING STUDIES OF COPV’S IN THE LABORATORY .....	27
4.1 Objective and Scope .....	27
4.1.1 Test Specimens .....	28
4.2 Pressure Testing.....	30
4.2.1 Health Monitoring System.....	31
4.2.2 Test Procedure .....	33
4.2.3 Preliminary Results.....	34
4.3 Dynamic Testing.....	37
4.3.1 Health Monitoring System.....	38
4.3.2 Test Procedure .....	40
4.3.3 Collection and Pre-Processing of Data .....	41

CHAPTER 5: RESULTS AND INTERPRETATIONS OF COPV MONITORING .....	44
5.1 Statistical Analysis Using Histograms.....	44
5.1.1 Hoop v Axial 2-1 Relationship .....	45
5.1.2 Comparison of Hoop Sensors 1 & 2 .....	48
5.2 Cross Correlation Analysis .....	52
5.2.1 Correlation between Hoop Sensors 1 & 2.....	52
5.3 ARX (Auto-Regressive models with eXogenous outputs) Analysis .....	55
5.3.1 Pressure and Strain Data .....	55
5.3.2 Acceleration Data.....	60
5.4 Summary of COPV Results .....	66
CHAPTER 6: TESTING AND MONITORING STUDIES OF THE ARFL TANK IN THE FIELD .....	70
6.1 Fiber Bragg Grating (Fbg) Monitoring System .....	71
6.1.1 Fiber Optic Sensors (FOS).....	71
6.1.2 In-House Developed FBG System.....	73
6.1.3 Installation of Sensors.....	75
6.2 7 PSI Test Field Test at NASA’s Kennedy Space Center (KSC).....	77
6.2.1 Preliminary Test Results .....	78
6.3 Full Burst Test at NASA’s MSFC .....	92

6.4 Conclusion .....	103
CHAPTER 7: SUMMARY, FINDINGS, CONCLUSIONS AND RECOMMENDATIONS FOR FUTURE WORK.....	108
7.1 Recommendations for Future Work.....	114
REFERENCES .....	117

## LIST OF FIGURES

Figure 2:1: Stresses in a Circular Cylindrical Pressure Vessel (adapted from Gere and Goodno (2009)).....	8
Figure 2:2: Stresses in the Hoop Direction in a Circular Cylindrical Pressure Vessel (adapted from Gere and Goodno (2009)).....	9
Figure 2:3: Stresses in the Axial Direction in a Circular Cylindrical Pressure Vessel (adapted from Gere and Goodno (2009)).....	10
Figure 2:4: Multiple COPVs in Different Shapes and Sizes.....	12
Figure 2:5: Components of the COPV Liner .....	13
Figure 2:6: AFRL Tank Stored at KSC .....	15
Figure 3:1: The Block Diagram of an ARMAX Model (adapted from Ljung (1999)).....	22
Figure 3:2: The Block Diagram of an AR Model (adapted from Ljung (1999)).....	22
Figure 3:3: The Block Diagram of an ARMA Model (adapted from Ljung (1999)) .....	23
Figure 3:4: The Block Diagram of an ARX Model (adapted from Ljung (1999)).....	24
Figure 4:1: Two Test Specimens (left) COPV End Cap (right).....	28
Figure 4:2: COPV Dimensions .....	29
Figure 4:3: COPV Pressure Testing Instrumentation Plan .....	30
Figure 4:4: Installed Strain Gage on COPV .....	31
Figure 4:5: Definition of Strain (Measuring Strain with Strain Gages).....	32
Figure 4:6: End Connection, Consisting of Pressure Transducer, Pressure Valve, and T-fitting.	32
Figure 4:7: Pressure Transducer Diagram .....	33

Figure 4:8: COPV Pressure Test.....	34
Figure 4:9: Time Response of Tank 1.....	35
Figure 4:10: Time Response of Tank 2.....	35
Figure 4:11: Time Response of Tank 3.....	36
Figure 4:12: Time Response of Tank 4.....	36
Figure 4:13: Time Response of Tank 5.....	37
Figure 4:14: COPV Dynamic Testing Instrumentation Plan .....	38
Figure 4:15: Dynamic Testing Health Monitoring System .....	39
Figure 4:16: Schematic of Accelerometer (left) Installed PCB Accelerometer (right) .....	40
Figure 4:17: Exciting the COPV with the Impact Hammer.....	41
Figure 4:18: Sample Raw Data from Tank 1 .....	42
Figure 4:19: Sample Acceleration Data; Raw (Top) and Free-Response (Bottom).....	43
Figure 5:1: Hoop v Axial Histogram for Tank 1 .....	45
Figure 5:2: Hoop v Axial Histogram for Tank 2 .....	46
Figure 5:3: Hoop v Axial Histogram for Tank 3 .....	46
Figure 5:4: Hoop v Axial Histogram for Tank 4 .....	47
Figure 5:5: Hoop v Axial Histogram for Tank 5 .....	47
Figure 5:6: Hoop 1 v Hoop 2 Histogram for Tank 1 .....	49
Figure 5:7: Hoop 1 v Hoop 2 Histogram for Tank 2 .....	49
Figure 5:8: Hoop 1 v Hoop 2 Histogram for Tank 3 .....	50
Figure 5:9: Hoop 1 v Hoop 2 Histogram for Tank 4 .....	50
Figure 5:10: Hoop 1 v Hoop 2 Histogram for Tank 5 .....	51

Figure 5:11: Correlation between Hoop Sensors 1 & 2 for Tank 1 .....	52
Figure 5:12: Correlation between Hoop Sensors 1 & 2 for Tanks 1 & 2 .....	53
Figure 5:13: Correlation between Hoop Sensors 1 & 2 for Tanks 1 & 3 .....	53
Figure 5:14: Correlation between Hoop Sensors 1 & 2 for Tanks 1 & 4 .....	54
Figure 5:15: Correlation between Hoop Sensors 1 & 2 for Tanks 1 & 5 .....	54
Figure 5:16: Time Response Comparison of Hoop Strain for Tank 1 .....	56
Figure 5:17: Time Response Comparison of Hoop Strain for Tank 2 .....	57
Figure 5:18: Time Response Comparison of Hoop Strain for Tank 3 .....	57
Figure 5:19: Time Response Comparison of Hoop Strain for Tank 4 .....	58
Figure 5:20: Time Response Comparison of Hoop Strain for Tank 5 .....	58
Figure 5:21: Threshold Level for Pressure and Strain Data .....	59
Figure 5:22: DF Tend Plot for Pressure and Strain Data .....	60
Figure 5:23: Time Response Comparison of the Acceleration Data for Tank 1 .....	61
Figure 5:24: Zoomed in View of the Time Response Comparison of the Acceleration Data for Tank 1 .....	62
Figure 5:25: Time Response Comparison of the Acceleration Data for Tank 5 .....	62
Figure 5:26: Zoomed in View of the Time Response Comparison of the Acceleration Data for Tank 5 .....	63
Figure 5:27: Threshold Level for Acceleration Data .....	65
Figure 5:28: DF Tend Plot for Acceleration Data .....	66
Figure 6:1: AFRL Tank in NASA's Clamshell Structure.....	71

Figure 6:2: Fundamental Concepts of Fiber Optic Technology (adapted from Malekzadeh & Catbas 2014) .....	73
Figure 6:3: UCF In-House Developed FBG System .....	74
Figure 6:4: FBG Sensor Type and Orientation .....	75
Figure 6:5: Mixing AE-10 Epoxy .....	76
Figure 6:6: Installed FBG Sensor .....	76
Figure 6:7: KSC Near Clamshell AFRL Checkout Test Area .....	77
Figure 6:8: UCF FBG Sensors .....	78
Figure 6:9: Strain in the Hoop Direction at the Mid-Section of the Panels .....	79
Figure 6:10: Strain in the Hoop Direction of the First Panel .....	80
Figure 6:11: Strain in the Axial Direction of the First Panel .....	81
Figure 6:12: Strain in Dome Portion of the Tank .....	82
Figure 6:13: KSC Instrumentation Plan .....	83
Figure 6:14: Strain in the Hoop Direction at the Mid-Section of the Panels .....	84
Figure 6:15: Strain in the Hoop Direction at the Lower Section of the Panels .....	85
Figure 6:16: Strain in the Hoop Direction of the First Panel .....	86
Figure 6:17: Strain in the Axial Direction of the First Panel .....	87
Figure 6:18: Comparison of Hoop Strain in the Mid-Section of Panel 1 .....	88
Figure 6:19: Comparison of Hoop Strain in the Lower Section of Panel 1 .....	88
Figure 6:20: Comparison of Axial Strain in the Mid-Section of Panel 1 .....	89
Figure 6:21: Comparison of Axial Strain in the Lower Section of Panel 1 .....	90
Figure 6:22: Strain at the Mid-Section of Panel 1 (UCF left and KSC right) .....	91

Figure 6:23: Ratio of Hoop v Axial Strain at the Mid-Section of Panel 1 (UCF left and KSC right)	91
.....	
Figure 6:24: Instrumented AFRL Tank in Flame Trench (left) AFRL Tank Filled with LN2 During Testing (right)	93
.....	
Figure 6:25: KSC Instrumentation Plan	95
.....	
Figure 6:26: Hoop v Axial at the Lower Section of Panel 1	96
.....	
Figure 6:27: Hoop v Axial at the Lower Section of Panel 1	97
.....	
Figure 6:28: Hoop v Axial at the Mid-Section of Panel 1	98
.....	
Figure 6:29: Hoop v Axial at the Mid-Section of Panel 1	99
.....	
Figure 6:30: Comparison of Axial Strain	101
.....	
Figure 6:31: Comparison of Axial Strain	102
.....	
Figure 6:32: Strain in the Hoop Direction at the Mid-Section of the Panels (UCF top and KSC bottom)	104
.....	
Figure 6:33: Axial strain at mid-panel for KSC vs. UCF dome reading at panel 1 at the 200psi peak	106
.....	
Figure 6:34: Axial strain at mid-panel for KSC vs. UCF dome reading at panel 1 at the 300psi peak	107
.....	

## LIST OF TABLES

Table 4-1: COPV Test Specimen Characteristics .....	29
Table 5-1: Hoop v Axial Histogram Summary.....	48
Table 5-2: Hoop 1 v Hoop 2 Histogram Summary.....	51
Table 5-3: Correlation between Hoop Sensors 1 & 2 Summary .....	55
Table 5-4: Inputs and Outputs of the ARX Models.....	60
Table 5-5: ARX Model 1 Fit Ratio .....	63
Table 5-6: ARX Model 2 Fit Ratio.....	64
Table 5-7: ARX Model 3 Fit Ratio.....	64
Table 5-8: Summary of Results from Various Data Analysis Methodologies .....	67

# **CHAPTER 1: INTRODUCTION**

## **1.1 Structural Health Monitoring (SHM)**

Structural engineers that specialize in Structural Health Monitoring (SHM) are comparable to physicians who take care of patients. For such engineers, their primary patients are structures. Their job is to ensure the structural integrity of civil structures. They use sensors to gather information about the structure or their patient, just as a doctor would utilize various instruments to gauge the status of his or her respective patient.

SHM is the measurement of the operating and loading environment as well as the critical responses of a structure to track and evaluate the symptoms of incidents, anomalies, damage and/or deterioration that may affect operation, serviceability, or safety and reliability (Aktan, Catbas et al. 2000). SHM provides non-biased decision making information on what actions need to be implemented concerning the safety and serviceability of the given structure.

## **1.2 SHM Applications**

The first modern SHM applications began within the aerospace industry during the late 1970's and early 1980's. Since as early as 1980, SHM and vibration-based damage assessment of bridges and buildings has existed in the civil engineering community (Farrar and Worden 2007). More recently, with advances in SHM technology, SHM has expanded throughout the engineering disciplines, making it more interdisciplinary than ever before. A complete and successful SHM

application, therefore, must also consider the socio-organizational and non-technical challenges which are highly interrelated with both the fundamental knowledge needs and technological needs (Catbas, Brown et al. 2004).

The two components of a SHM system are as follows:

- 1) The acquisition of data using sensing technologies – Generally a SHM system collects information on the response of the structure at various locations. Sometimes, if applicable, the system will also record input information related to the structure. Information of the system can be collected using a wide range of sensing technologies (accelerometers, strain gages, and displacement are examples). The sensors relay the measurements to the data acquisition (DAQ) system where it will be stored for further use. The type and quantity of the sensors DAQ have a direct effect on the accuracy and reliability of the monitoring process (Terrell 2011), and should be carefully chosen.
- 2) The data analysis methodologies and the decision-making process – Once the data is collected it must be analyzed to extract useful information. Without the analysis process the raw measurements are basically useless. After the useful information of the structure is processed, decisions need to be made in order to determine the “Health” of the structure. In addition to the analysis of experimental data, the data analysis process may require modeling and simulation. These models can then be used for comparison purposes with experimental findings, predicting future performance, etc (Terrell 2011).

Damage detection is a critical component of SHM; a thorough review of SHM applications and associated damage detection methods can be found in (Brownjohn, Tjin et al. 2004). Structural damage is when the material or properties of a structure change that affects the behavior of the structure adversely which can potentially result in failure. The four levels of damage identification, are 1) detection of the damage, 2) localization of the damage, 3) quantification of damage, and 4) decision making (Rytter 1993).

### **1.3 Objectives and Scope**

SHM offers a proactive approach to monitoring the existing condition of our nation's aging infrastructure, which will help ensure the safety and reliability of these types of structures. However, even though the current state of our infrastructure is a significant issue and will probably be one of the largest applications of current and future SHM; the main focus of this thesis will be on monitoring composite pressure vessels.

The development of new data analysis techniques along with the use of new sensor technologies will help contribute to the relatively new and growing field of SHM. It is known that all sensors and health monitoring techniques cannot be implemented for every application. Therefore the use of already developed sensors and techniques to new applications of SHM will also add to the field. The accuracy and limitations of these techniques will be better understood as well as which applications they work best with.

The overall objectives of this study are to:

- 1) Investigate the obtaining indices/features related to the performance and/or condition of pressure vessels
- 2) Explore different sensing technologies and SHM systems
- 3) Explore different types of data analysis methodologies to detect damage, cross-correlation and ARX models
- 4) Compare differences in various types of pressure vessels

First an introduction to theoretical pressure vessels which will be used to compare to actual test specimens. Next will be a background review of the test specimens including their applications and importance. Next a review of related SHM applications to this study. Followed by the theoretical background of the data analysis methodologies used to detect damage in this study, cross-correlation and ARX. These methodologies will be applied to a laboratory using Composite Overwrapped Pressure Vessels (COPVs) study to determine the effectiveness of these techniques for a particular application. Next another study on the Air Force Research Laboratory (AFRL) Tank will be implemented along with preliminary results. Finally the results and interpretations of both studies will be summarized and discussed.

#### **1.4 Organization of the Thesis**

The organization of the thesis is as follows.

- Chapter 2: Mechanics of Pressure Vessels and Related SHM Applications – This chapter provides an introduction to theoretical properties of pressure vessels as well as practical

applications. It introduces the test specimens of concern and provides background information on such. This chapter also provides theoretical support and background information related to the research of pressure vessels and health monitoring.

- Chapter 3: Data Analysis Techniques for Damage Detection – This chapter provides a review of the implemented data analysis techniques used in this study. The background for statistical methods to detect damage are explored, especially that of the cross-correlation method. Also theoretical background on time series modeling is conducted, focusing on the implementation of the ARX model. Finally the method of how Damage Features are obtained from ARX model comparisons is explained.
- Chapter 4: Testing and Monitoring Studies of COPV's in the Laboratory – This chapter details the first experimental study conducted, using NASA's COPV's in UCF's Structures Laboratory. It explains the procedure and mythology of the different types of test conducted; pressurization and dynamic testing. It provides information on the types of sensing technologies as well as the specification of the DAQs and monitoring system.
- Chapter 5: Results and Interpretations of COPV Monitoring – This chapter shows the results of the first experimental study using the COPV's. Damage detection is explored using multiple methodologies; including cross-correlation analysis, comparison of the theoretical properties of pressure vessels, and a comparison of the ARX models to the experimental data for both the pressure and dynamic test. The Damage Features from the ARX models are also computed to better explain the extent of damage. Finally a comparison of these data analysis methodologies will be conducted to see which was most accurate for detecting damage.

- Chapter 6: Testing and Monitoring Studies of the AFRL Tank in the Field – This chapter details another experimental study conducted exploring the condition and assessment of the AFRL Tank. This extensive study was conducted along with partners from NASA; Mr. Rudy Werlink and Dr. Curtis Banks and was tested to failure in the field. It provides information on the types of sensing technologies as well as the specification of the DAQs and monitoring system. Also preliminary results are presented
- Chapter 7: Summary, Conclusions and Recommendations for Future Work – This chapter presents a summary of the thesis along with the conclusions from the studies of the COPV's and the AFRL tanks. Also the recommendations for future studies are provided.

## **CHAPTER 2: MECHANICS OF PRESSURE VESSELS AND RELATED SHM APPLICATIONS**

### **2.1 Mechanics of Pressure Vessels**

Pressure vessels are structures containing fluids (liquids or gases) under pressure. Some common examples are: tanks, pipes, and pressurized cabins in aircraft and space vehicles. The stresses and strains in the walls of these structures due to the internal pressures from the compressed fluids can be determined using the theoretical methodologies of this type of geometry. Assuming only positive internal pressure (not the effects of external loads, reactions, the weight of the contents, and the weight of the structure) is considered. Linear-elastic behavior is assumed, and the formulas for hoop and axial stresses in cylindrical tanks are only valid in regions of the tank away from stress concentrations caused by openings, changes in geometry, and/or support brackets (Gere and Goodno 2009).

The analysis of cylindrical pressure vessels starts by determining the normal stresses in a thin-walled circular tank AB (Figure 2-1) subjected to internal pressure. A stress element with its faces parallel and perpendicular to the axis of the tank is shown on the wall of the tank. No shear stresses act on these faces because of the symmetry of the vessel and its loading. Therefore, the stresses  $\sigma_1$  and  $\sigma_2$  are principal stresses.

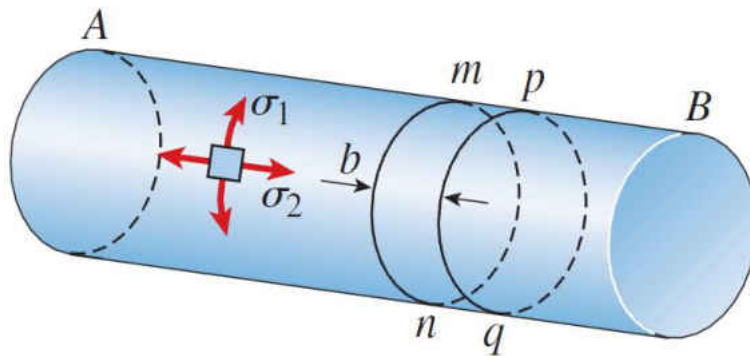


Figure 2:1: Stresses in a Circular Cylindrical Pressure Vessel (adapted from Gere and Goodno (2009))

Because of their directions, the stress  $\sigma_1$  is called the circumferential stress or the **hoop** stress, and the stress  $\sigma_2$  is called the longitudinal stress or the **axial** stress. Each of these stresses can be calculated from equilibrium by using appropriate free-body diagrams.

### 2.1.1 Hoop Stress

To determine the hoop stress  $s_1$ , two cuts (mn and pq) are made perpendicular to the longitudinal axis and distance  $b$  apart (Figure 2-1). Then a third cut is made in a vertical plane through the longitudinal axis of the tank, resulting in the free body shown in Figure 2-2. This free body consists not only of the half-circular piece of the tank but also of the fluid contained within the cuts. Acting on the axial cut (plane mpqn) are the hoop stresses  $\sigma_1$  and the internal pressure  $p$ .

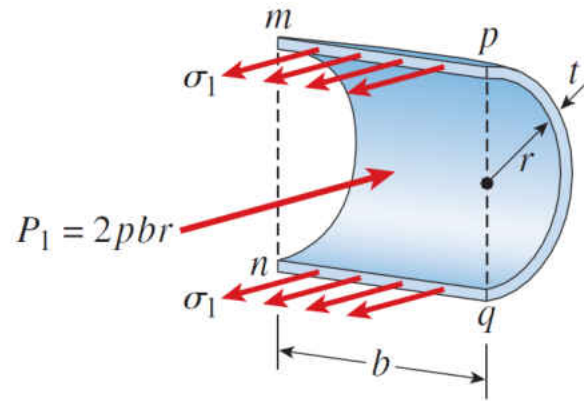


Figure 2:2: Stresses in the Hoop Direction in a Circular Cylindrical Pressure Vessel (adapted from Gere and Goodno (2009))

The hoop stresses  $\sigma_1$  acting in the wall of the vessel have a resultant equal to  $\sigma_1(2bt)$ , where  $t$  is the thickness of the wall. Also, the resultant force  $P_1$  of the internal pressure is equal to  $2pbr$ , where  $r$  is the inner radius of the cylinder. Hence, we have the following equation of equilibrium (Gere and Goodno 2009):

$$\sigma_1(2bt) - 2pbr = 0 \quad (1)$$

From rearranging equation (1), the stress uniformly distributed along the hoop direction of the pressure vessel is:

$$\sigma_1 = \frac{pr}{t} \quad (2)$$

### 2.1.2 Axial Stress

The axial stress  $\sigma_2$  is obtained from the equilibrium of the free body of the part of the vessel to the left of cross section  $mn$  (Figure 2-3).

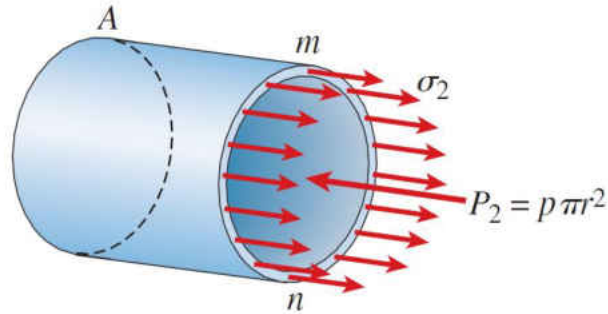


Figure 2:3: Stresses in the Axial Direction in a Circular Cylindrical Pressure Vessel (adapted from Gere and Goodno (2009))

Again, the free body includes not only part of the tank but also its contents. The stresses  $\sigma_2$  act longitudinally and have a resultant force equal to  $\sigma_2 (2\pi r t)$ . The resultant force  $P_2$  of the internal pressure is a force equal to  $p\pi r^2$ . Thus, the equation of equilibrium for the free body is (Gere and Goodno 2009):

$$\sigma_2 (2\pi r t) - p\pi r^2 = 0 \quad (3)$$

From rearranging equation (3), the stress uniformly distributed along the axial direction of the pressure vessel is:

$$\sigma_2 = \frac{pr}{2t} \quad (4)$$

Comparing equations (2) and (4) it is apparent that the relationship between the hoop ( $\sigma_1$ ) and axial ( $\sigma_2$ ) stresses are:

$$\sigma_1 = 2\sigma_2 \quad (5)$$

Still assuming a linear elastic relationship with a constant modulus of elasticity ( $E$ ), the stress ( $\sigma$ ) strain ( $\epsilon$ ) relationship is expressed by Hooke's Law:

$$\sigma = E\varepsilon \quad (6)$$

After substituting equation (6) into equation (5), for the hoop and axial directions. The relationship between the hoop ( $\varepsilon_1$ ) and axial ( $\varepsilon_2$ ) strains are:

$$\varepsilon_1 = 2\varepsilon_2 \quad (7)$$

### 2.1.3 General Comments

The preceding formulas for stresses in a circular cylinder are valid in parts of the cylinder away from any discontinuities that cause stress concentrations, as discussed previously for spherical shells. An obvious discontinuity exists at the ends of the cylinder where the heads are attached, because the geometry of the structure changes abruptly. Other stress concentrations occur at openings, at points of support, and wherever objects or fittings are attached to the cylinder. The stresses at such points cannot be determined solely from equilibrium equations; instead, more advanced methods of analysis (such as finite-element analysis) must be used (Gere and Goodno 2009).

## **2.2 Pressure Vessel Applications and Test Specimens**

As mentioned above, pressure vessels have many applications in multiple different industries today. This thesis will mostly focus on circular cylindrical pressure vessels, made from composite materials, which will be used for aircraft applications. The composite material allows for significant reduction in weight that will result in precious energy conservation. The two

different types of pressure vessels explored in this thesis are the Composite Overwrapped Pressure Vessel (COPV) and the Air Force Research Laboratory (AFRL) Tank.

### 2.2.1 Composite Overwrapped Pressure Vessel (COPV)

A Composite Overwrapped Pressure Vessel (COPV) is a vessel consisting of a thin, non-structural liner wrapped with a structural fiber composite, designed to hold a liquid or gas under pressure (Figure 2-4). The most commonly used composites are fiber reinforced polymers such as carbon, Kevlar, and/or zylon fibers. COPV's are currently used at NASA to contain high-pressure liquids and or gases in life support systems, propulsions, and science experiments.



Figure 2:4: Multiple COPVs in Different Shapes and Sizes

A composite, as defined for this COPV application, is a matrix of continuous fibers contained within a resin. This matrix of continuous fibers provides added tensile strength while

the resin handles shear loads in the composite and maintains the fiber position. The fiber/resin composite is applied over a fluid-retention barrier that provides an interior liner for the composite. The fluid-retention barrier may be either a rubber, plastic or a thin ductile metal liner. In this case study, the COPV has a load-sharing liner that is made of titanium (Figure 2-5) and provides structural integrity by carrying a portion of the pressure load. The rigid titanium liner also acts as a spindle upon which the wet fiber/resin composite is wrapped around to form the COPV.



Figure 2:5: Components of the COPV Liner

COPVs offer many unique advantages over other similarly sized metallic pressure vessels such as a significant weight advantage and high efficiency. Efficiency is the ratio of product capacity to vessel weight. However, three distinct and important differences exist between composite and metal vessels. The first difference is that COPVs do not lose significant structural strength due to minor surface damage. The next difference is that the composites are subjected to

an effect known as stress rupture. Stress rupture is a function of time and tensile stress in the overwrap, in which the composite fails as a function of time while at operating pressure. The final main contrast is that nondestructive testing methods currently used to screen thick-walled metal vessels for flaws are generally not applicable to COPV designs. COPVs possess thin metallic liners and/or composite materials both of which are not accurately measured by the well-established nondestructive evaluation methods currently used in the industry. Although, significant progress has been made in composite NDE methods, techniques and technology.

NASA COPVs are commonly used for propellant storage in spacecraft and launch vehicles. Most of which store these gases or liquids at very high pressures. The consequence of a COPV rupture can be catastrophic to surrounding spacecraft structure and components. Therefore, various rupture failure modes are addressed during design and stress rupture modes are studied after manufacturing. Since the result of a COPV failure due to stress rupture would most likely lead to the loss of the spacecraft, experimental testing of long term stress rupture modes has become very significant.

### 2.2.2 Air Force Research Laboratory (AFRL) Tank

The tank was originally purchased for Air Force Research Laboratory (AFRL) Future Responsive Access to Space Technology (FAST) project as a Cryo-structural test article and originally planned to be tested with flight loads under cryogenic conditions. The tank was fabricated in 2008 by Scorpius Space Launch Company, Hawthorne, CA and Delivered directly from Scorpius to the Kennedy Space Center (KSC) in January 2009 (Werlink, Banks et al. 2014).

Made to hold 515 gallons, the AFRL Tank is of a cylindrical shape with two spherical ends (Figure 2-6). The ends of the tank are not a perfect sphere, and the curvature of the shape was not given. With a total length of 95 inches and a cylindrical diameter of 42 inches, the tank came with Aluminum alloy skirts for load transfer and an Aluminum support structure. Being a large composite cylindrical tank it has longitudinal composite stiffeners and circumferential composite stiffeners with an exterior of carbon cloth and wound tow fibers (IM7 Carbon Fiber Tow plus CTD-7.1 plus resin). The tank is specifically all composite and has no metal liner.



Figure 2:6: AFRL Tank Stored at KSC

Due to space flight being very resource intensive, a constant effort is being made into finding the most efficient way to safely explore. The AFRL tank is one of many possible ways to accomplish this goal. Since weight is a critical factor in the cost and fuel efficiency of space travel, by exploring different materials and pressurized vessels NASA intends to find the perfect method of space exploration. As a result, a significant effort was made into understanding the construction

as well as limits of the composite tank. It is expected that by better understanding the pros and cons of the technology an informed decision can be made as to what would best contribute in the effort of space exploration.

### **2.3 Related Work**

Two methods were performed using the Auto-Regressive models with eXogenous input (ARX) to identify, locate, and estimate the amount of structural changes. The ARX models are used in a time series analysis for different sensor clusters by using the free response of the structure. Both of the methods are used for extracting Damage Features from ARX models. The first method the coefficients of the ARX models are directly used as the Damage Features. The second method is based on using the ARX model fit ratios as the Damage Features, to help deliberate the effects of noise and model complexity. This second method is successful for diverse damage cases. The Damage Features level was detected to be a good gauge for estimating the extent of the damage (Gul and Catbas 2011).

Different methodologies of identifying structural problems were explored to find the most practical and cost-effective. The method used was tracking correlation coefficients between strain time histories at different locations. A lab test was first performed, and then testing on a real-life bridge. Monitoring for the bridge was done before, during, and after damage occurred. The results of the structural changes was detected and located for both testing conditions using the variations in the correlation matrices. The differences in the different testing conditions were also taken into account. The method has the possibility to be easily applicable (Catbas Gokce et al. 2011).

The safe life of carbon composite overwrapped pressure vessels (COPVs) were evaluated by the NASA White Sands Test Facility – Jet Propulsion Laboratory. COPVs are largely used for propellant storage and actuation pressure storage. Advantages with COPV technology over other similar technologies (amorphous technology) is the savings in weight. The objects tested were comprised of an aluminum liner and a carbon fiber overwrap in an industry standard epoxy resin system. 120 test articles were manufactured, 110 were delivered, and the remaining 10 were burst tested to establish the delivered fiber stress (Greene Yoder et al. 2007).

Analysis and tests were performed on a designed pressure tank. Its design was centered on a flight-qualified pressure tank. The tank is a titanium-lined, composite overwrapped pressure vessel for helium pressure storage to be used for commercial spacecraft. Risks and costs were lessened by using the existing technology, processes, procedures, and the tooling to the fullest degree. Stress analysis proved positive safety for pressure cycle and vibration fatigue. Qualification testing also proved to be conservative. Commercially pure titanium was chosen as the material for the liner because of its excellent manufacturability, comparative high strength, exceptional corrosion and oxidation resistance characteristics, and good low and high cycle fatigue. A complete and successful qualification testing was performed on the tank (Tam and Griffin 2002).

Testing was done to help calculate and prolong the lifetime of flight vessels. The type of testing done was stress rupture of Kevlar composite overwrapped pressure vessels (COPVs), which were tested until failure occurred. The testing occurred over a six year time period at the NASA

White Sands Test Facility. The purpose of these tests were to distinguish control parameters for stress rupture testing, and predict vessel life by statistical modeling. This testing generated substantial information that will be used in the future to boost the development of improved NDE (Non Destructive Examination) methods and predictive modeling techniques. This will lead to an improved understanding of stress rupture and other composite durability concerns that affect pressure vessel safety, reliability, and mission assurance (Greene Saulsberry et al. 2010).

Auto-Regressive Integrated Moving Average (ARIMA) models were used to analyze static strain data from a bridge while it was being used and during its construction. The information taken showed the ability of damage detection, but was limited on the nature, severity, and location (Omenzetter and Brownjohn 2006).

A recent three month study of the Golden Gate Bridge was conducted using the peak picking method and an ARMA model. The high spatial density of the sensor network permitted for precise identification of the first three modes in each direction (Shamim and Gregory 2009).

## **CHAPTER 3: DATA ANALYSIS TECHNIQUES FOR DAMAGE DETECTION**

In SHM there are two main categories of analyzing data; Parametric and Nonparametric modeling methods. Where parametric models use the physical parameters of the structure to create the model, for example stiffness, geometry, supports, etc. Alternatively nonparametric models do not require these physical parameters. A non-parametric model still has parameters; however, they are not directly related to the physical characteristics of the system (Gul 2009).

In many cases parametric methods can be more difficult, time consuming and expensive than nonparametric methods. This is true in the case of complex structures that have unique geometry, material, and/or other difficult parameter to identify or model. Because of the complexity of composite pressure vessels I will focus on nonparametric techniques to analyze data and detect damage. The nonparametric methods used are Cross-Correlation Analysis (CCA) and Auto-Regressive models with eXogenous outputs (ARX)

### **3.1 Cross-Correlation Analysis**

In this study correlation of the strain data is employed in order to detect data. In theory, correlation coefficient is a measure of similarity of two data sets and may take a value between +1 and -1. Having similar behavior in data sets gives high magnitude correlation (values close to +1 and -1) while low magnitude correlation (values close to 0) indicates either low or no correlated response (Catbas, Gokce, et al. 2011). For the continuous monitoring of data, for a given window, the correlation coefficient between two sensors is shown in equation (8).

$$\rho_{ij}(t_n) = \frac{\sum_{k=1}^n ((S_i(t_k) - \mu_i)(S_j(t_k) - \mu_j))}{\sqrt{\sum_{k=1}^n (S_i(t_k) - \mu_i)^2} \sqrt{\sum_{k=1}^n (S_j(t_k) - \mu_j)^2}} \quad (8)$$

Where  $\rho_{ij}$  is the correlation between the sensors  $i$  and  $j$ ,  $n$  is the total number of time observations during the monitoring duration,  $S_i(t_k)$  and  $S_j(t_k)$  are the values of the sensors  $i$  and  $j$  at time  $t_k$ , and,  $\mu_i$ ,  $\mu_j$  are the mean values of the sensors  $i$  and  $j$ .

Baseline correlation matrices are generated based on the data captured from undamaged structure. For each baseline data set, a baseline correlation matrix, which consists of the correlation of individual pairs of sensors, is generated. Baseline correlation matrix is an  $n \times n$  matrix where  $n$  refers to number of sensors existing on monitored structure. Each row (or column) in the matrix is presenting the correlation of a sensor with the rest of sensors (Malekzadeh 2014). After obtaining these matrices for baseline and damaged conditions, they are compared to detect and locate the damage (Malekzadeh, Gul, & Catbas 2013). This methodology is based on the premise if the baseline structure remains unchanged then there should be no change in correlation coefficient, and if there is a change in the correlation coefficient then there must be a change in the structure.

### **3.2 Time Series Modeling**

Time series modeling is statistical modeling of a sequence of data points that are observed in time. It has been used in many different fields including structural dynamics and system identification. The following subsections provide a condense description and discussion about time series modeling and its related applications. For more details concerning the theory behind time series modeling (outside the scope of this study) can be found in literature (Pandit and Wu 1993; Box et al. 1994; Ljung 1999).

### 3.2.1 Formulations of Time Series Modeling

A linear time series model representing the relationship of the input, output and the error terms of a system can be written with the difference equation shown in equation (9) (Ljung 1999).

$$y(t) + a_1y(t - 1) + \dots + a_{n_a}y(t - n_a) = b_1u(t - 1) + \dots + b_{n_b}u(t - n_b) + e(t) + d_1e(t - 1) + \dots + d_{n_d}e(t - n_d) \quad (9)$$

A simplified version of equation (9) is shown in equation (10).

$$A(q)y(t) = B(q)u(t) + D(q)e(t) \quad (10)$$

Where in equation (9),  $y(t)$  is the output of the model,  $u(t)$  is the input to the model and  $e(t)$  is the error term. The unknown parameters of the model are shown with  $a_i$ ,  $b_i$ , and  $d_i$  and the model orders are shown with  $n_a$ ,  $n_b$  and  $n_d$ . In equation (10),  $A(q)$ ,  $B(q)$ , and  $D(q)$  are polynomials in the delay operator  $q^{-1}$  as shown below in equation (11). The model shown in equation (9) can also be referred as an ARMAX model (Auto-Regressive Moving Average model with eXogenous input) and a block diagram of an ARMAX model can be shown as in Figure 3-1.

$$\begin{aligned} A(q) &= 1 + a_1q^{-1} + a_2q^{-2} + \dots + a_{n_a}q^{-n_a} \\ B(q) &= b_1q^{-1} + b_2q^{-2} + \dots + b_{n_b}q^{-n_b} \\ D(q) &= 1 + d_1q^{-1} + d_2q^{-2} + \dots + d_{n_d}q^{-n_d} \end{aligned} \quad (11)$$

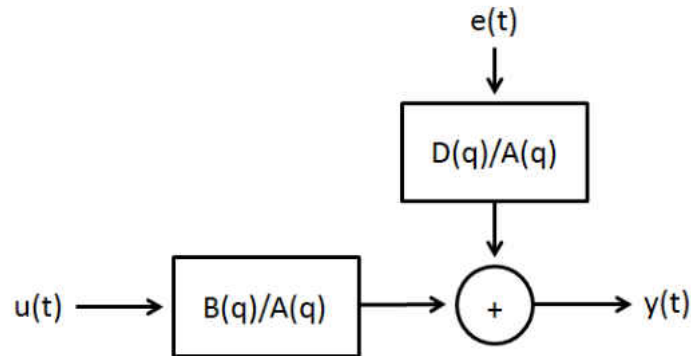


Figure 3:1: The Block Diagram of an ARMAX Model (adapted from Ljung (1999))

By changing the model order of an ARMAX model, different types of similar time series models can be made. If the  $n_b$  and  $n_d$  terms are set to zero, the model will be referred as an AR (Auto- Regressive) model. The structure of an AR model is shown in equation (12) and the block diagram of the model is shown in Figure 3-2.

$$A(q)y(t) = u(t) + e(t) \tag{12}$$

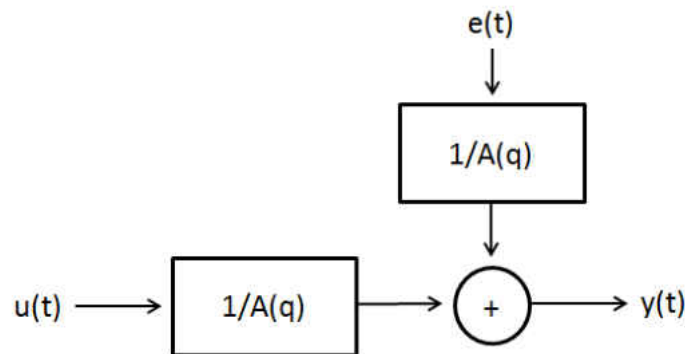


Figure 3:2: The Block Diagram of an AR Model (adapted from Ljung (1999))

If the  $n_b$  term is set to zero, the model will be referred as an ARMA (Auto- Regressive Moving Average) model. The structure of an ARMA model is shown in equation (13) and the block diagram of the model is shown in Figure 3-3.

$$A(q)y(t) = u(t) + D(q)e(t) \quad (13)$$

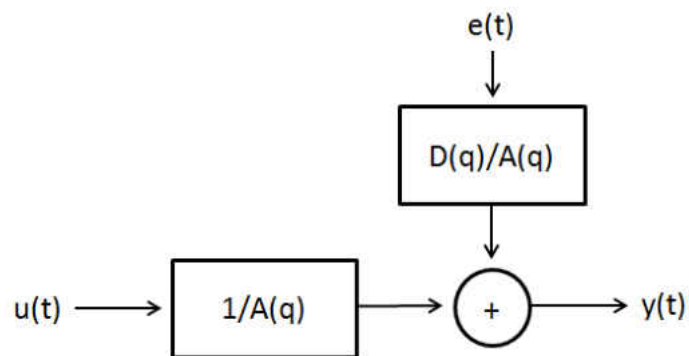


Figure 3:3: The Block Diagram of an ARMA Model (adapted from Ljung (1999))

If the  $n_d$  term is set to zero, the model will be referred as an ARX (Auto-Regressive models with eXogenous outputs) model. The structure of an ARX model is shown in equation (14) and the block diagram of the model is shown in Figure 3-4.

$$A(q)y(t) = B(q)u(t) + e(t) \quad (14)$$

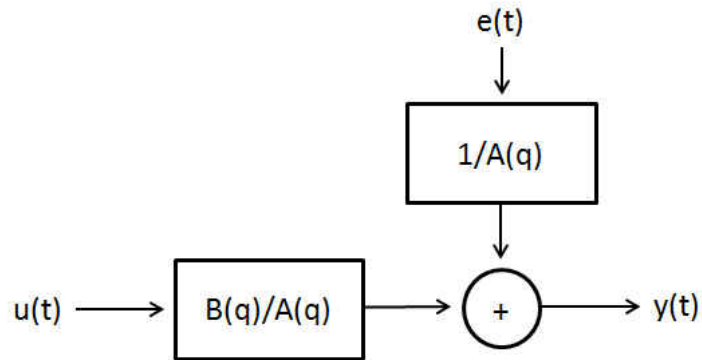


Figure 3:4: The Block Diagram of an ARX Model (adapted from Ljung (1999))

Instead of the previous models (Figures 3-1 to 3-3), the ARX model (Figures 3-4) was the type of time series model selected for this study, since modeling of the disturbance dynamics did not affect the end results significantly (Gul 2009). ARX model estimation is the most efficient of the polynomial estimation methods due to the fact that it is the result of solving linear regression equations in analytic form (Instruments 2009).

### 3.2.2 Time Series Modeling for Structural Dynamics

From Figure 3-4 and equation (14) it is clear that the ARX model requires both the input and output of the system to be defined in order to create the model. However for many civil engineering applications, especially those which use acceleration/dynamic data, collecting input data can be very difficult and is not yet practical in health monitoring. Therefore using techniques to determine the health of such structures using only the output data is extremely important. Proposed by Gul and Catbas (2011), a new time series methodology was used to identify damage in structures using only the output component of the acceleration data.

For N degrees of freedom (DOF), the equation of motion of a linear dynamic system can be written in matrix form as seen in equation (15) below.

$$\begin{bmatrix} m_{11} & \cdots & m_{1N} \\ \vdots & \ddots & \vdots \\ m_{N1} & \cdots & m_{NN} \end{bmatrix} \begin{Bmatrix} \ddot{x}_1 \\ \vdots \\ \ddot{x}_N \end{Bmatrix} + \begin{bmatrix} c_{11} & \cdots & c_{1N} \\ \vdots & \ddots & \vdots \\ c_{N1} & \cdots & c_{NN} \end{bmatrix} \begin{Bmatrix} \dot{x}_1 \\ \vdots \\ \dot{x}_N \end{Bmatrix} + \begin{bmatrix} k_{11} & \cdots & k_{1N} \\ \vdots & \ddots & \vdots \\ k_{N1} & \cdots & k_{NN} \end{bmatrix} \begin{Bmatrix} x_1 \\ \vdots \\ x_N \end{Bmatrix} = \begin{Bmatrix} f_1 \\ \vdots \\ f_N \end{Bmatrix} \quad (15)$$

Where [M] is the mass matrix, [C] is the damping matrix, and [K] is the stiffness matrix;  $\{\ddot{x}\}$  is the acceleration vector,  $\{\dot{x}\}$  is the velocity vector,  $\{x\}$  is the displacement vector, and  $\{f\}$  is the force vector. The equality in equation (16) is obtained if the first row of equation (15) is written separately. By rearranging equation (16) the output of the first DOF can be written in term of the excitation force, the physical parameters of the structure, and the outputs of the other DOFs, as seen in equation (17). Finally, in the free response case, the excitation force will be zero and therefore equation (17) will simplify into equation (18).

$$(m_{11}\ddot{x}_1 + \cdots + m_{1N}\ddot{x}_N) + (c_{11}\dot{x}_1 + \cdots + c_{1N}\dot{x}_N) + (k_{11}x_1 + \cdots + k_{1N}x_N) = f_1 \quad (16)$$

$$\ddot{x}_1 = \frac{f_1 - (m_{12}\ddot{x}_2 + \cdots + m_{1N}\ddot{x}_N) + (c_{11}\dot{x}_1 + \cdots + c_{1N}\dot{x}_N) + (k_{11}x_1 + \cdots + k_{1N}x_N)}{m_{11}} \quad (17)$$

$$\ddot{x}_1 = - \frac{(m_{12}\ddot{x}_2 + \cdots + m_{1N}\ddot{x}_N) + (c_{11}\dot{x}_1 + \cdots + c_{1N}\dot{x}_N) + (k_{11}x_1 + \cdots + k_{1N}x_N)}{m_{11}} \quad (18)$$

It is seen from equation (18) that if a model is created to predict the output of the first DOF by using the DOFs connected to it (neighbor DOFs); the change in this model can reveal important information about the change in the properties of that part of the system. Obviously, similar equalities can be written for each row of equation (15) and different models can be created for each equation. Each row of equation (15) can be considered as a sensor cluster with a reference DOF and its neighbor DOFs (Gul 2009). The reference DOF for equation (18) is the first DOF and

neighbor DOFs are the DOFs that are directly connected to the first DOF. Therefore different linear time series models can be created to establish different models for each sensor cluster, and inconsistencies between the models and experimental data will result in the detection of damage explained below.

### 3.2.3 Damage Feature (DF)

Once the ARX models are created for the baseline structure; they will be used to predict the expected outputs of the other structures of interest. The fit ratio (FR) is how closely the predicted model is to the actual data, shown below in equation (19).

$$\text{Fit Ratio (FR)} = \left(1 - \frac{|y - \hat{y}|}{|y - \bar{y}|}\right) \times 100 \quad (19)$$

Where  $y$  is the measured output,  $\hat{y}$  is the predicted output and,  $\bar{y}$  is the mean of  $y$ . After determining the FR for each case the damage feature (DF) can be determined by the difference in FRs between the baseline and damaged cases, shown below in equation (20).

$$\text{Damage Feature (DF)} = \frac{\text{FR}_{\text{healthy}} - \text{FR}_{\text{damaged}}}{\text{FR}_{\text{healthy}}} \times 100 \quad (20)$$

Damage Features using Auto-Regressive models with eXogenous outputs (ARX) Analysis will be implemented using the pressure input and strain responses and also the acceleration responses. ARX models will be established and then compared with the measured data. From there, the Damage Feature (DF) will be identified based on the established threshold limits. This approach was well-documented by Catbas' previous publications.

## **CHAPTER 4: TESTING AND MONITORING STUDIES OF COPV'S IN THE LABORATORY**

### **4.1 Objective and Scope**

Concerns regarding the catastrophic nature of COPV failure have prompted NASA's to perform an independent assessment of COPV safety and their flight worthiness since they have been in operation for over 25 years. A small scale experiment was performed to obtain indices/features related to the performance and/or condition of COPVs. We will research further about the safety of the COPV due to the complexity of the material. And explore to see if the lifespan or sudden changes of the tank can be identified.

Therefore the specific objectives of this experiment are to:

- Establish strain/stress levels in the hoop and longitudinal directions under different pressure levels. Then compare the stresses at different locations for material/structural consistency.
- Compare how each specimen performs to each other. See if damage/flaws can be detected.

In order to find the stress/strain levels and the dynamic properties of the COPVs, multiple test must be conducted on each test specimen. One test required to determine the stress stain levels in the COPVs is a hydrostat pressure test. Each tank will be filled with water (for safety and a

more practical use) and then pressurized in certain pressure steps while the stain is recorded. Then in order to determine the dynamic properties of the tank a hammer test is conducted.

#### 4.1.1 Test Specimens

The experimental testing comparing the differences in the COPVs will contain five different specimens. Each tank is identical geometry; a circular, cylindrical, pressure vessel fourteen and a half inches long and six and a half inches in diameter. Each specimen will have two dome end caps and can be seen in the following figure below (Figure 4-1):



Figure 4:1: Two Test Specimens (left) COPV End Cap (right)

The dimensions of the COPVs can be seen on the following AutoCad schematic figure below (Figure 4-2):

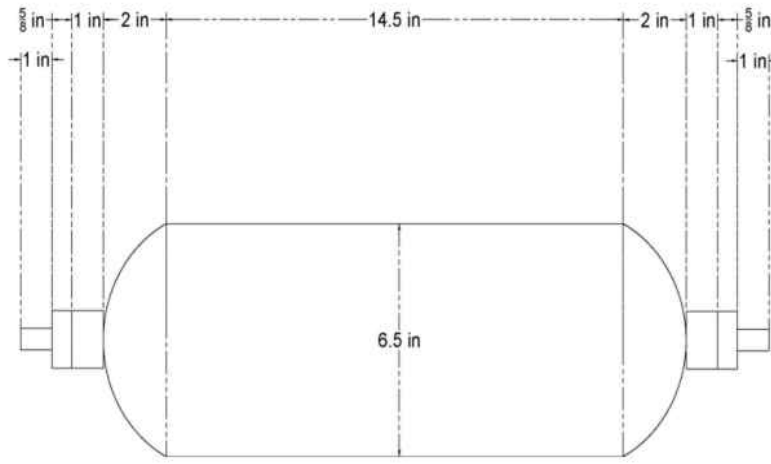


Figure 4:2: COPV Dimensions

Two of the specimens have no defects and should only have normal manufacturing differences. While the other three COPVs have known voids, flaws, or changes in material. The following table (Table 4-1) further explains the different specimens:

Table 4-1: COPV Test Specimen Characteristics

Identifying Number	Description	Condition Simulated
1	No defects TRH-50 -5 hoop, helical over-wraps	Comparison-normal manufacturing variances
2	No defects TRH-50 -5 hoop, helical over-wraps	Comparison-normal manufacturing variances
3	Zylon Ring midpoint after 2nd hoop wrap	Thermally similar hidden delamination or void
4	Teflon Tape X after 3rd hoop wrap	Thermally different hidden delamination or void
5	Zebra pattern 50/50 TRH-50 and Zylon	two materials intergrated in helical pattern

## 4.2 Pressure Testing

The hydrostat pressure test was conducted in order to collect pressure and strain data and see how they compare. This test was ideal to retrieve this type of data because it gradually increases the pressure and strain which makes the data clean and easy to work with. There will be a pressure transducer to record pressure data as well as three electrical strain gages for each pressure vessel. Two strain gage will be on one side (one in the axial direction and the other in the hoop), while the third strain gage will be opposite to the first hoop gage; the instrumentation of these sensors can be seen on Figure 4-3. All the strain gages will be located in the center on the vessel because that's the area that's furthest away from the geometry change and will better resemble an ideal cylinder.

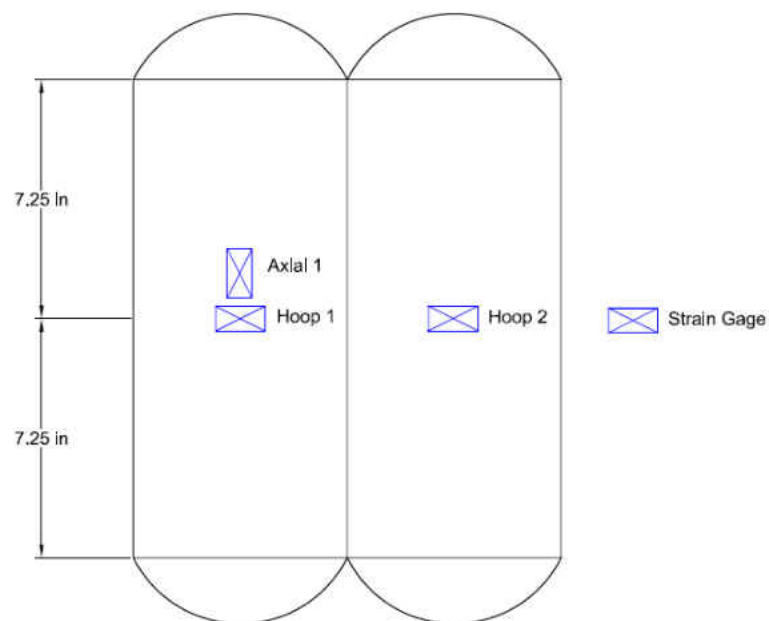


Figure 4:3: COPV Pressure Testing Instrumentation Plan

#### 4.2.1 Health Monitoring System

For this part of the experiment the National Instruments (NI) SCXI-1001 Data Acquisition System (DAQ) was used in conjunction with the LabView software. A simple code was written in LabView in order to collect data from the three strain gages and pressure transducer. The specifications of the sensors used in this portion of the experiment are explained below:

The three strain gauges that were used throughout the experiment were all Omega KFG-5-350-C1-11L1M2R, which were installed with super glue, shown in Figure 4-4 below:



Figure 4:4: Installed Strain Gage on COPV

Strain gauges are designed to measure strain that is being caused by structures, COPV. “Strain is the amount of deformation of a body due to an applied force. More specifically, strain is defined as the fractional change in length, as shown in Figure 4-5. Strain can be positive (tensile) or negative (compressive)” (Measuring Strain with Strain Gages). The strain gauge in this case study was used to find the thickness of the COPV. Also, the strain gauge was used in a comparison of the FBG vs. strain and strain hoop vs. strain axial.

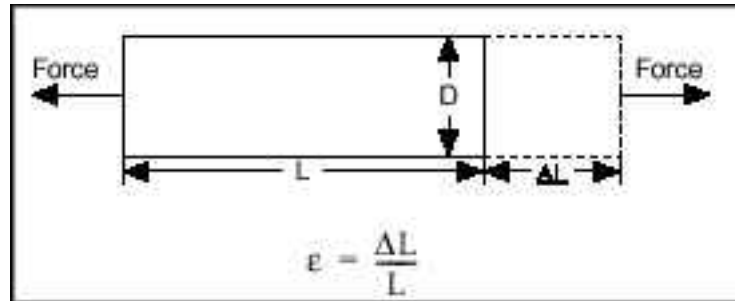


Figure 4:5: Definition of Strain (Measuring Strain with Strain Gages)

The pressure transducer that was used in the case study was an Omega dyne Inc. model type PX309-300GV. It was connected to the COPV using a T-fitting, allowing the sensor to sense the pressure without disturbing the experiment, seen in Figure 4-6 below.



Figure 4:6: End Connection, Consisting of Pressure Transducer, Pressure Valve, and T-fitting

The pressure transducer diagram seen in Figure 4-7 allowed air pressure to come through the pressure port. Once the air pressure was inside the pressure transducer it hit the sensing element

and then was converted from air pressure to voltage. The voltage was then converted back into pressure in order to find the thickness of the tank.

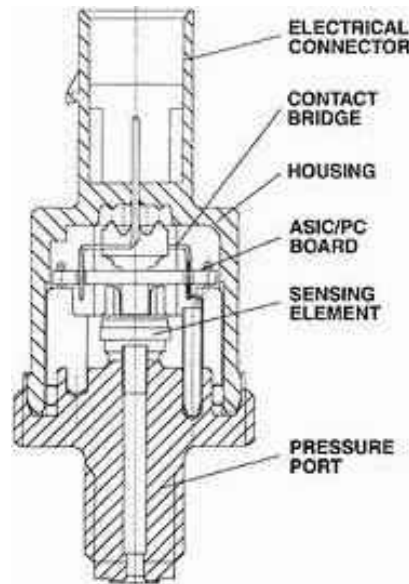


Figure 4:7: Pressure Transducer Diagram

#### 4.2.2 Test Procedure

Initially before the experiment started the COPV was filled with water. Then the COPV was placed inside the frame. The air compressor was connected to the pressure transducer and the gauges were connected to the data acquisition system (DAQ). Once the gauges and DAQ were connected power was turned on to the computer systems and the DAQs. Once all the systems were powered up and collecting data, pressure was applied to the tank. Pressure was applied at 50, 100, 150 and 200 psi pressure steps. When the pressure was stopped, the system kept running to allow for the pressure to normalize inside the tank. Once the normalization occurred, the air compressor was removed from the pressure transducer and the tank was vented. Each pressure step (50, 100, 150 and 200 psi) was repeated five times for consistency. Once completed the test

and re-done on each of the eight tanks, the computers and the DAQ were shut down and gauges removed.



Figure 4:8: COPV Pressure Test

#### 4.2.3 Preliminary Results

Once the data was collected, it was pre-processed by the MatLab built-in filter function “decimate”. This reduces the noise of the data which results in a more stream-lined, accurate data set. The filtered Input-Output (Pressure-Strain) data for each tank can be seen in Figures 4-9 through 4-13 below:

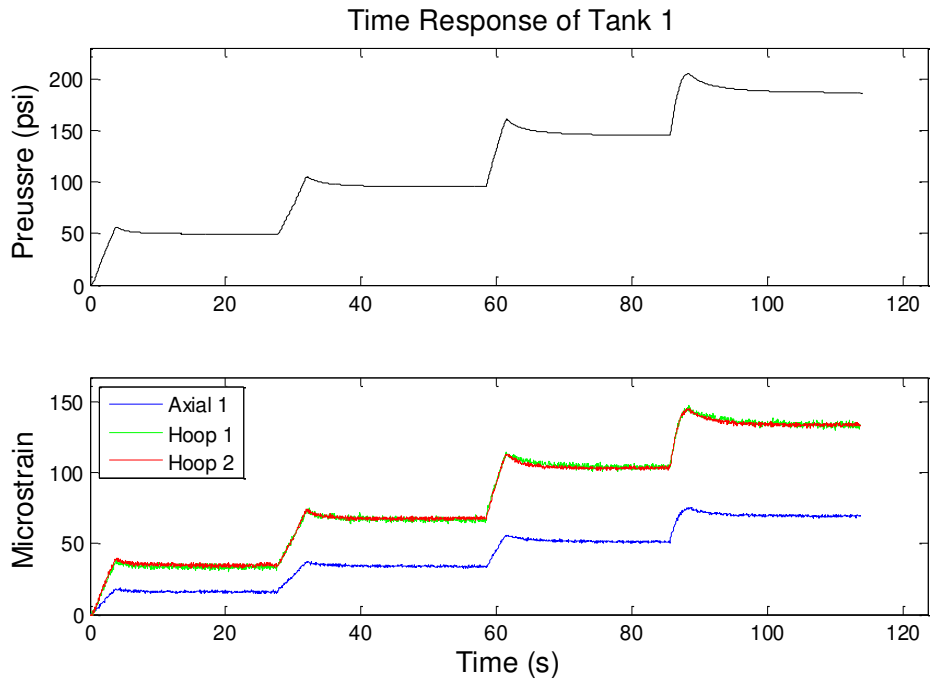


Figure 4:9: Time Response of Tank 1

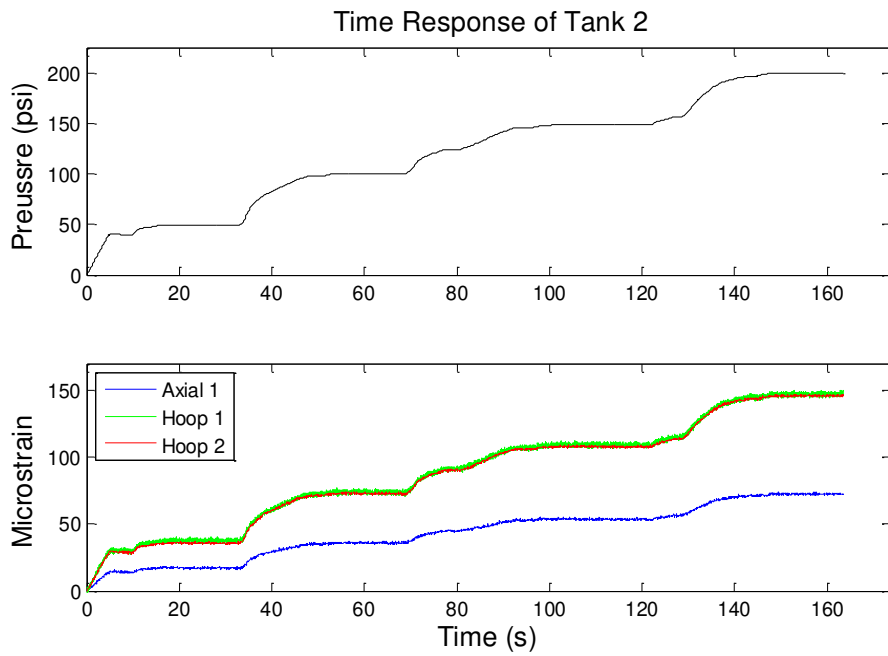


Figure 4:10: Time Response of Tank 2

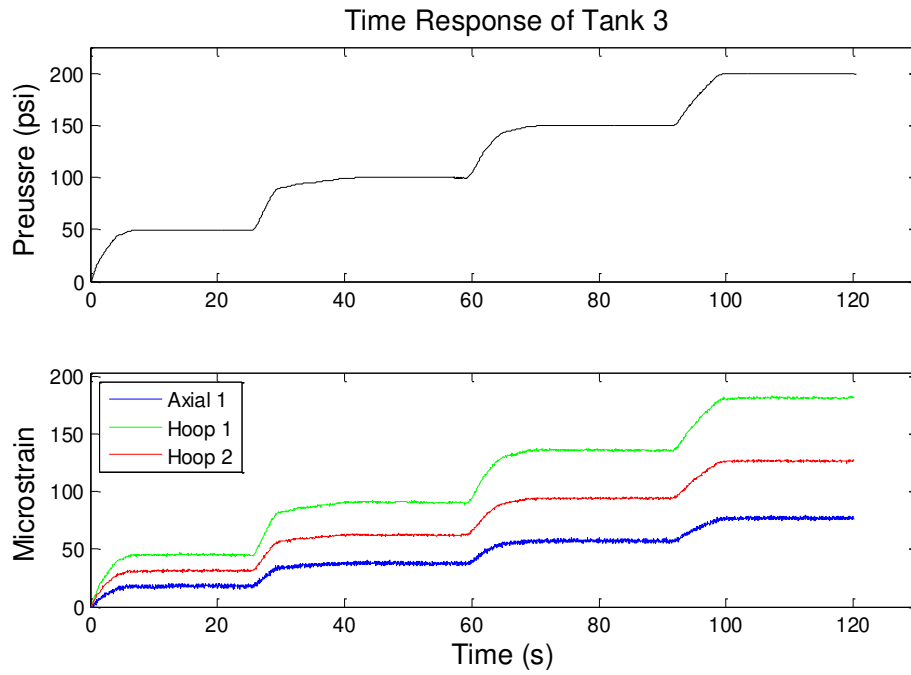


Figure 4:11: Time Response of Tank 3

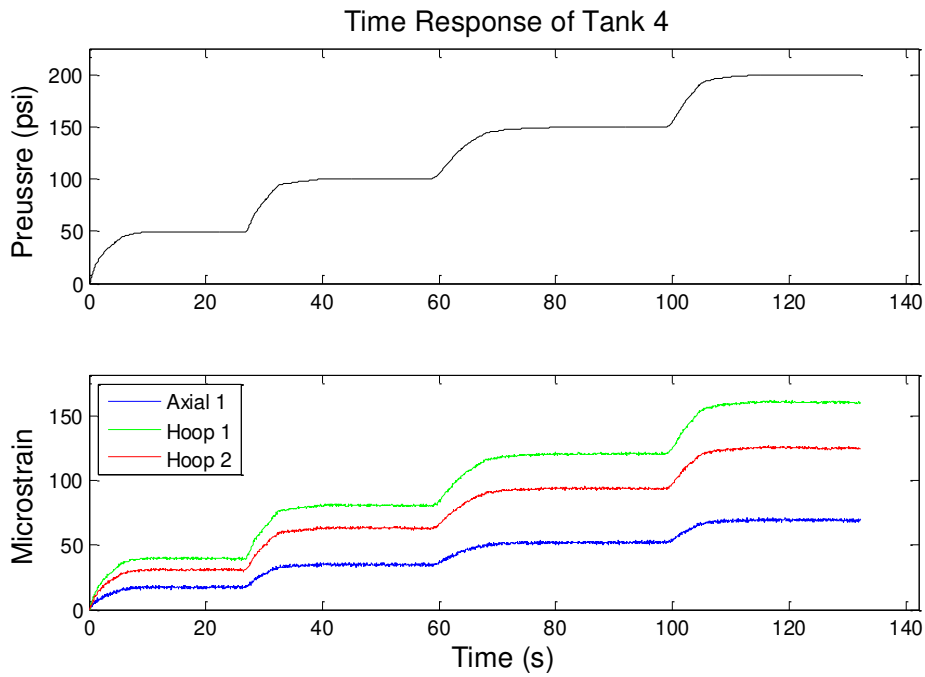


Figure 4:12: Time Response of Tank 4

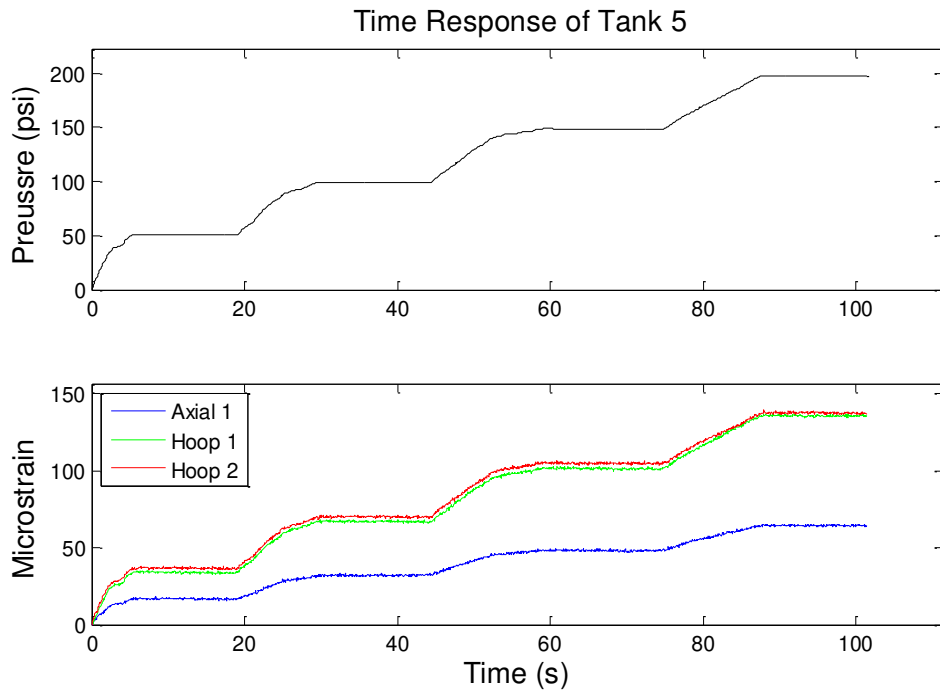


Figure 4:13: Time Response of Tank 5

### 4.3 Dynamic Testing

The hammer tapping test was performed in order to excite the tank's natural frequencies. This was possible due to the relative size of the vessel compared to the hammer. When applying the force of the hammer onto the tank, the hammer was swung lightly. In order to excite higher and more frequencies, a very hard/stiff hammer head was used. The stiffness of the contacting surfaces, hammer head and tank, affected the shape and size of the force pulse, which is necessary to determine the frequency content.

Three accelerometers were used in this test; they are separated quarterly in the vertical (axial) direction and by thirds in the horizontal (hoop) direction. The instrumentation of these sensors can be seen on Figure 4-14.

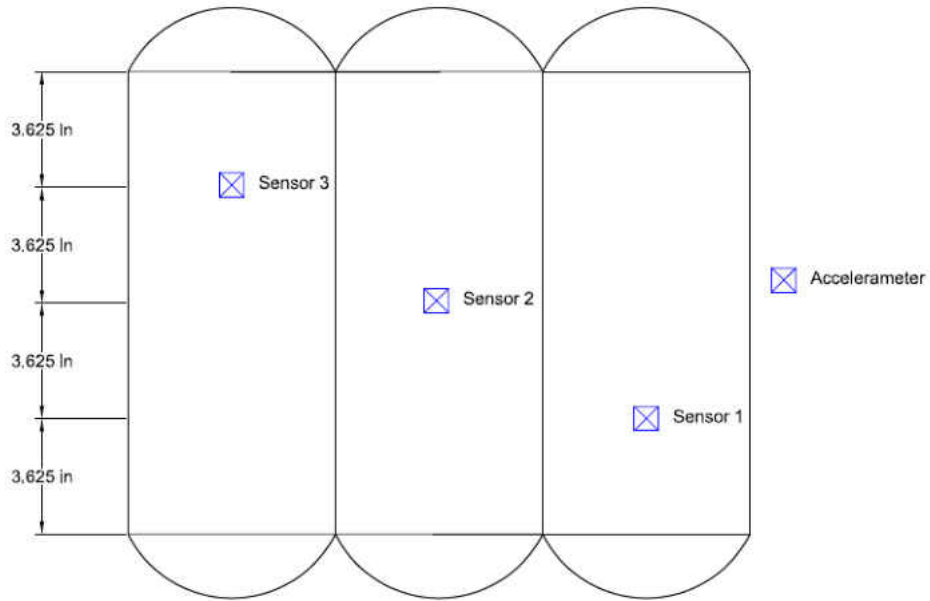


Figure 4:14: COPV Dynamic Testing Instrumentation Plan

#### 4.3.1 Health Monitoring System

The three PCB accelerometers were connected individually to the CT-100C data acquisition system from VXI. A signal conditioner from PCB Piezotronics conditioned the continuous electrical signal before it was discretized into finite values by the digitizer. A PC link then enabled the data to be stored on the desktop PC. DAQ Express software was used for controlling the data acquisition and recording. Figure 4-15 shows the health monitoring system; the PC, PCB Piezotronics conditioner, and the VXI data acquisition system.



Figure 4:15: Dynamic Testing Health Monitoring System

The accelerometers that were used for the experiment were the PCB Series 3801 capacitive accelerometers; they were installed using hot glue, seen in Figure 4-16. An accelerometer works when the housing of a piezoelectric crystal is compressed between the base and a small weight called the seismic mass this can be seen in Figure 4-16. When the accelerometer vibrates along its axis this arrangement applies an alternating force of compression and extension to the crystal. This vibration generates a minute, constantly changing electric charge proportional to the force, and thus the acceleration. An accelerometer measures the force of acceleration, allowing them to sense movement, speed and direction. The accelerometers were used to find the natural frequency and modal shapes of the tanks due to an impact force.

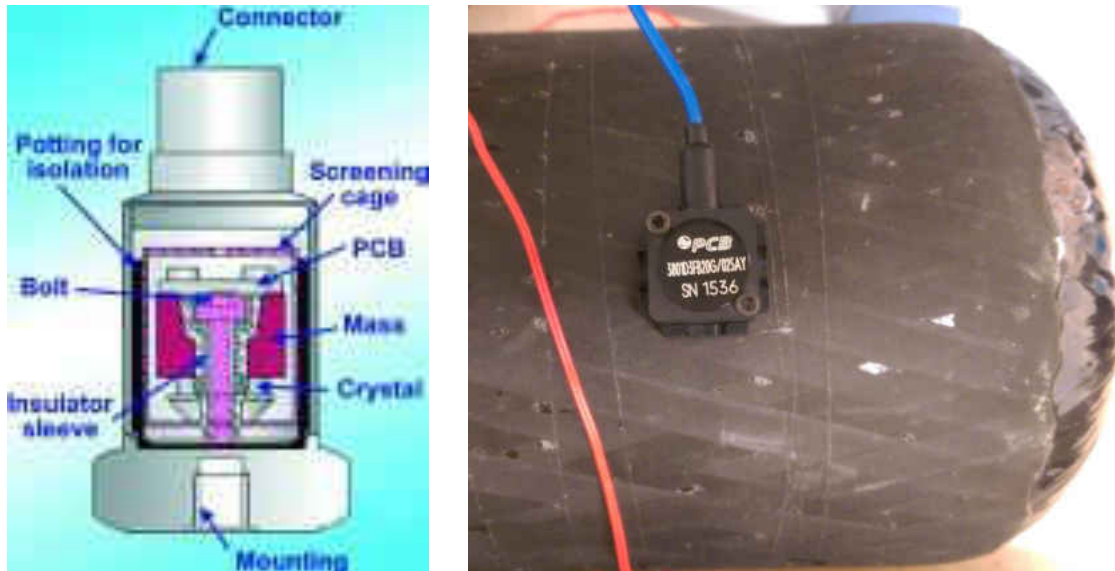


Figure 4:16: Schematic of Accelerometer (left) Installed PCB Accelerometer (right)

#### 4.3.2 Test Procedure

The COPV was hung from a bungee cord, shown in Figure 4-17. The accelerometers were then connected to the data acquisition system (DAQ) and the power was turned on to the computer systems and the DAQs. Once all the systems were powered up and collecting data, the hammer was hit in various locations on the tank. The hammer-hitting locations were strategically placed next to the accelerometers in order to get a full representation of the vessel. If this were to happen some natural frequencies could not be observed and therefore there will be missing information. Each hammer location was struck four times and the average acceleration data was used for analysis. Once all the data was saved to the systems, the computers and the DAQ were shut down and the sensors were removed and placed on the next tank for testing.



Figure 4:17: Exciting the COPV with the Impact Hammer

#### 4.3.3 Collection and Pre-Processing of Data

Once the data was collected by the DAQ it was transferred to another computer for processing. The raw acceleration data (one input and 3 outputs) for one sample data set can be seen in Figure 4-18 below.

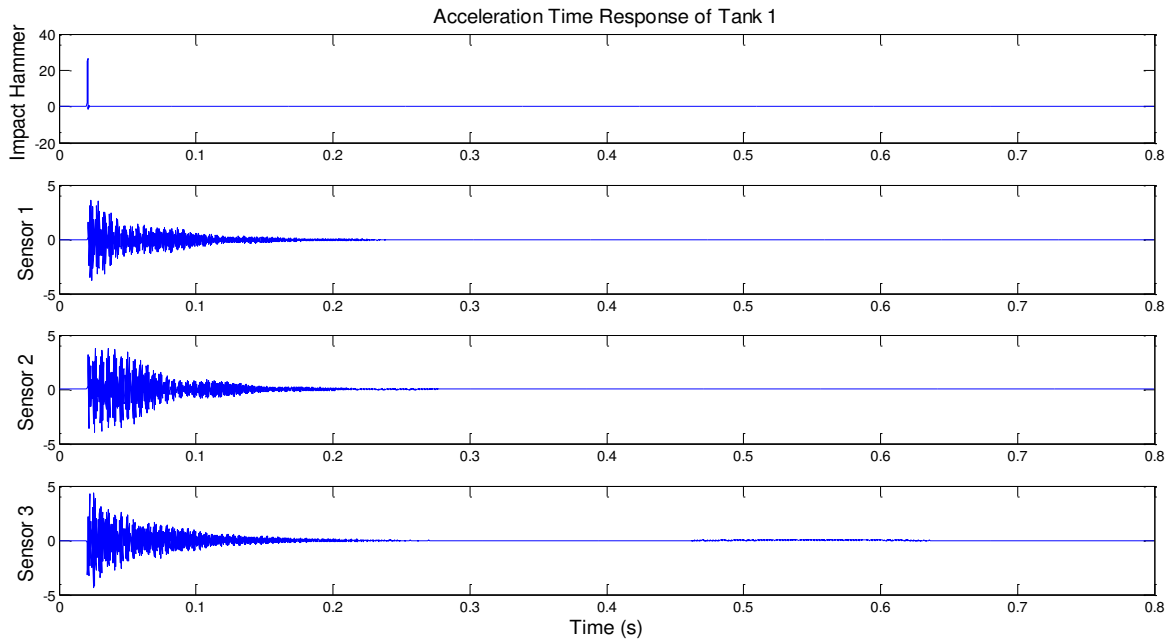


Figure 4:18: Sample Raw Data from Tank 1

As stated in Chapter 3, it is necessary that the ARX models that are going to be generated are based on only the free response of the structure (not the impact event itself). The next step in pre-processing is creating a window in which only the free response data is used. Windowing of the free vibration region of the data was done by locating the maximum acceleration value of the impact hammer and then selecting a starting point for the window shifted 20 data points to the right, thus ensuring that the impulse input itself was not modeled (Terrell 2011). Figure 4-19 below shows a sample of free-response acceleration data from one accelerometer in the experiment.

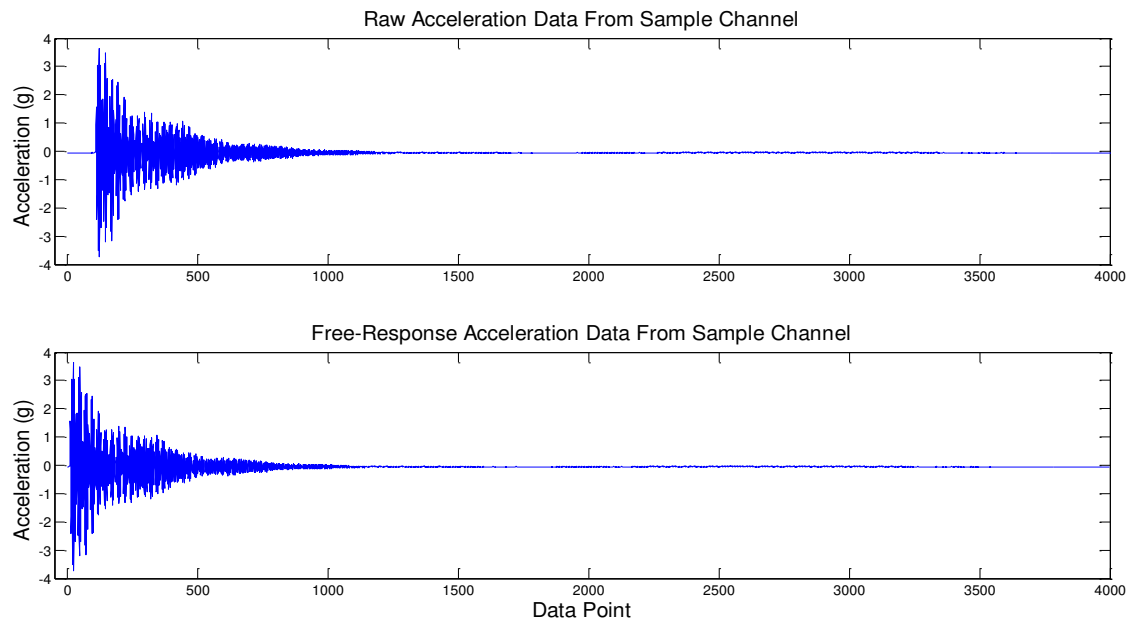


Figure 4:19: Sample Acceleration Data; Raw (Top) and Free-Response (Bottom)

## **CHAPTER 5: RESULTS AND INTERPRETATIONS OF COPV MONITORING**

In this chapter the results from the previous chapter, “Testing and Monitoring Studies of COPVs in the Laboratory”, will be presented using multiple types of data analysis techniques. First statistical analysis techniques using histograms will be implemented to examine the theoretical properties of cylindrical pressure vessels in both the axial and hoop direction. Then the Cross Correlation Analysis technique will be implemented to examine how the hoop strain in the tanks differs from one another. Next using ARX (Auto-Regressive models with eXogenous outputs) Analysis, both the pressure and strain data along with the acceleration data will be used to generate individual models which will compare to the experimental data. Finally after all the analysis results are presented, a summary of each method and weather damage was accurately was detected is displayed. It is worth mentioning that statistical analysis is used in different fields of studies to evaluate data such as in sustainable infrastructure (Malekzadeh et al. 2015), and transportation (Consoli et al. 2015, Noori 2015).

### **5.1 Statistical Analysis Using Histograms**

As mentioned before there are many different types of methods to analyze and interpret data. This section will focus on using statistical histograms as means to detect damage. This approach has been used in other civil engineering related field of studies to analyze data such as in pavement rehabilitation (Noori et al. 2014; Nam et al. 2014) and pavement design (Kucukvar et al. 2014). The section 2.1 “Mechanics of Pressure Vessels” discusses the theoretical properties of

thin walled, cylindrical pressure vessels. Such as the relationship of how stress is distributed within the vessel. These parameters will be further examined in subsections 5.1.1 and 5.1.2 below.

### 5.1.1 Hoop v Axial 2-1 Relationship

As discussed in section 2.1 and equation (5), the hoop and axial stresses within a cylindrical pressure vessel have 2 to 1 relationship. Also from equation (7) the relationship between hoop and axial strain is similar, where the hoop strain is twice the strain in the axial direction. Therefore in this study the ratio of the hoop and axial strain, for each data point, of each individual tank was computed. These values were used to create a histogram in MatLab using the built in function “histfit”. The results of these plots for each tank are shown in Figures 5-1 through 5-5 below.

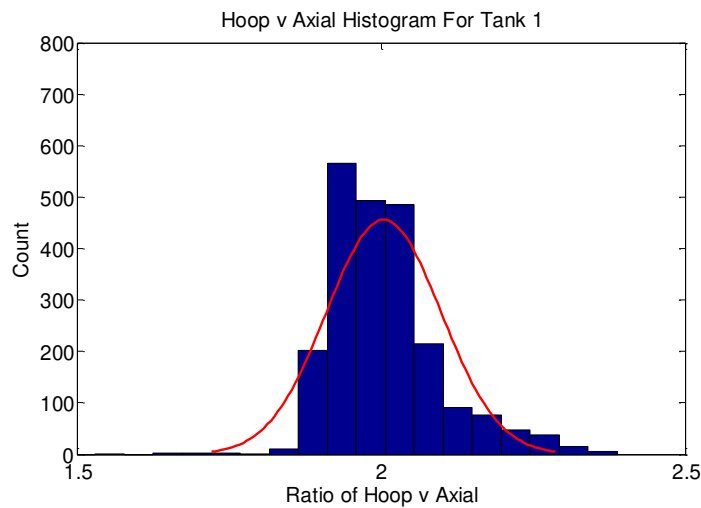


Figure 5:1: Hoop v Axial Histogram for Tank 1

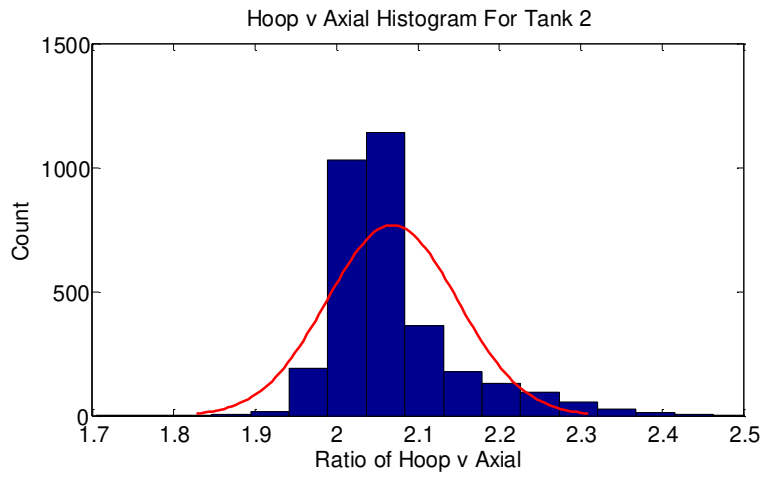


Figure 5:2: Hoop v Axial Histogram for Tank 2

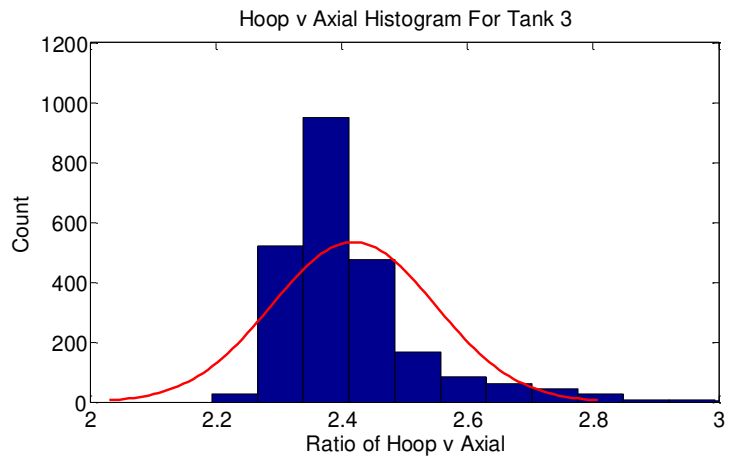


Figure 5:3: Hoop v Axial Histogram for Tank 3

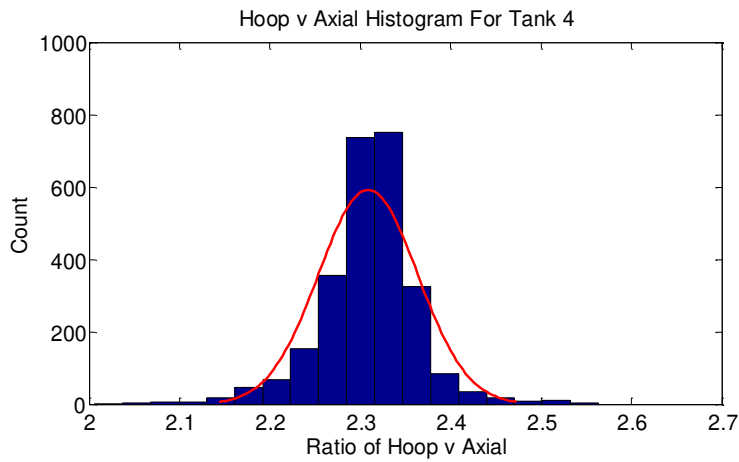


Figure 5:4: Hoop v Axial Histogram for Tank 4

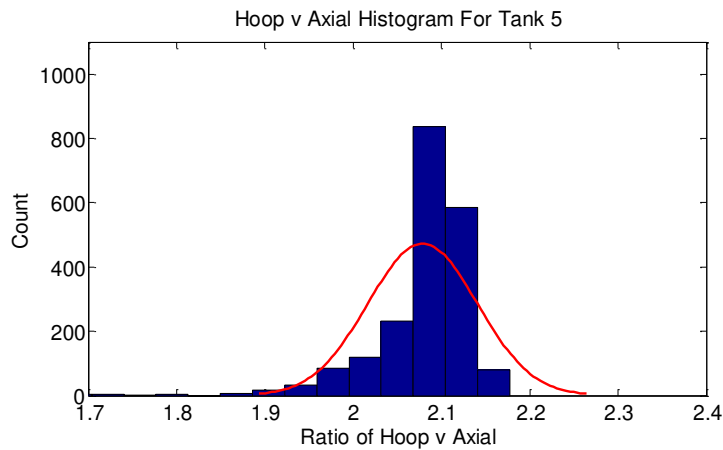


Figure 5:5: Hoop v Axial Histogram for Tank 5

As seen from the five figures above each tank shows a relationship of hoop to axial strain close to the theoretical value of 2 to 1. However tanks 1, 2 and 5 are significantly closer than tanks 3 and 4. This makes sense because only tanks 3 and 4 were induced with damage, shown in Table 4-1. Table 5-1 below shows the average of each plot along with the corresponding percent error.

Table 5-1: Hoop v Axial Histogram Summary

Tank	Mean	% Error
1	1.9043	4.78
2	2.0868	4.34
3	2.4192	20.96
4	2.3087	15.44
5	2.1287	6.43

### 5.1.2 Comparison of Hoop Sensors 1 & 2

As discussed in section 2.1 and equation (2), the hoop stress along a cylindrical pressure vessel has constant uniform stress. Therefore the relationship between various hoop strains should have a 1 to 1 relationship at any location as long as it's in the hoop direction. Furthermore this study will compare the ratio of the hoop strains at locations 1 and 2 (shown in Figure 4-3). The ratio for each data point, of each individual tank was computed. These values were used to create a histogram in MatLab using the built in function "histfit" similar to what was done in 5.1.1. The results of these plots for each tank are shown in Figures 5-6 through 5-10 below.

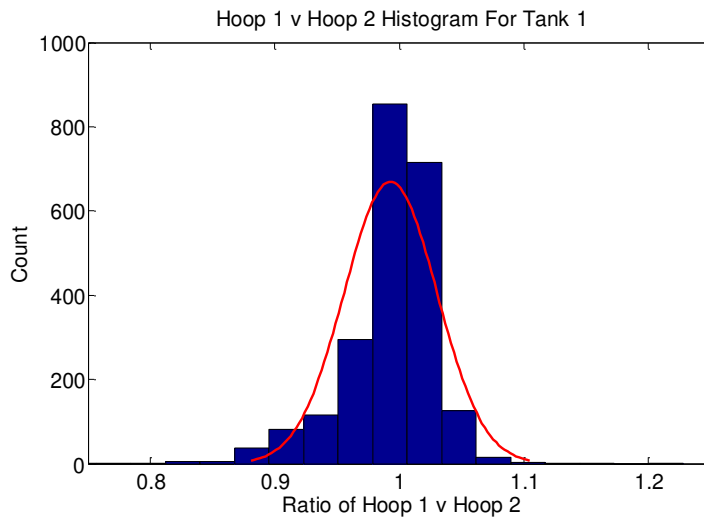


Figure 5:6: Hoop 1 v Hoop 2 Histogram for Tank 1

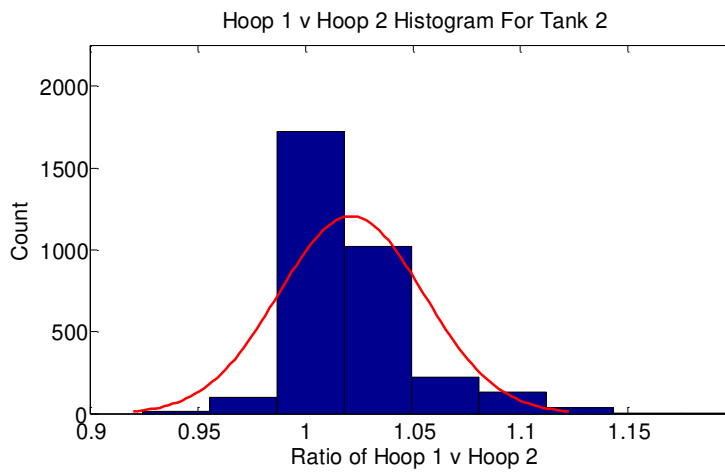


Figure 5:7: Hoop 1 v Hoop 2 Histogram for Tank 2

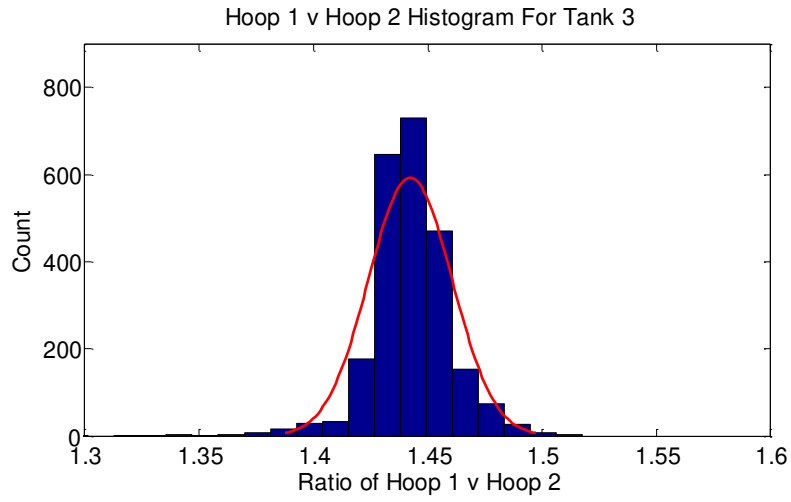


Figure 5:8: Hoop 1 v Hoop 2 Histogram for Tank 3

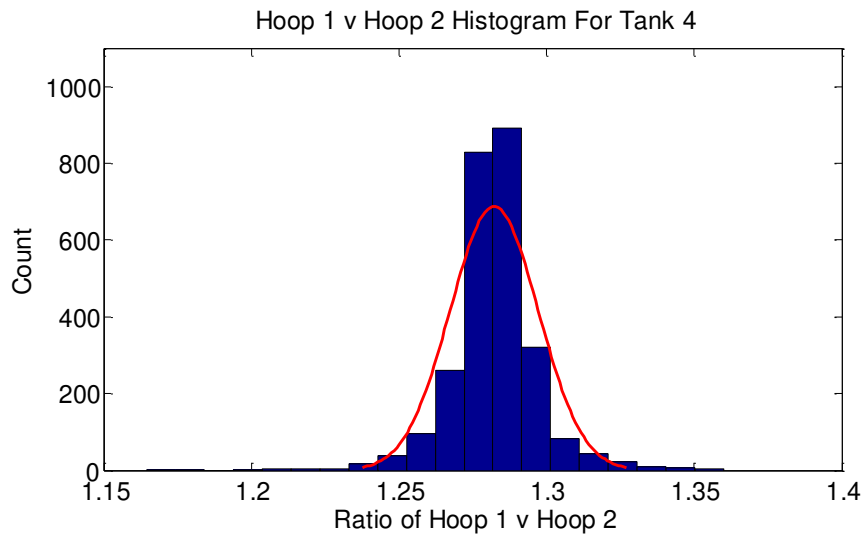


Figure 5:9: Hoop 1 v Hoop 2 Histogram for Tank 4

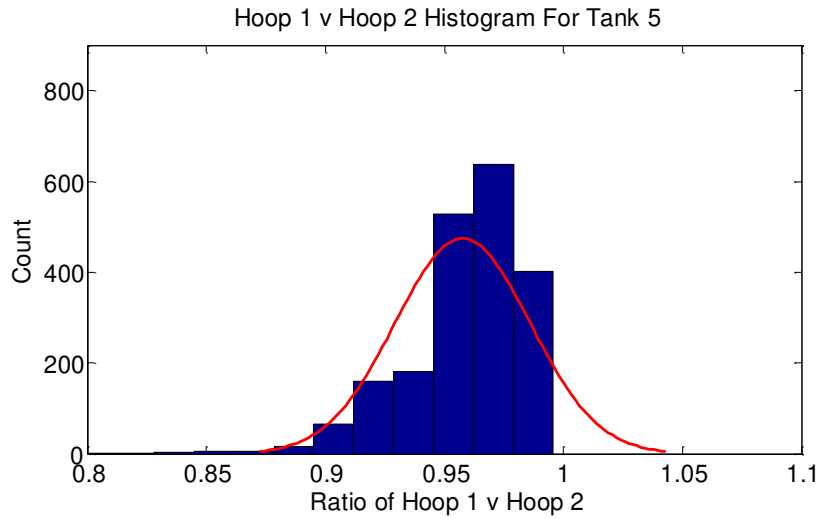


Figure 5:10: Hoop 1 v Hoop 2 Histogram for Tank 5

As seen from the five figures above each tank shows a relationship of hoop strains at different locations close to the theoretical value of 1 to 1. However tanks 1, 2 and 5 are significantly closer than tanks 3 and 4. This makes sense because only tanks 3 and 4 were induced with damage, shown in Table 4-1. This is consistent with the results presented in subsection 5.1.1 above. Table 5-2 below shows the average of each plot along with the corresponding percent error.

Table 5-2: Hoop 1 v Hoop 2 Histogram Summary

Tank	Mean	% Error
1	0.993	0.70
2	1.0212	2.12
3	1.4423	44.23
4	1.2822	28.22
5	0.9576	4.24

## 5.2 Cross Correlation Analysis

This section will focus on using cross correlation analysis as means to detect damage. The section 3.1 “Cross Correlation Analysis” discusses the theoretical methodology for this technique and how it’s implemented. The correlation of strain data will be further examined in subsection 5.2.1 below.

### 5.2.1 Correlation between Hoop Sensors 1 & 2

First the correlation of tank 1 (baseline/healthy structure) for hoop sensors 1 and 2 is calculated and plotted in Figure 5-11 below. Where each data point is the relationship of hoop strains 1 and 2, the red lines are a confidence interval for the baseline condition and the correlation is shown on the upper left hand side of the plot.

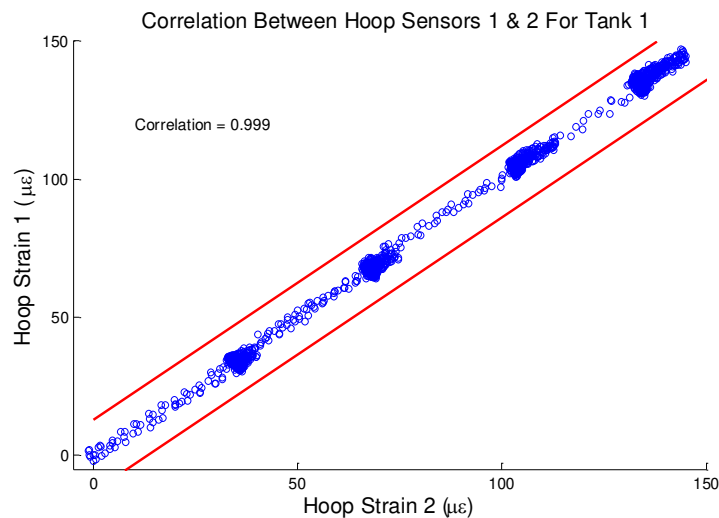


Figure 5:11: Correlation between Hoop Sensors 1 & 2 for Tank 1

Once the baseline plot is populated each of the other tanks will be compared to the baseline and the correlation between both is shown. Figures 5-12 through 5-15 show the results.

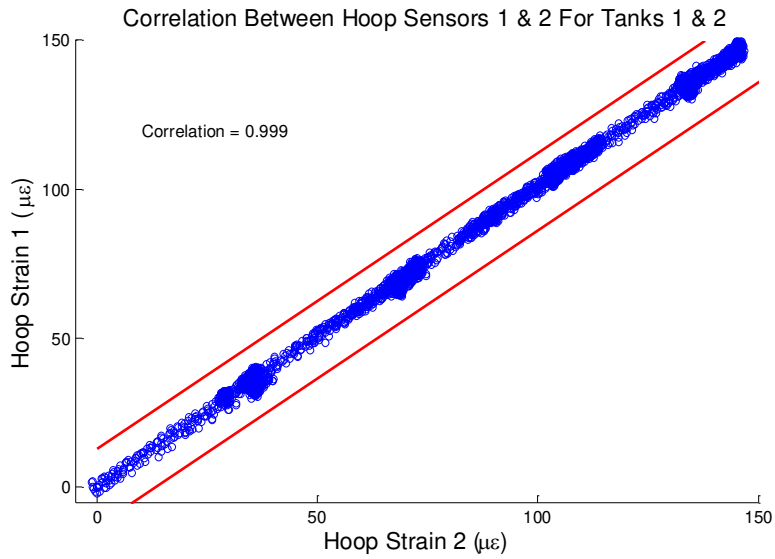


Figure 5:12: Correlation between Hoop Sensors 1 & 2 for Tanks 1 & 2

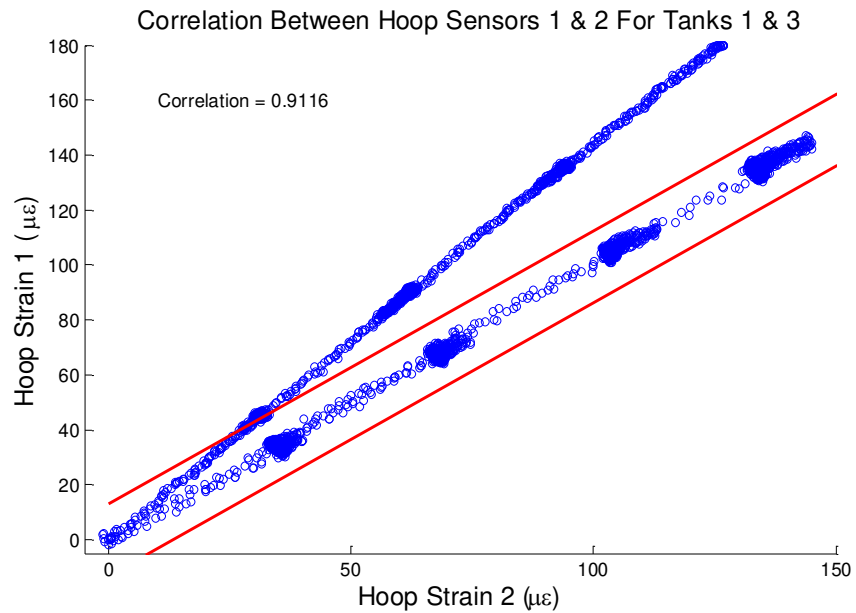


Figure 5:13: Correlation between Hoop Sensors 1 & 2 for Tanks 1 & 3

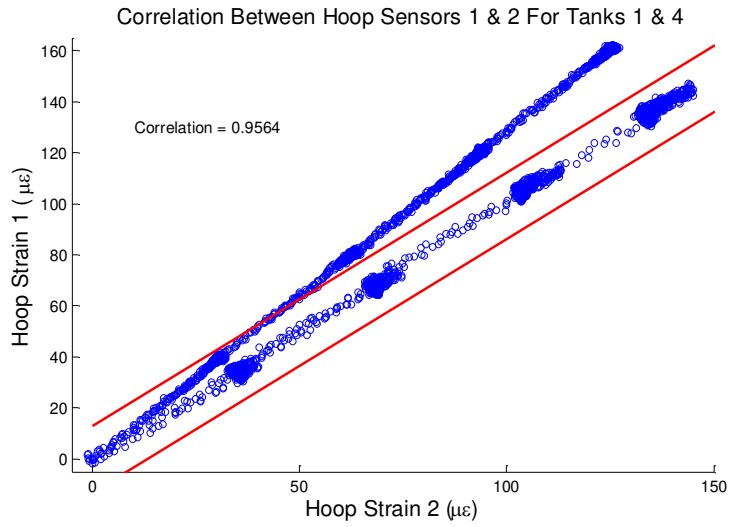


Figure 5:14: Correlation between Hoop Sensors 1 & 2 for Tanks 1 & 4

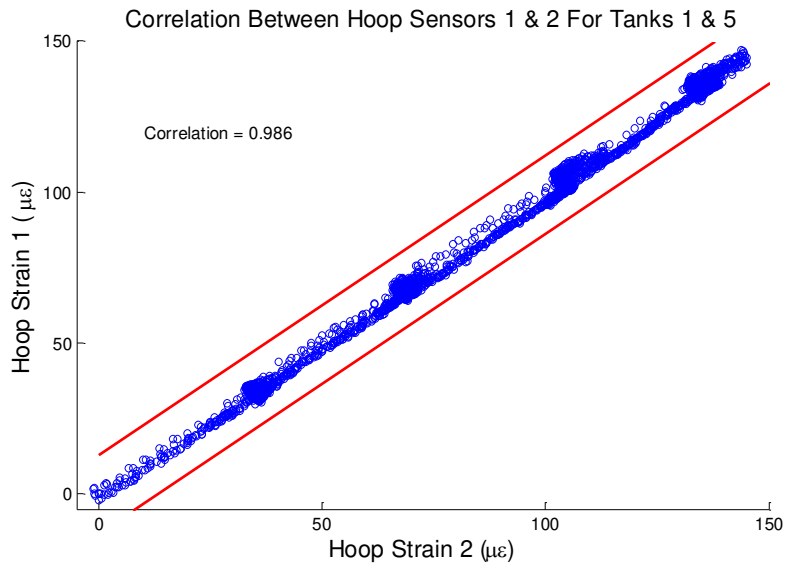


Figure 5:15: Correlation between Hoop Sensors 1 & 2 for Tanks 1 & 5

As seen from the four figures above, each tank shows high correlation of hoop strain data when compared to tank 1. However tanks 2 and 5 are significantly closer than tanks 3 and 4. This makes sense because only tanks 3 and 4 were induced with damage, shown in Table 4-1. This is consistent with the results presented in section 5.1 above. Table 5-3 below shows the correlation of each plot along with the corresponding correlation difference compared with tank 1.

Table 5-3: Correlation between Hoop Sensors 1 & 2 Summary

Tank	Correlation	Difference
1	0.999	0
2	0.999	0
3	0.9116	0.0874
4	0.9564	0.0426
5	0.986	0.013

### **5.3 ARX (Auto-Regressive models with eXogenous outputs) Analysis**

As discussed in Section 3.2, “Time Series Modeling”, many different types of time series models can be generated to analyze data and in this study the ARX Model is implemented. Multiple models are generated for the different types of data sets; pressure versus strain and acceleration. Once the models are created they will be used to compare to the experimental data and will result in the extraction of the Damage Feature (DF). Once the DFs are developed, a threshold will be determined to decide if and how severe damage is.

#### 5.3.1 Pressure and Strain Data

The first step in performing ARX analysis is to create corresponding ARX models to compare predicted results with the experimental values. First the input and output data needs to be

transformed into “iddata”, which was performed using the MatLab built in function “idpoly”. The ARX modeling pressure and strain data, the model will give theoretical hoop strain given an input pressure. For a model as such, single input single output, MatLab built in functions “selstruc” and “arxstruc” were implemented to the best model orders for this system. After using a range of 0 to 50 and baseline data from tank 1 as reference, the model orders for this particular ARX model are 25 and 14 for  $n_a$  and  $n_b$  respectively. The results of the ARX model plotted along with the experimental data are shown on Figures 5-16 through 5-20 below.

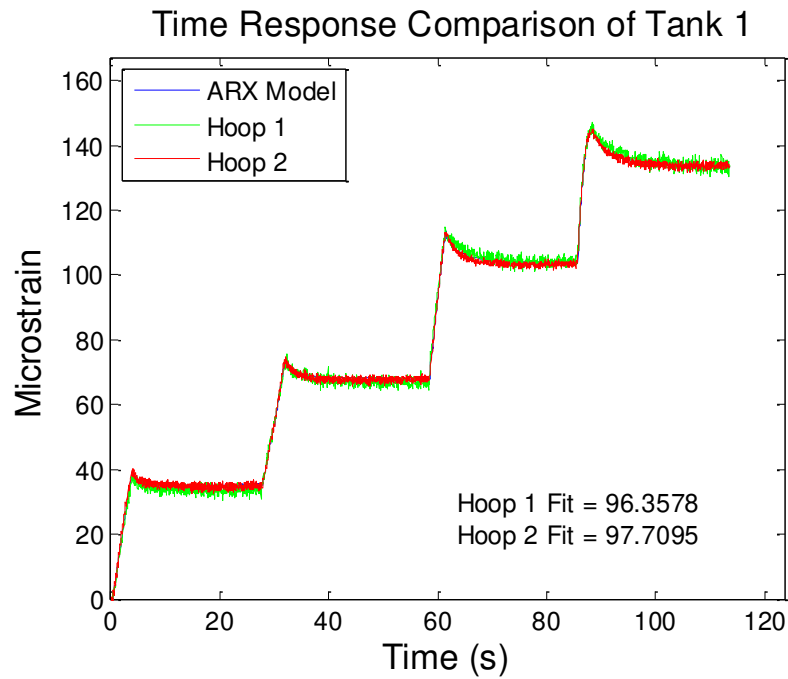


Figure 5:16: Time Response Comparison of Hoop Strain for Tank 1

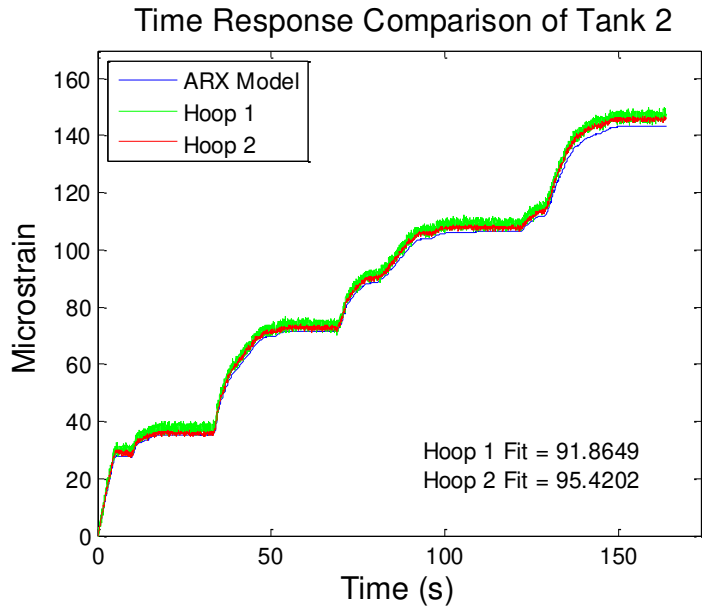


Figure 5:17: Time Response Comparison of Hoop Strain for Tank 2

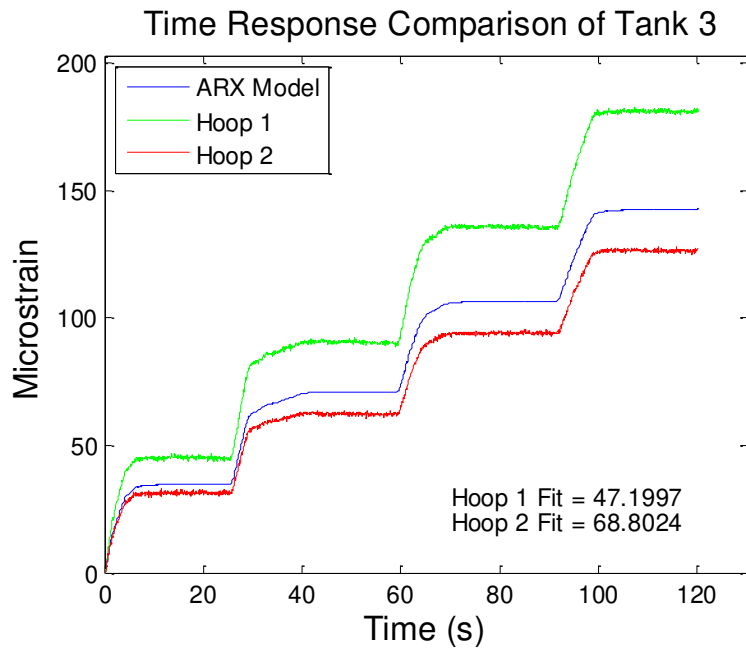


Figure 5:18: Time Response Comparison of Hoop Strain for Tank 3

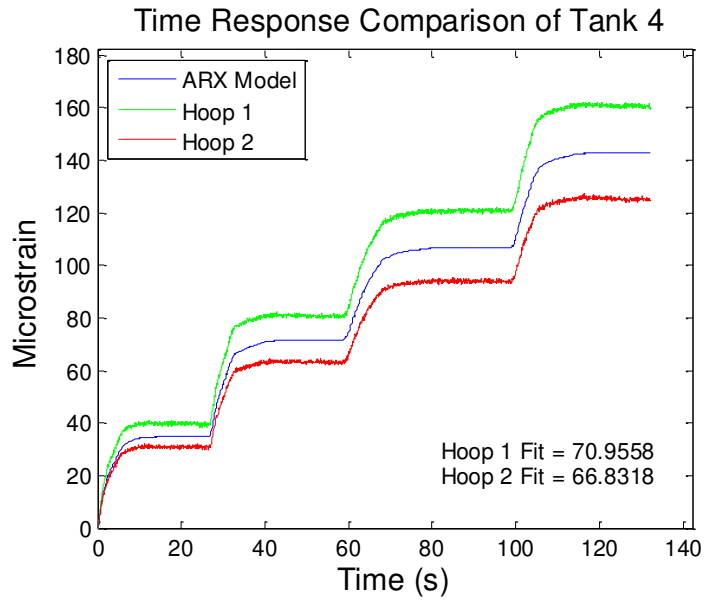


Figure 5:19: Time Response Comparison of Hoop Strain for Tank 4

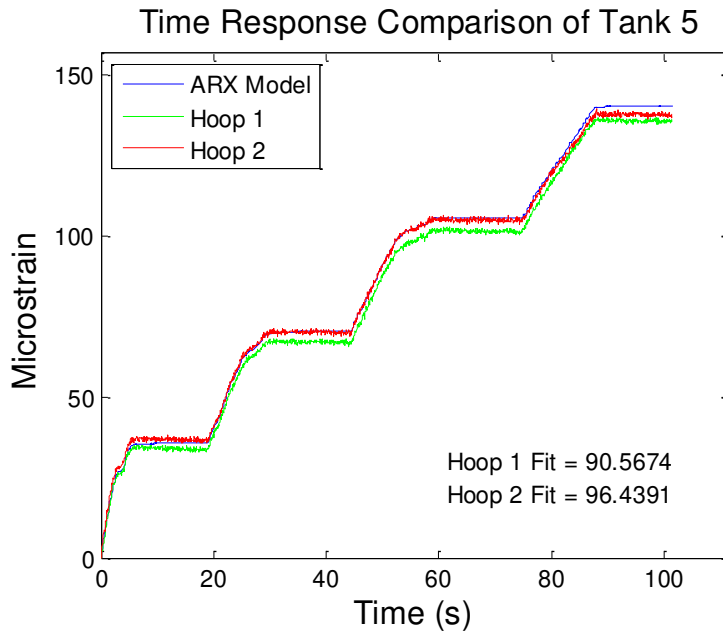


Figure 5:20: Time Response Comparison of Hoop Strain for Tank 5

To determine the damage threshold level, the damage feature (DF) for hoop sensors 1 and 2 were computed for each tank using equation (20) and the methodology in subsection 3.2.3. The DFs for the undamaged tank (tank 2) are shown on Figure 5-21. Noting that all DFs are under 5, this was selected for the threshold and will be used to compare for the remaining tanks.

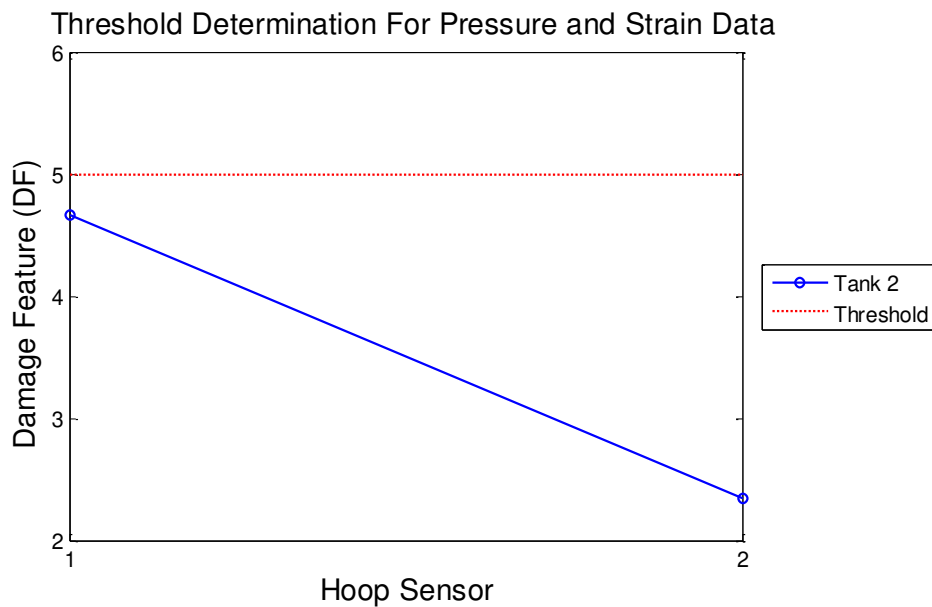


Figure 5:21: Threshold Level for Pressure and Strain Data

Figure 5-22 shows all the DFs for the tanks of interest. The plot shows that tank 3 has the most damage followed by tank 4. Furthermore tank 5 borders the threshold line and therefore damage cannot be confidently detected, however there are some inconsistencies.

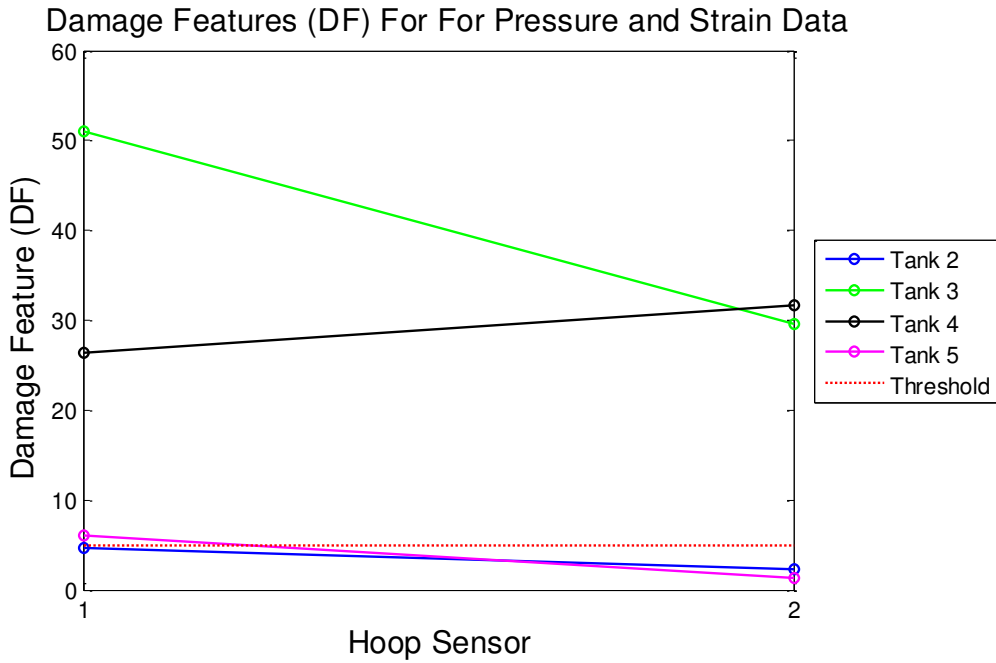


Figure 5:22: DF Tend Plot for Pressure and Strain Data

### 5.3.2 Acceleration Data

Similar to the previous subsection 5.3.1, the raw data was converted to “iddata”. Also the raw data was preprocessed removing the initial impact of the excitation hammer, shown in Figure 4-19. The ARX model in this subsection will use the acceleration data collected in section 4.3. Three ARX models were created using output only data relating to the sensor clusters shown in Table 5-4 below.

Table 5-4: Inputs and Outputs of the ARX Models

Sensor Cluster	Output of the ARX Model (Reference Channel)	Inputs of the ARX Model (Adjacent Channels)
1	N1	N1, N2, N3
2	N2	N1, N2, N3
3	N3	N1, N2, N3

The model order,  $n_a$ , of the Baseline ARX models corresponds to the input term and was set to 1. The model order,  $n_b$ , and was determined through an iterative process. Model orders of  $n_b=20, 30, 40, 50$ , and  $70$  were all investigated. However, a model order of  $n_b=50$  was selected due to optimization between high fit ratios and processing time. This model order was used to develop all Baseline ARX models in subsection 5.3.2. Sample results from tanks 1 and 5 of the first ARX model are plotted along with the experimental data; they can be seen on Figures 5-23 and 5-25 below. Furthermore a more closely look of each plot can be seen on Figures 5-24 and 5-26.

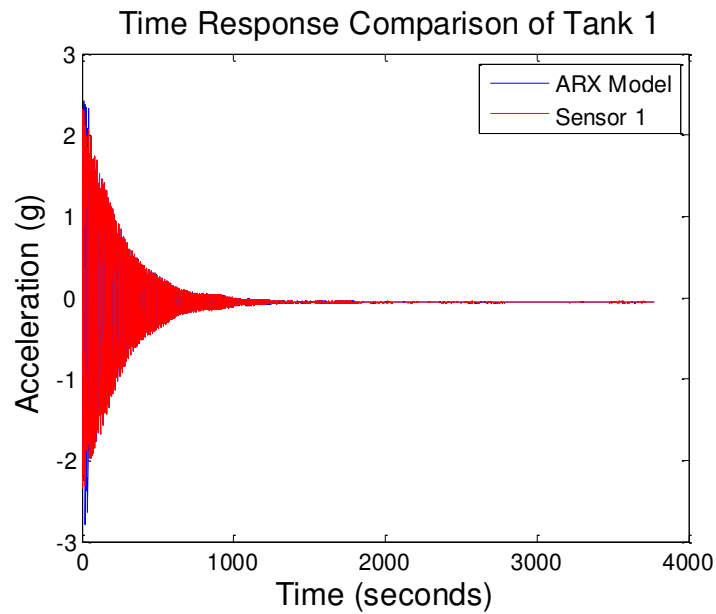


Figure 5:23: Time Response Comparison of the Acceleration Data for Tank 1

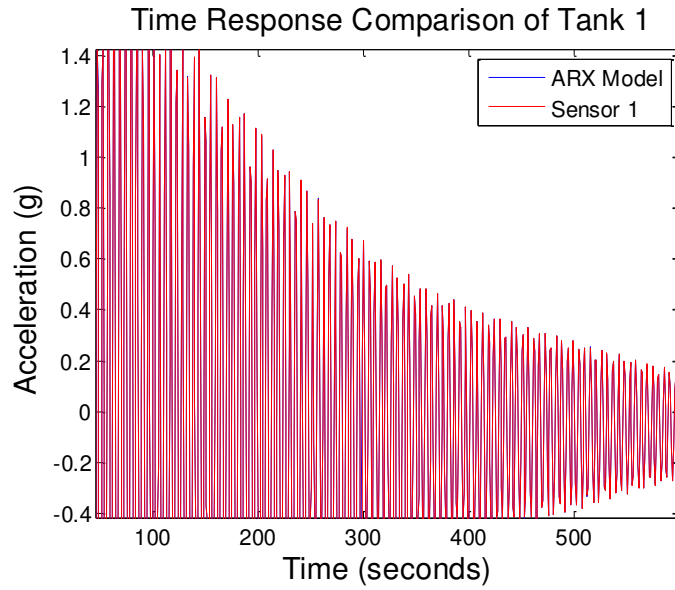


Figure 5:24: Zoomed in View of the Time Response Comparison of the Acceleration Data for Tank 1

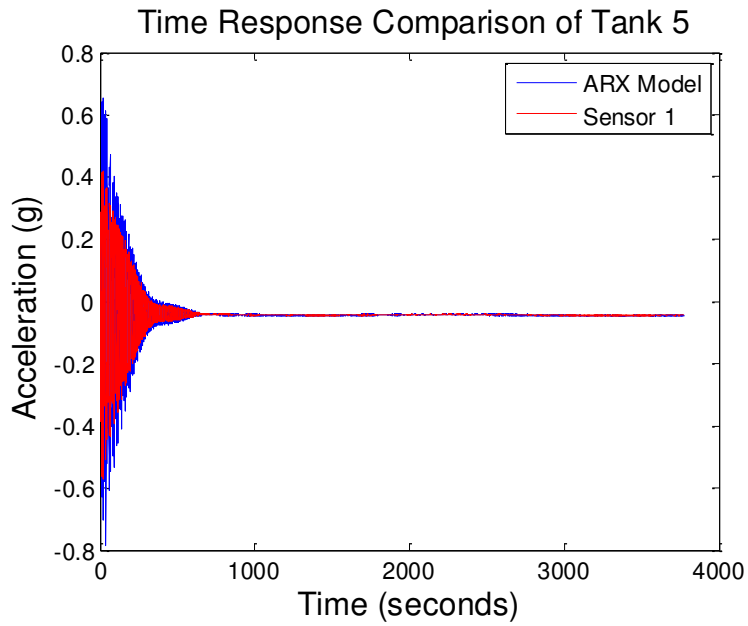


Figure 5:25: Time Response Comparison of the Acceleration Data for Tank 5

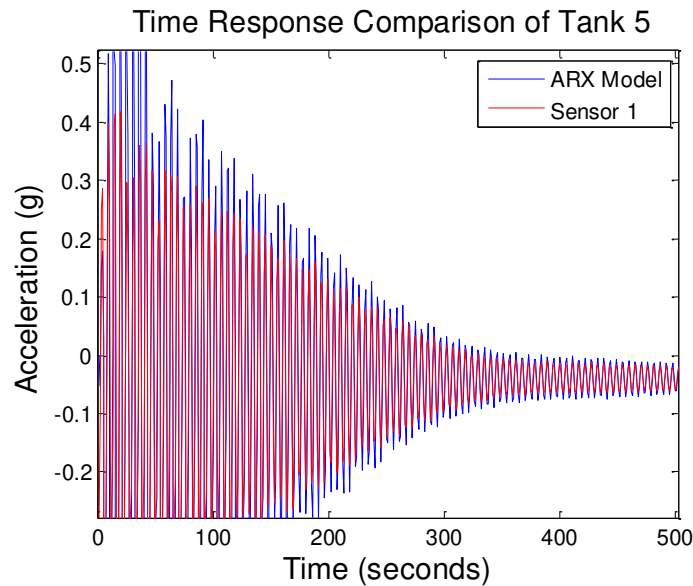


Figure 5:26: Zoomed in View of the Time Response Comparison of the Acceleration Data for Tank 5

Comparing Figure 5-24 and 5-26 it can be seen that tank 1 (Figure 5-24) shows a much closer relationship between the ARX model and the experimental data than tank 5 (Figure 5-26). The fit ratios for all the tanks at each location and for each ARX model are presented in Tables 5-5 through 5-8 below.

Table 5-5: ARX Model 1 Fit Ratio

Tank	Position 1	Position 2	Position 3
1	99.43	99.32	99.43
2	94.22	95.59	94.87
3	84.53	88.41	85.46
4	79.01	83.63	72.69
5	64.19	72.87	65.09

Table 5-6: ARX Model 2 Fit Ratio

Tank	Position 1	Position 2	Position 3
1	99.66	99.38	99.62
2	93.11	97.55	97.17
3	92.02	94.68	91.46
4	85.85	74.37	81.55
5	68.8	73.8	75.47

Table 5-7: ARX Model 3 Fit Ratio

Tank	Position 1	Position 2	Position 3
1	99.71	99.24	99.73
2	94.44	97.13	98.41
3	92.03	91.34	91.01
4	78.12	82.43	70.49
5	72.05	73.82	71.79

Similarly to subsection 5.3.1, the damage threshold level corresponding to the damage feature (DF) computed for each tank using equation (20) was calculated. The DFs of each ARX

model for the undamaged tank (tank 2) are shown on Figure 5-27. Noting that all DFs are under 7, this was selected for the threshold and will be used to compare for the remaining tanks.

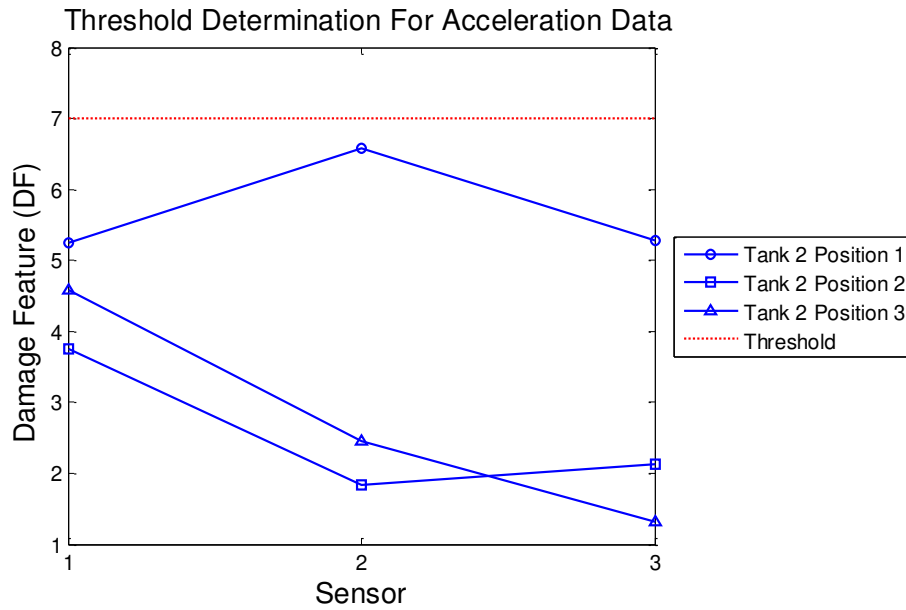


Figure 5:27: Threshold Level for Acceleration Data

Figure 5-28 shows all the DFs for the tanks of interest. The plot shows that tank 5 has the most damage followed by tank 4. Furthermore tank 3 borders the threshold line and therefore damage cannot be confidently detected, however there are some inconsistencies.

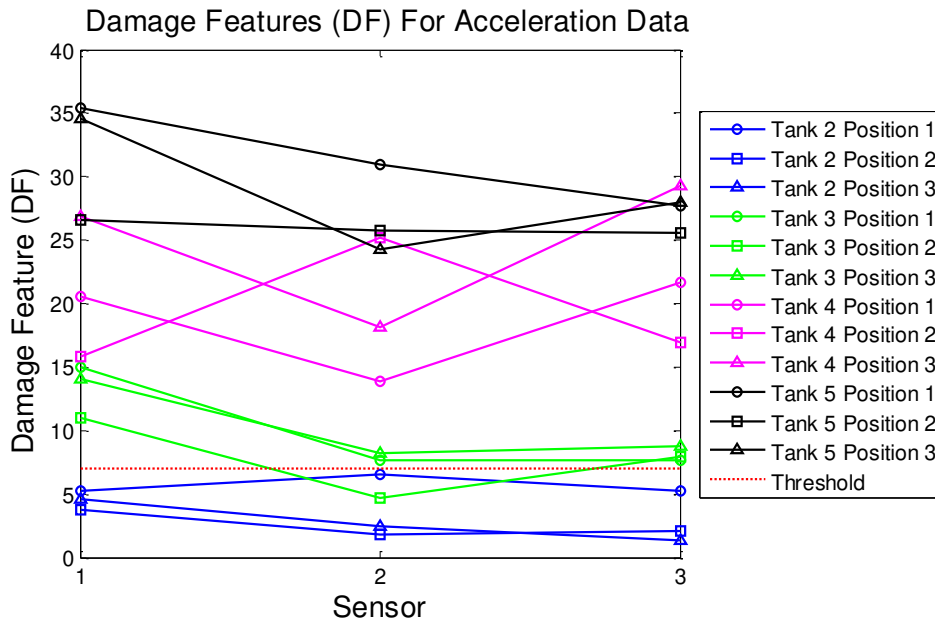


Figure 5:28: DF Tend Plot for Acceleration Data

### 5.4 Summary of COPV Results

Table 5-8 below shows the results of all the different methodologies studied in this chapter. Each method was able to detect certain changes within the different tanks. And obviously the most accurate and complete form of health monitoring would be to apply all of them if not more. In the Table the darker the color indicates more damaged detected. All of the results are consistent with the anticipated outcomes of the specimens.

Table 5-8: Summary of Results from Various Data Analysis Methodologies

Method Tank	Statistical Analysis		Cross Correlation Analysis	ARX Models	
	Hoop v Axial	Hoop 1 v Hoop 2		Pressure & Strain	Acceleration
1					
2					
3					
4					
5					

Based on the thin walled pressure vessel theory well-defined in mechanics of materials theory, there is a relationship between the hoop and axial stressed. Hoop-to-axial strain response (also eliminating the need to use input/pressure) data were generated. Histograms of these data sets for each tank were plotted. Theoretically, the ratio should be around 2.00 with slight variations for undamaged and well-manufactured COPVs. It was seen this ratio was very close to 2.00 for Tanks 1, 2 and 5 with 4-6% error with respect to the theoretical 2.00 ratio. For Tanks 3 and 4, the ratio were found to be 2.42 (21% error) and 2.31 (15% error), clearly indicating the damage and variation from an undamaged tank behavior.

In addition to hoop-to-axial ratio, hoop 1 -to- hoop 2 response data (for two different locations) were also analyzed (also eliminating the need to use input/pressure). Theoretically, the ratio should be around 1.00 with slight variations for undamaged and well-manufactured COPVs. It was seen this ratio was very close to 1.00 for Tanks 1, 2 and 5 with 1-4 % error with respect to the theoretical

1.00 ratio. For Tanks 3 and 4, the ratio were found to be 1.44 (44% error) and 1.28 (28% error), clearly indicating the damage and variation from an undamaged tank behavior.

The cross-correlation of hoop 1 -to- hoop 2 response data were analyzed and compared with respect to the Tank 1 which is showing almost perfect correlation (0.999%) for different sensors. For Tanks 1, 2 and 5, the correlation were found to be between 0.999 to 0.986 with about 1% error with respect to Tank 1's 0.999 correlation. Tanks 3 and 4 correlation was 0.912 and 0.956, which is indicating high correlation, however, less than the other tanks.

Damage Features using Auto-Regressive models with eXogenous outputs (ARX) Analysis was first implemented using the pressure input and strain responses. ARX models were established and then compared with the measured data. From there, the Damage Feature (DF) was identified based on the established threshold limits. It was observed that the deviation of the DF from the threshold was much higher for Tanks 3 and 4 while others were below the threshold level.

Damage Features using Auto-Regressive models with eXogenous outputs (ARX) Analysis was then implemented using the acceleration responses without using the input data. In this case, the input was considered as all response measurement for a given response data. This approach was well-documented by Dr. Catbas' previous publications. This approach also indicated that the deviation of the DF from the threshold was much higher for Tanks 3 and 4, however, it was also observed that Tank 5 indicated (false positive) values above the threshold level. The false positive was probably detected due to the difference in material, with the zebra pattern, addition of zylon material, the mass and stiffness of the COPV is noticeably different and therefore damage was detected.

A number of experimental technologies, algorithms and damage features were presented building up a collection of various methodologies. A composite index or a table such as the one given in Table 5-8 can be utilized for better decision making.

## **CHAPTER 6: TESTING AND MONITORING STUDIES OF THE ARFL TANK IN THE FIELD**

The University of Central Florida was brought on to assist in the Structural Health Monitoring (SHM) process of the Air Force Research Lab (AFRL) composite tank (Figure 6-1), which was instrumented and tested to failure in the summer of 2013. The experiment consist of two test; one 7 psi pretest, held at the Kennedy Space Center, and one rupture test held at the Marshall Space Flight Center. The university has a custom, in-house built Fiber Optic Sensor (FOS) system which was previously used on laboratory experiments as well as in the field test. The system continually proves to produce successful results in measuring strain, detecting damage, and in finding dynamic properties of various structures. The system was chosen due to its many advantages such as; a high sampling rate, portably of the system, susceptibility to moist/wet conditions, capability of measuring multiple parameters (wavelength, strain, temperature) and the ability to detect damage and dynamic characteristics. With that being said, the objectives of this study are to better understand capabilities of the Fiber Optic System, especially in cryogenic conditions, and to further understand the behavior and characteristics of composite pressure vessels.



Figure 6:1: AFRL Tank in NASA's Clamshell Structure

## **6.1 Fiber Bragg Grating (Fbg) Monitoring System**

### 6.1.1 Fiber Optic Sensors (FOS)

For quite a few decades, electrical based sensors have sat on top of sensor technology for measuring different types of phenomena. However, there were several deficiencies associated with electrical sensors such as being sensitive to electrical noise, heavy cabling labor etc. Conversely,

FOS technology overcomes most of these encounters by replacing electricity with light and copper wire with optical fiber. The use of FOS for SHM has increased tremendously over the last decade due to aforementioned advantages brought by these types of sensors. FBG sensors, which are point sensors, are among the most widely used FOS. The basic working principles of FOS and FBG sensors are reflection and filtration of different wavelengths of light (Kersey et al. 1997). For FBG sensors, grating property enables the optical fiber to transmit the entire wavelength except the particular reflected wavelength entitled as grating process. A brief introduction to theory of the optical fiber is presented in the following section (Malekzadeh et al. 2012).

FBG consist of article interrogator launching infrared light down the core of an optical fiber. As white color, broadband light, travels down the fiber it passes through grating segment, also identified as FBG, which is a series of article filters. They can filter certain wavelength or color while letting others pass through. This is happening by periodically altering the refractive index of fiber dictating which wavelengths pass and which get reflected. External factor such as heat and vibration will cause a shift in the wavelength of the reflected light (Catbas et al. 2014). These variations can then translate into physical engineering units such as amplitude, temperature and strain. The principal sensing technology of FBG is illustrated in Figure 6-2 below.

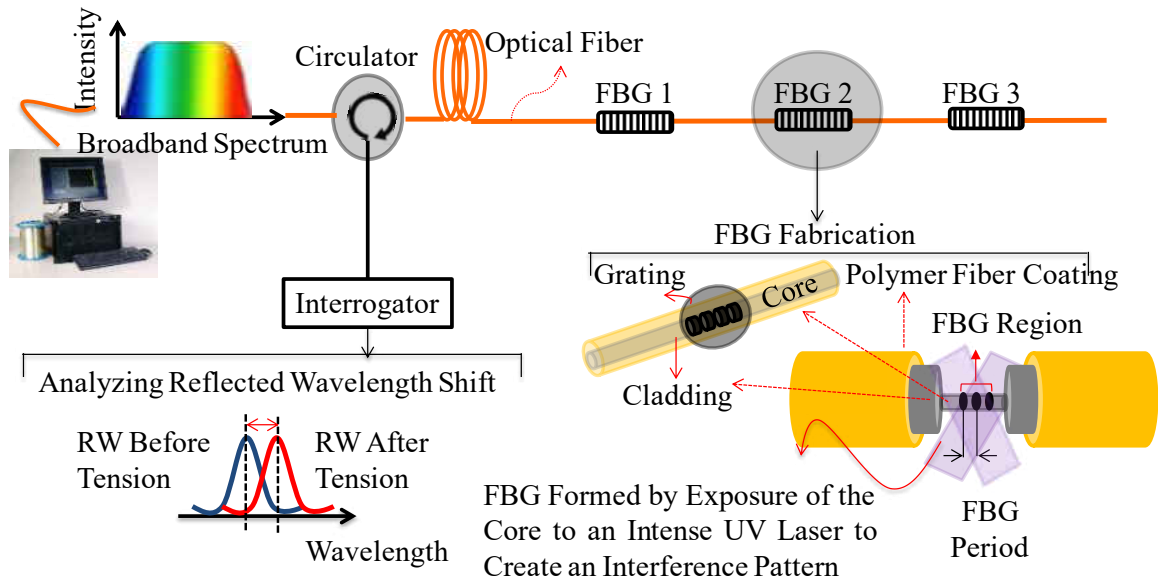


Figure 6:2: Fundamental Concepts of Fiber Optic Technology (adapted from Malekzadeh & Catbas 2014)

### 6.1.2 In-House Developed FBG System

The characteristic information of this FBG system is revealed in this section. The designed system consists of three main components including power source, interrogator and circulator. Each of these components has an individual operating characteristic, which has to be carefully considered. The power source as a first component needs a voltage of about 5V and 0.4-0.5A to assure that the light source can perform properly. The minilite light source (ASE source) has a wavelength range of 800-1650nm while having a spectral width of 100nm and an output power up to 30 mW.

The light source can operate in the temperature between 10-70 degrees Celsius. Finally, the most important part of the FBG system is the FBG interrogator. The FBG interrogator, which is used for this system, has the wavelength range of 1525-1565 nm, while the resolution is about

1 pm. The operating frequency of the system is around 5 kHz and interface with USB. The interrogator is operating in the temperature range of 0-70 Celsius. The last component of the system is the circulator.

The circulator is in charge of separating the reflected light and directing it to the FBG interrogator. Eventually the data is sent from the interrogator to the computer for further processing. The In-house developed FBG system and all the individual components are exhibited in the Figure 6-3.



Figure 6:3: UCF In-House Developed FBG System

The calibration and verification studies on this FOS system were presented in a separate paper (Kwon et al. 2011).

### 6.1.3 Installation of Sensors

For the AFRL Test UCF used seven arrays of fibers consisting of 15 FBG sensors. The orientation, type, and wavelength of sensors can be seen in Figure 6-4. The wavelengths of the individual sensors were chosen carefully. Each sensor corresponds to a unique wavelength and all the wavelengths are within the range of our system's interrogator. Also groups of sensors were chosen to be in arrays for easier installation and use.

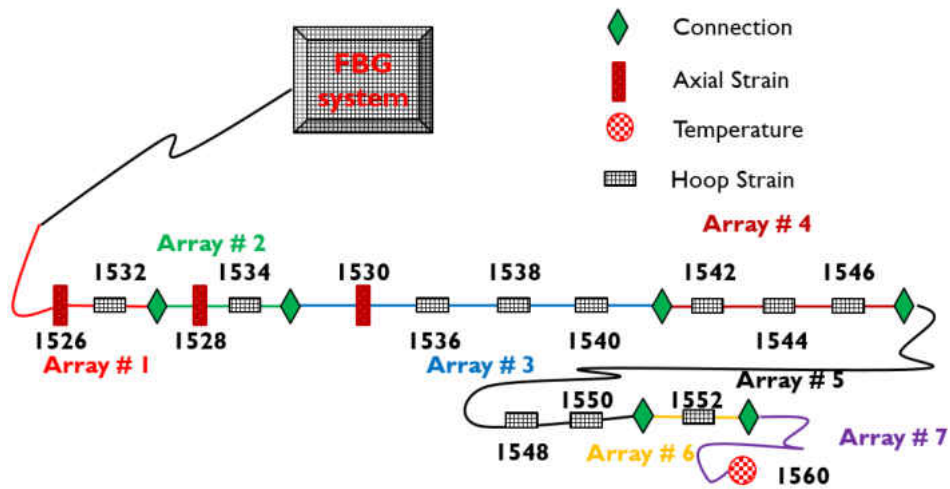


Figure 6:4: FBG Sensor Type and Orientation

In order to install the Fiber Optic Sensors a simply but delicate procedure was followed. First apply marking on the tank surface to show the location and orientation of the sensors. Then clean surface with acetone. Remove tape from back of sensor and apply adhesive side to the surface. Mix and prep AE-10 epoxy (FBG standard). Inject epoxy into sensor and let dry, shown in Figures 6-5 and 6-6.



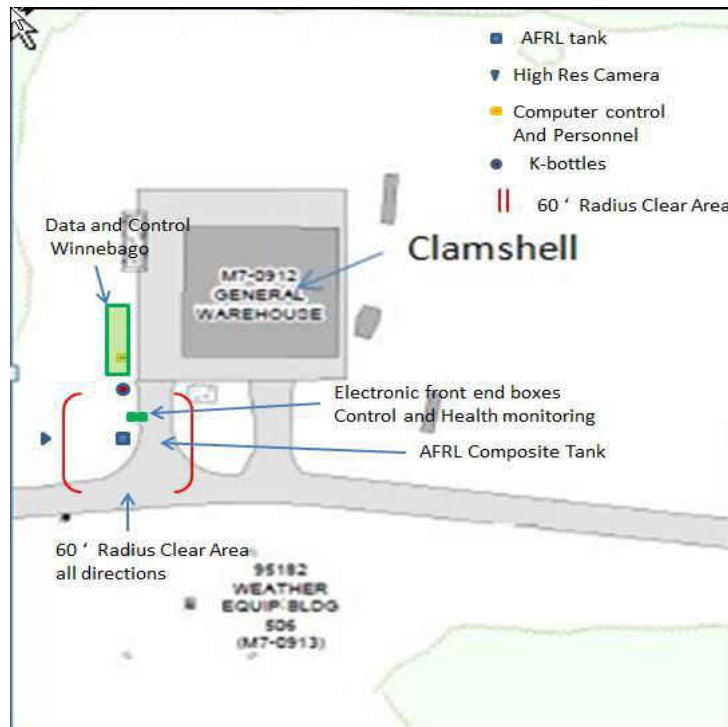
Figure 6:5: Mixing AE-10 Epoxy



Figure 6:6: Installed FBG Sensor

## 6.2 7 PSI Test Field Test at NASA's Kennedy Space Center (KSC)

The 7 psig checkout was accomplished at Kennedy Space Center (KSC) in July 2013 to verify operation, assemble and test the control and data systems required for a safe test using the much higher pressures and liquid nitrogen at MSFC test to failure site. Ambient Temperature Nitrogen and Helium were used, to verify remote valve sealing. The 7 psi limit was for Safety constraints at the Clamshell test area. The plan layout for this this at KSC is shown in Figure 6-6 below.



MSFC, Figure 6:7: KSC Near Clamshell AFRL Checkout Test Area systems.

The test configuration was basically the same with improvements that was used for the AFRL the liquid nitrogen Pressure steps to Failure testing at MSFC but with all the Health monitoring technology integrated at the MSFC test site.

From the experiment unfortunately MSFC was unable to record any strain data during the test. Rudy and his team from KSC was able to record strain data on all of their 12 gages located at different locations and orientations along the tank. And our team from UCF had a break in our fiber optic line; which would not allow us to collect data from our last 5 sensors. Therefore only our first 10 were able to record data during the test.

### 6.2.1 Preliminary Test Results

The FBG sensors from UCF that were working during the test can be seen as:

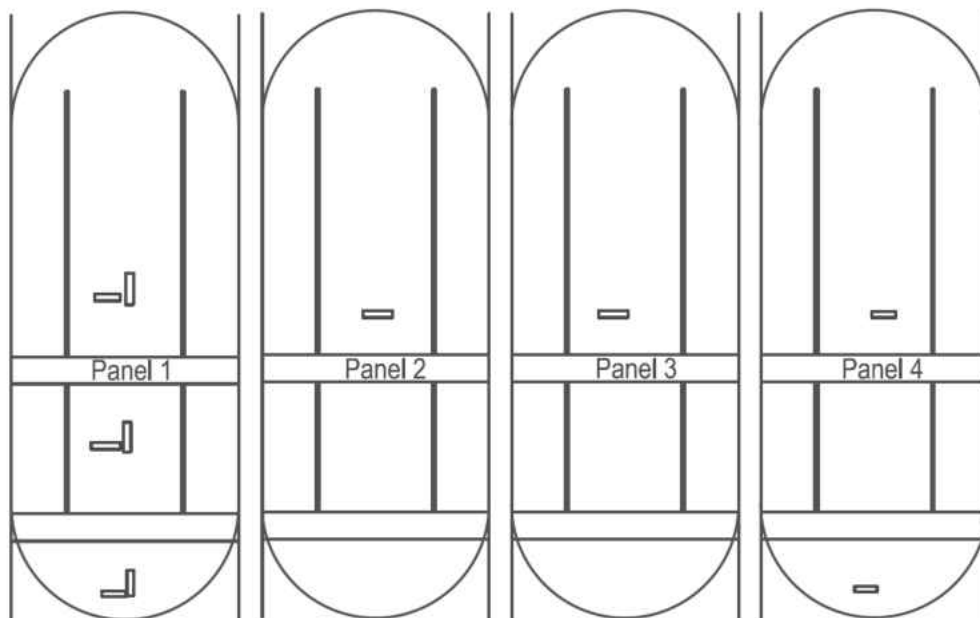


Figure 6:8: UCF FBG Sensors

The sensors are all FBG strain sensors. They are in series with each other flowing from the bottom to the top of each panel and then flowing to the next panel in cranial order. There

are 10 sensors, three in the axial direction and 7 in the hoop. The following figures will explain show the findings:

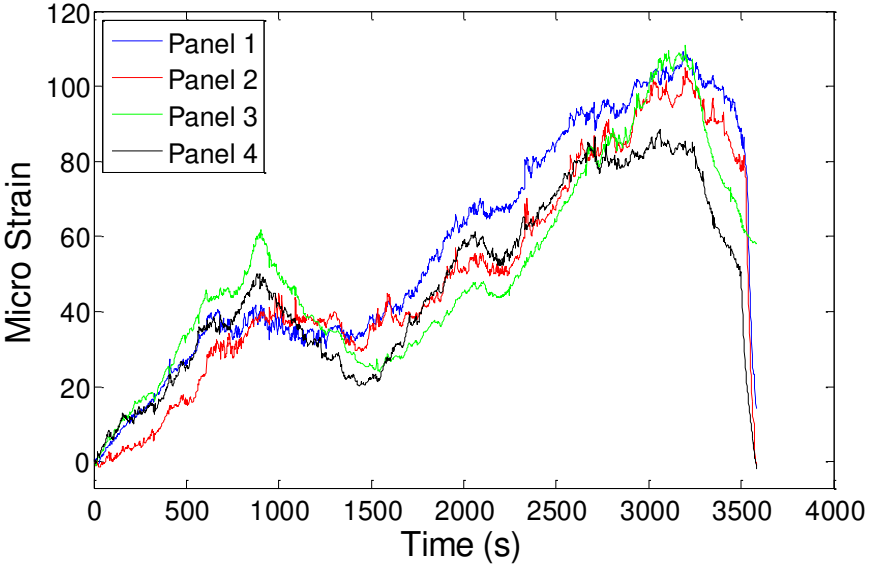
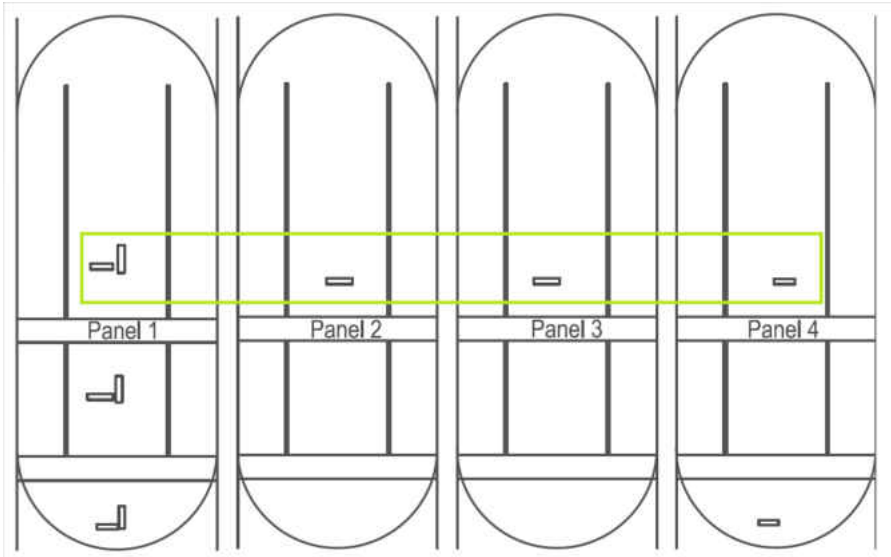


Figure 6:9: Strain in the Hoop Direction at the Mid-Section of the Panels

Figure 6-9 shows the overall run of the experiment. The graph shows all of the hoop strains in the mid-section of the panels. The figure shows similar strains in each panel; with panel one having the largest magnitude of strain and therefore appears to be the weakest.

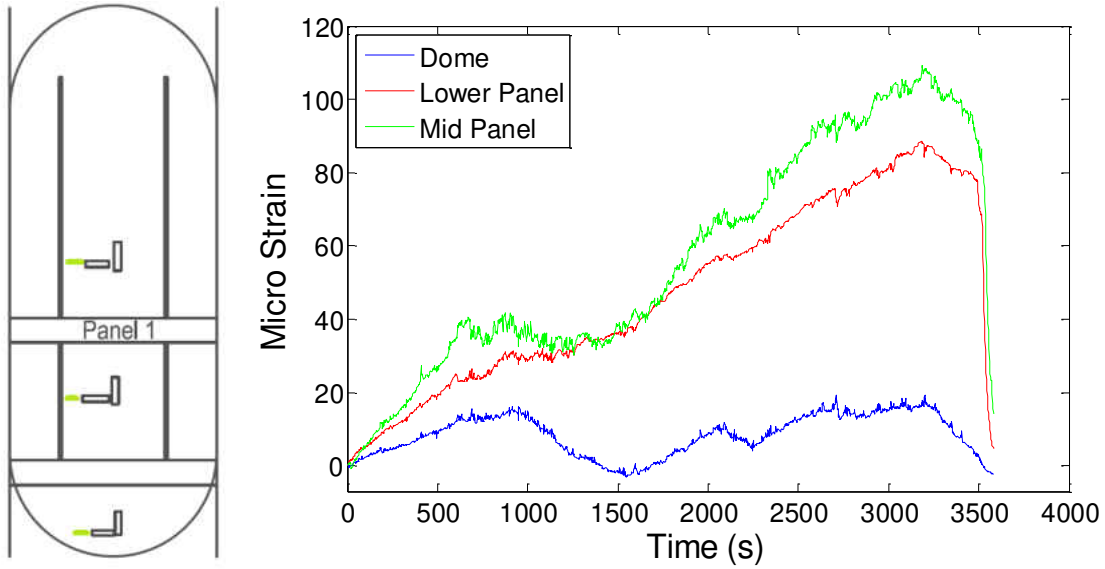


Figure 6:10: Strain in the Hoop Direction of the First Panel

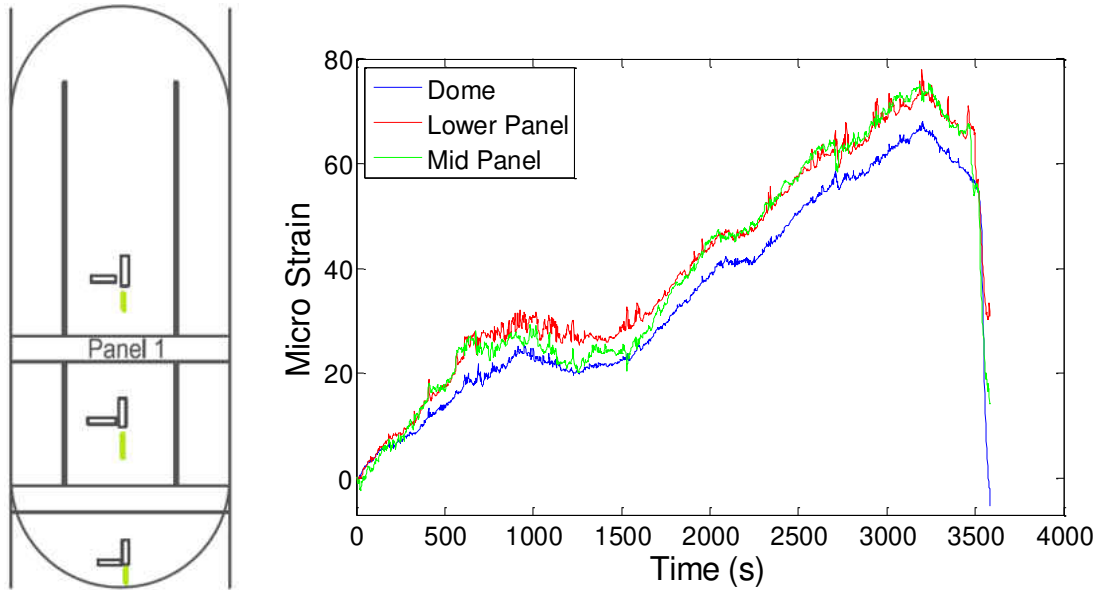


Figure 6:11: Strain in the Axial Direction of the First Panel

The graphs show the hoop (Figure 6-10) and axial (Figure 6-11) strains in the first panel. The hoop strain in the lower and middle panel show a strong correlation with the mid panel larger in magnitude. The hoop strain in the dome has corresponding peaks and valleys but is significantly smaller in value. While the axial strain in all sections appear to be consistent with each other. The middle and lower panels are nearly identical with the dome section slightly smaller in magnitude.

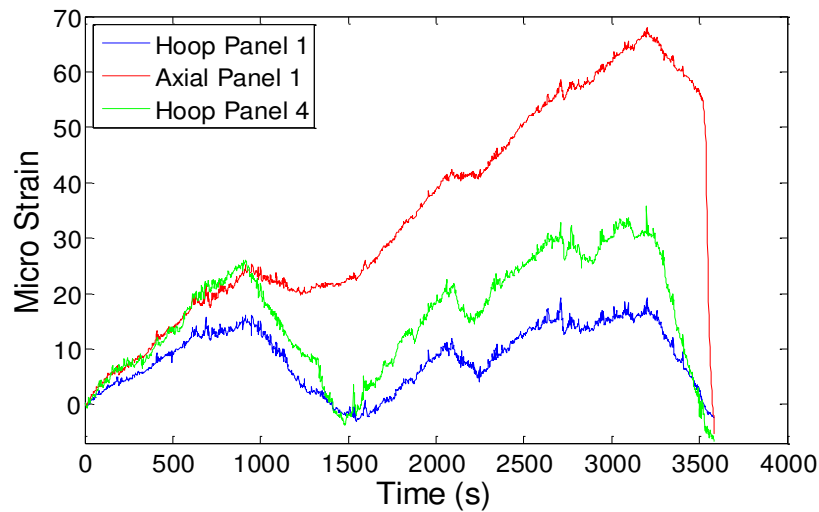
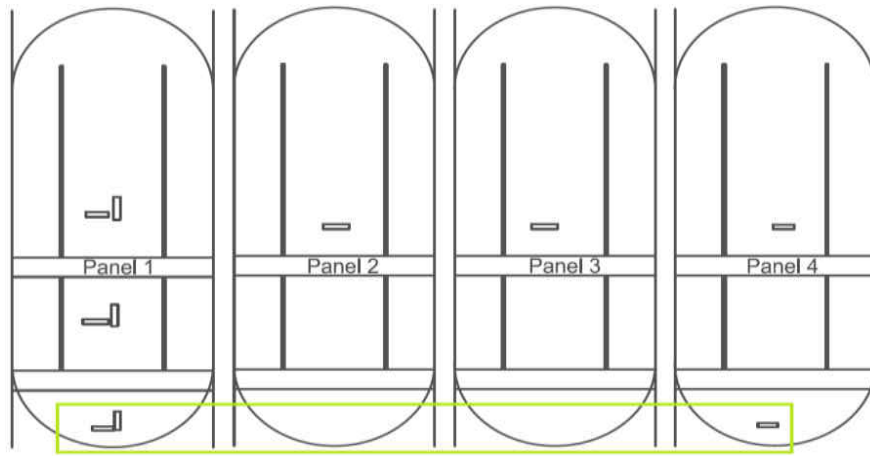


Figure 6:12: Strain in Dome Portion of the Tank

The graph (Figure 6-12) shows all of the sensors in the dome section of the tank. The hoop strains are consistent with each other but don't show significant strain compared to the other sensors on the tank. The axial strain appears similar in value to other strain values along the tank but is significantly larger than the hoop strain in the dome; and does not show the 2-1 hoop v axial relationship. This is due to the geometry of the dome, not being ideally cylindrical.

The strain gages from KSC are shown as:

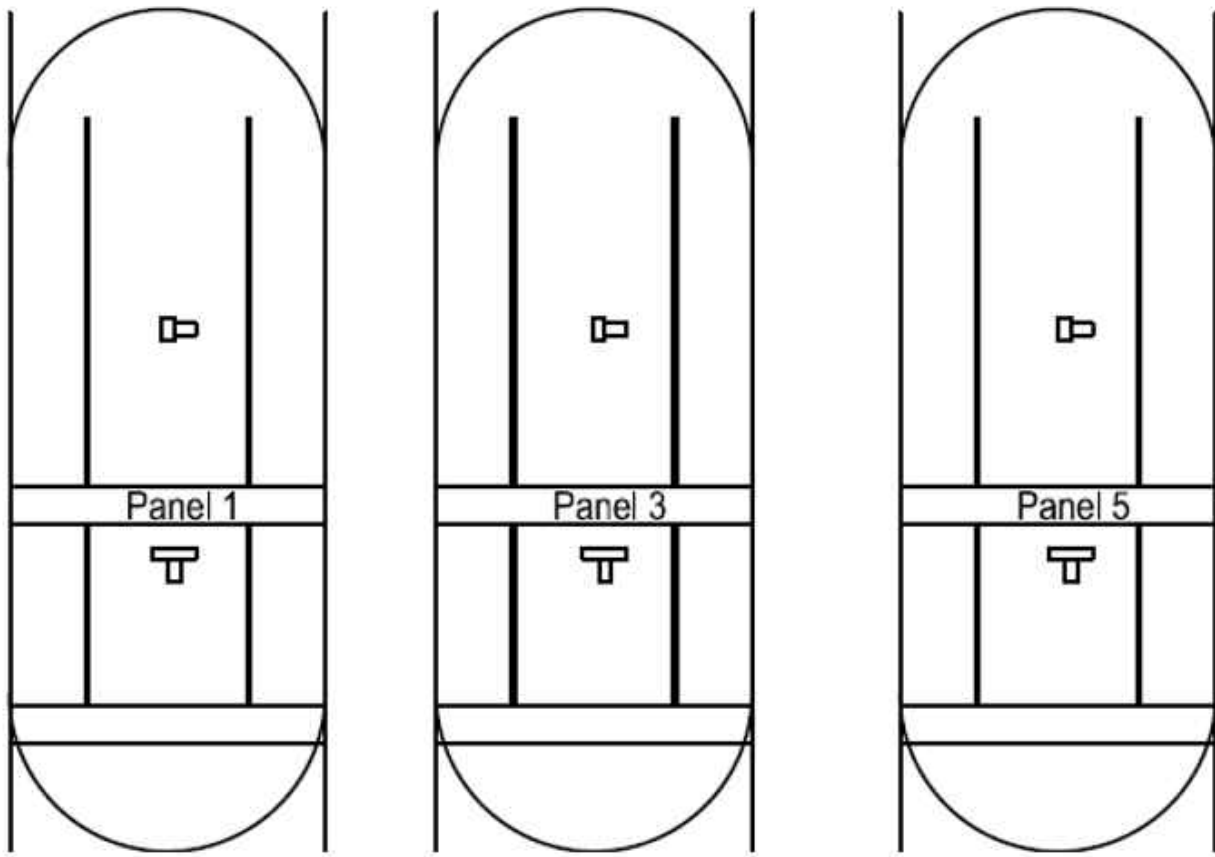


Figure 6:13: KSC Instrumentation Plan

Figure 6-13 shows the 12 strain sensors used and their locations on each panel. There are 4 sensors per panel. Two sensors in each panel section oriented in opposite directions (Hoop and Axial). However the first panel will be examined the most due to the fact it appears to be the weakest and also is the most instrumented panel by the UCF team.

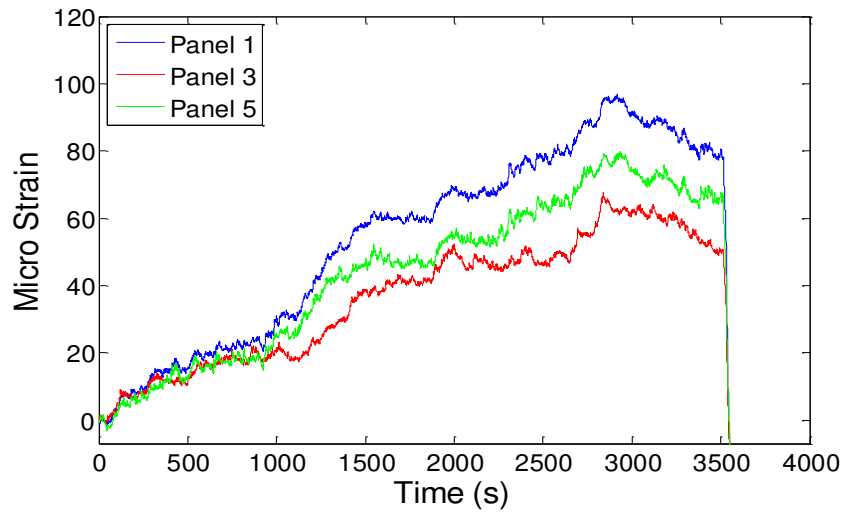
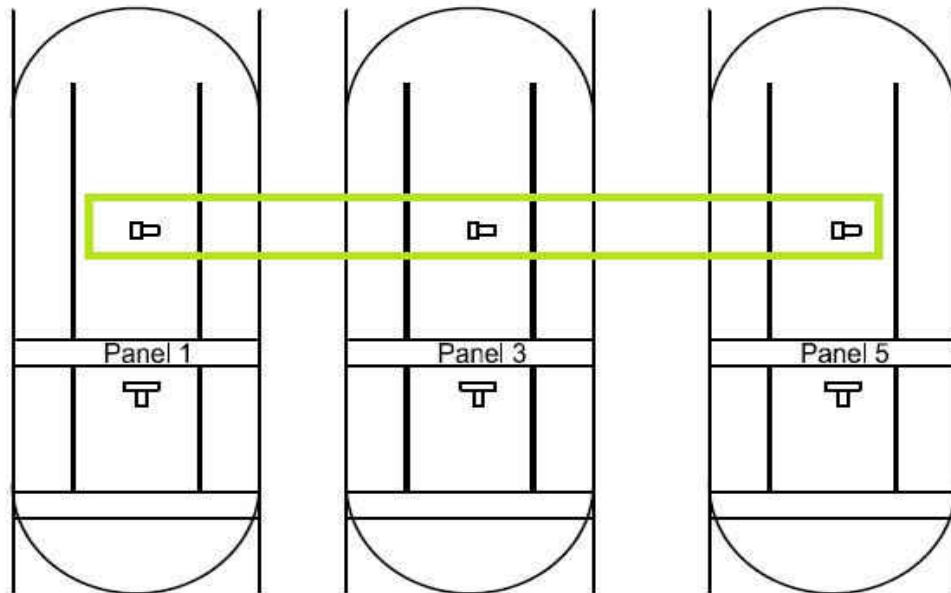


Figure 6:14: Strain in the Hoop Direction at the Mid-Section of the Panels

Figure 6-14 shows all of the hoop strains in the mid-section of the panels. The figure shows similar strains in each panel; with panel one having the largest magnitude of strain, followed by panels five and three respectively, and therefore appears to be the weakest. These results are consistent with the UCF's sensors.

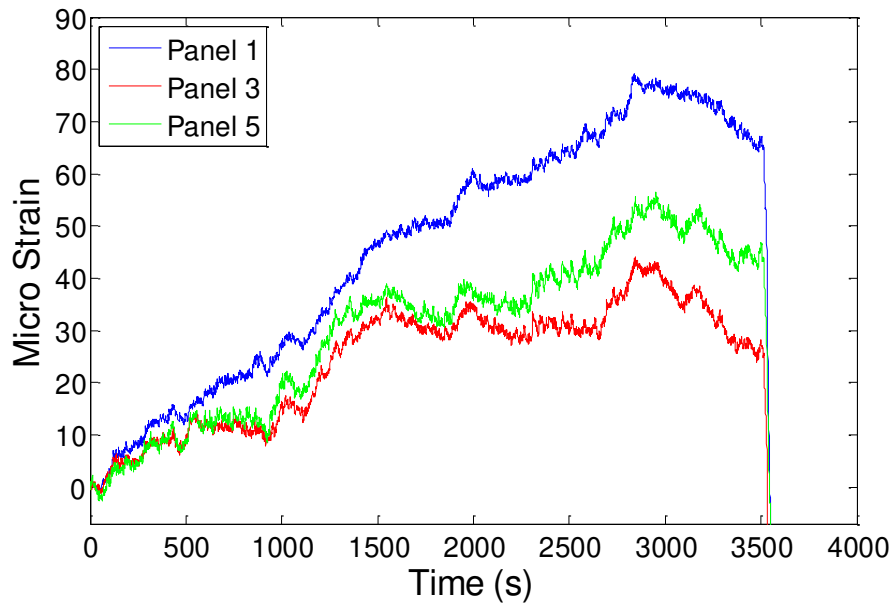
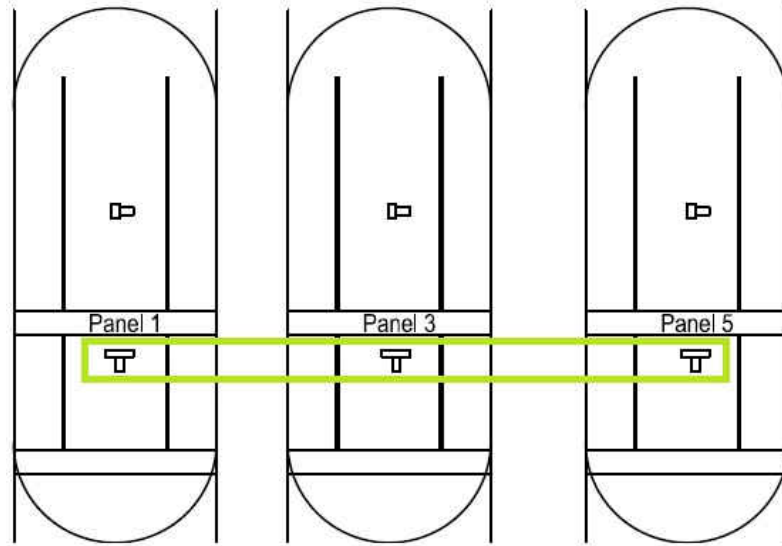


Figure 6:15: Strain in the Hoop Direction at the Lower Section of the Panels

Figure 6-15 shows all of the hoop strains in the lower-section of the panels. The figure shows similar strains in each panel; with panel one having the largest magnitude followed by

panels five and three respectively. Also the strain is slightly lower in the lower section compared to the mid-section. These results are consistent with the mid-section as well as UCF's sensors.

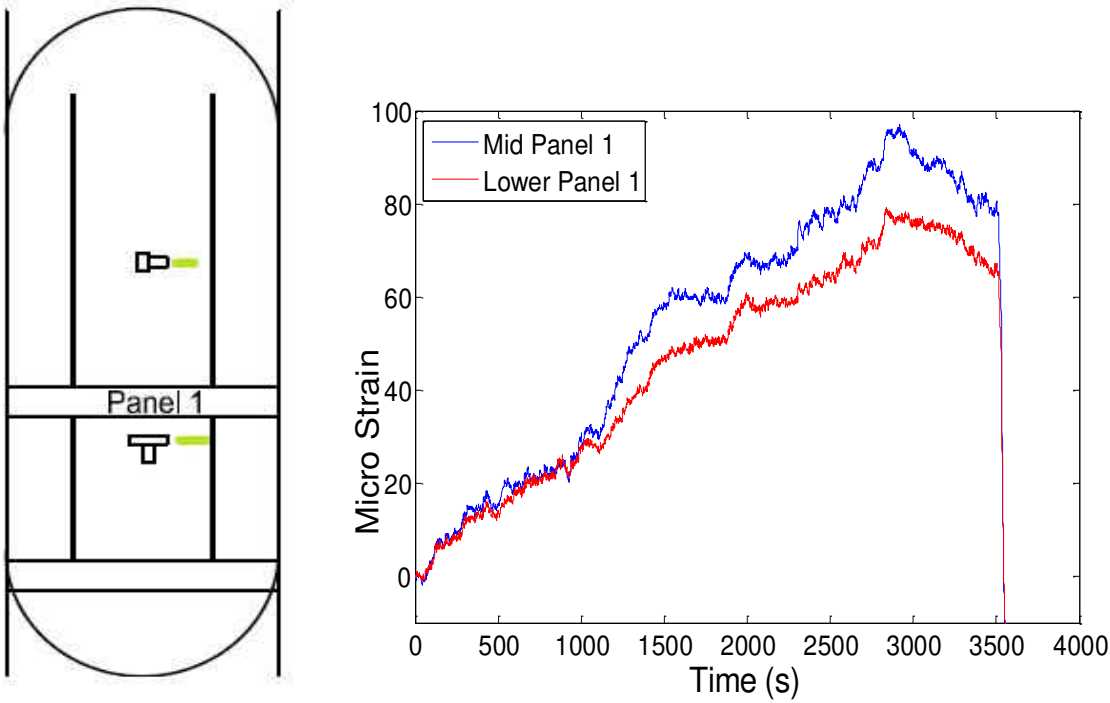


Figure 6:16: Strain in the Hoop Direction of the First Panel

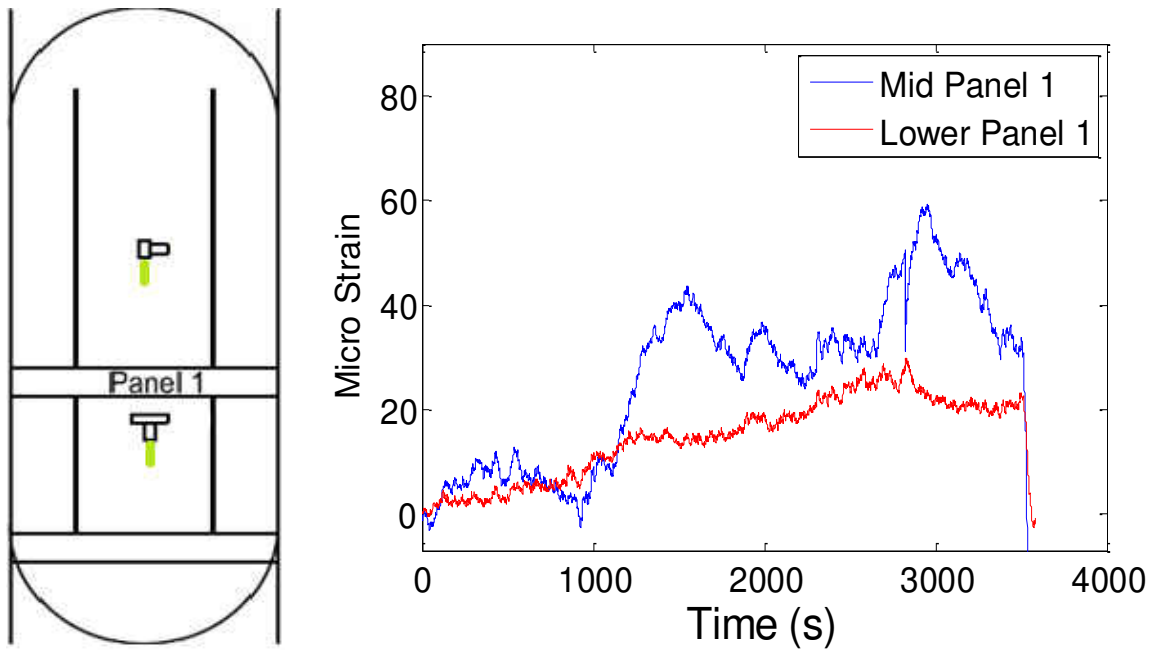


Figure 6:17: Strain in the Axial Direction of the First Panel

The graphs show the hoop (Figure 6-16) and axial (Figure 6-17) strains in the first panel. The hoop strain in the lower and middle panel show a strong correlation with the mid panel larger in magnitude. While the axial strains in each section show inconsistently with each other. However the axial strain in mid-section is larger in magnitude, which follows the trends of the other sensors.

The comparison of UCF's and KSC's strain data is as follows:

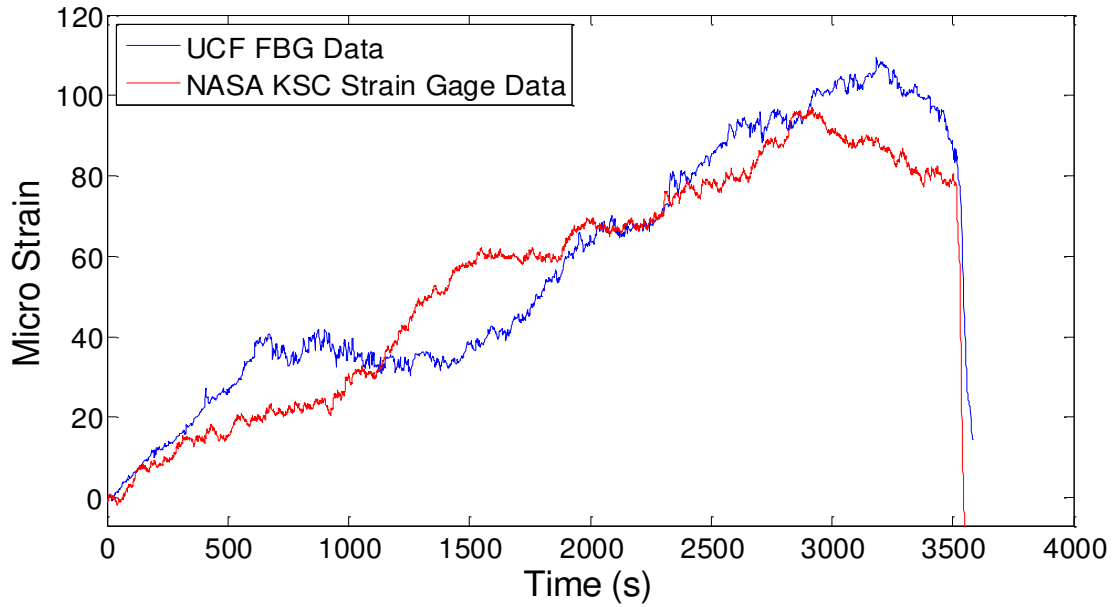


Figure 6:18: Comparison of Hoop Strain in the Mid-Section of Panel 1

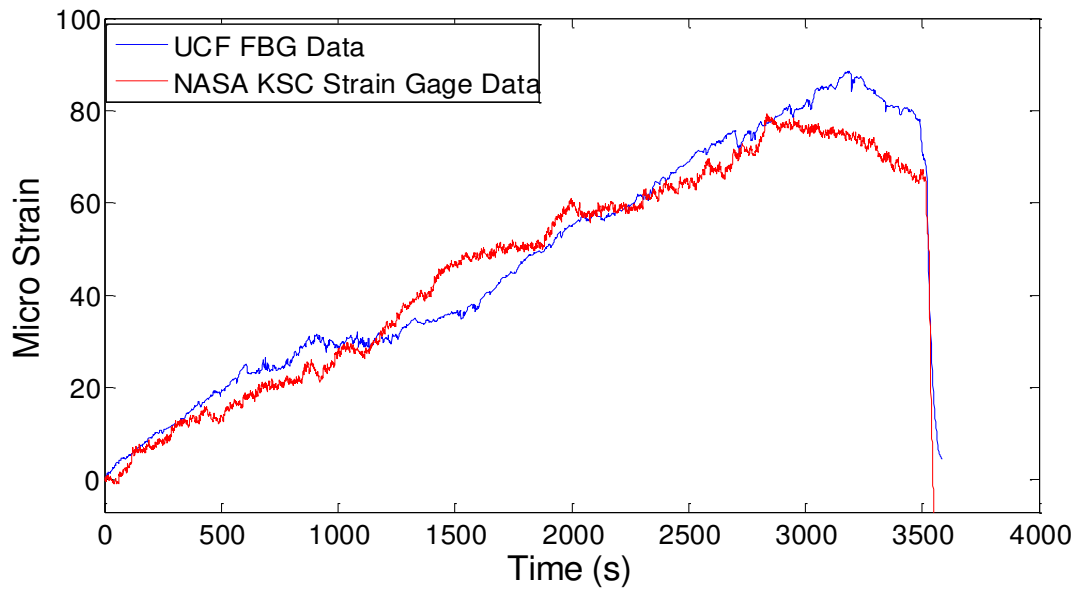


Figure 6:19: Comparison of Hoop Strain in the Lower Section of Panel 1

The graphs (Figures 6-18 and 6-19) show the comparison of the hoop strain in the first panel between UCF and KSC. The upper plot shows the strain in the mid-section of the tank while the lower plot shows the strain in the lower section. From the figures the strain in both sections of panel one have trends and values.

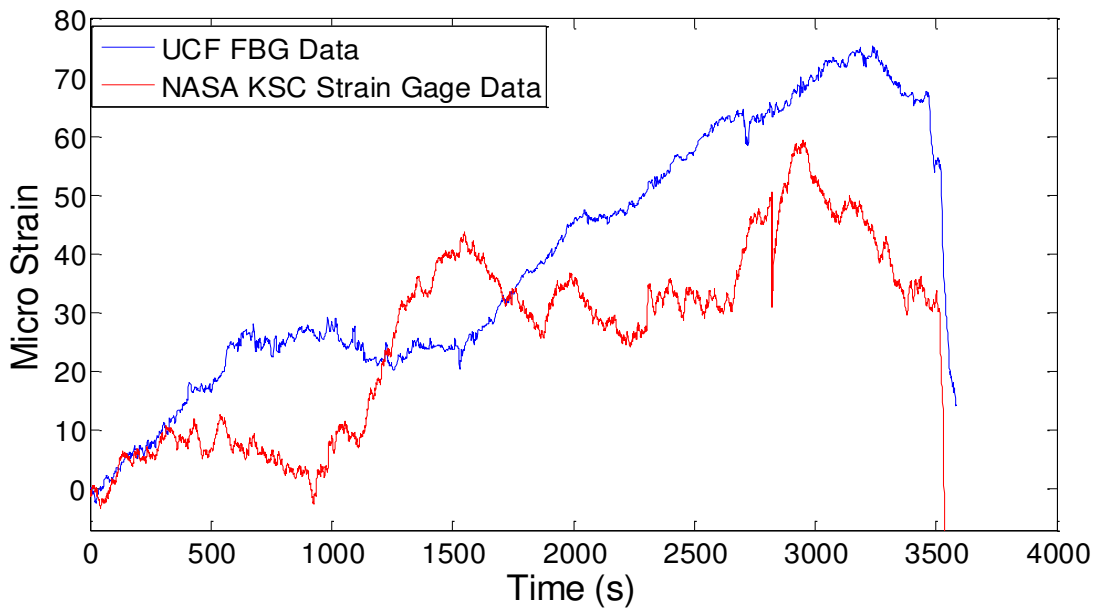


Figure 6:20: Comparison of Axial Strain in the Mid-Section of Panel 1

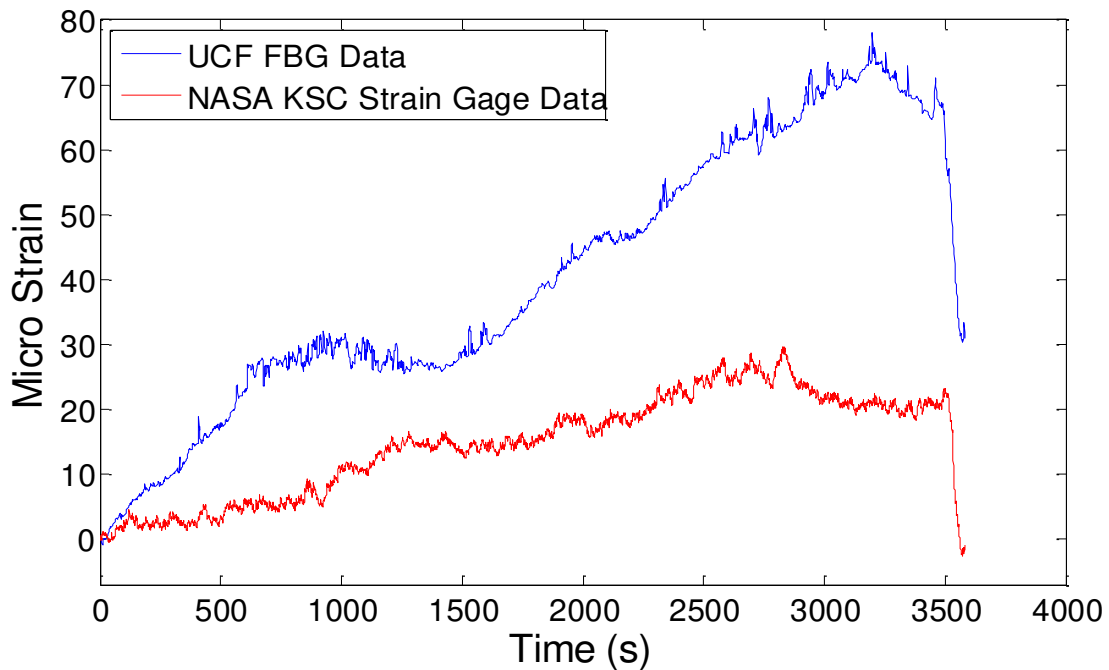


Figure 6:21: Comparison of Axial Strain in the Lower Section of Panel 1

The graphs (Figures 6-20 and 6-21) show the comparison of the axial strain in the first panel between UCF and KSC. The upper plot shows the strain in the mid-section of the tank while the lower plot shows the strain in the lower section. From the figures the strain in both sections of panel one show inconsistent results. The mid-section has about the value in strain but differs in the locations of the peaks. While the lower section has similar peak locations but is inconsistent in magnitude.

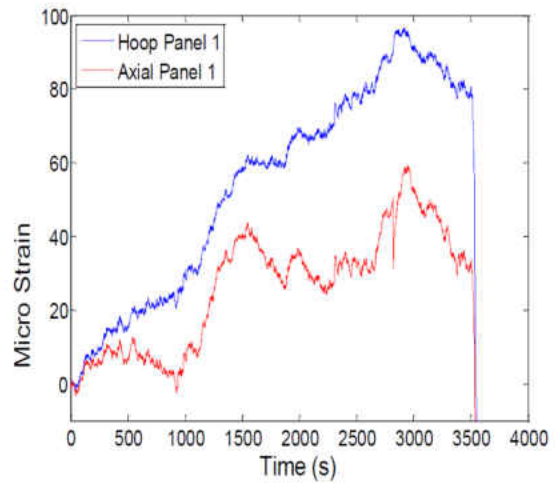
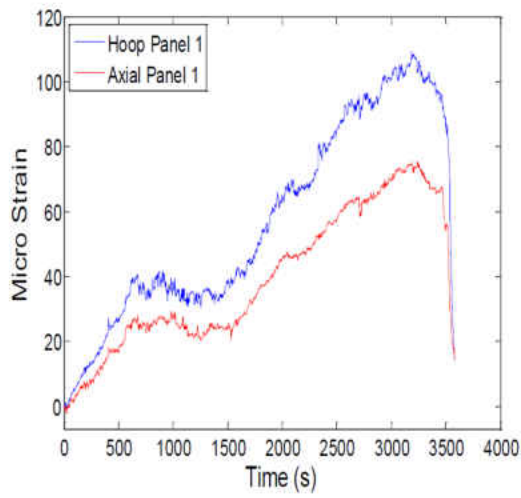


Figure 6:22: Strain at the Mid-Section of Panel 1 (UCF left and KSC right)

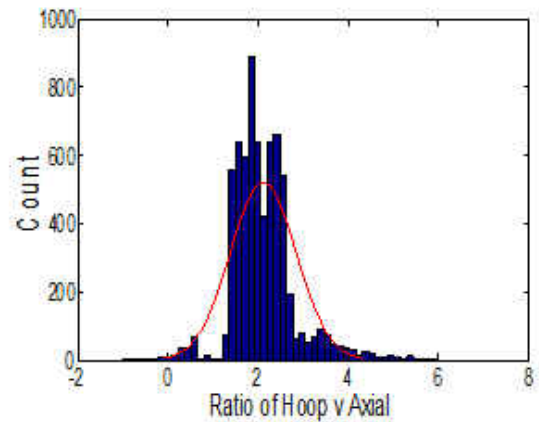
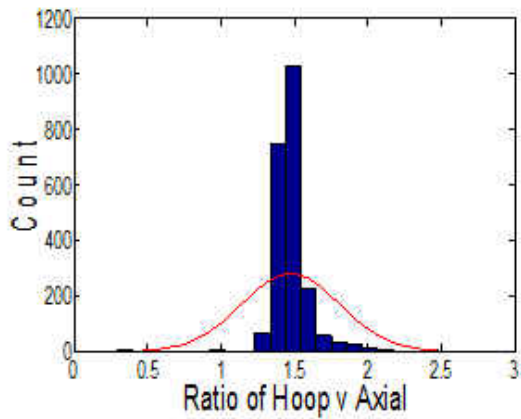


Figure 6:23: Ratio of Hoop v Axial Strain at the Mid-Section of Panel 1 (UCF left and KSC right)

The graphs (Figures 6-22 and 6-23) show the comparison of the hoop and axial of the mid-section of panel one as well as a histogram showing the ratios. The figures on the left correspond to UCF's sensors while the ones on the right correspond to KSC's. UCF's mean ratio is 1.5 and has a standard deviation of 0.334; while KSC's mean ratio is 2.1 with a standard deviation of 0.7298. Even though KSC's results were closer to the ideal 2-1 ratio, UCF's sensors had less variance.

### **6.3 Full Burst Test at NASA's MSFC**

After the tank was pressurized to 7 psi and checked out at KSC, it was shipped to the MSFC test site ET10 and lowered into the flame trench, shown in Figure 6-24, July 31st. The KSC team traveled on Sunday August 11th and continued setup on August 12th and 13th, On August 14th the tank was filled with LN<sub>2</sub>, pressurized to 32 and then 136 psig using GN<sub>2</sub> with Health Monitoring data gathering functioning. The maximum operational pressure was 136 psig from Scorpius.



Figure 6:24: Instrumented AFRL Tank in Flame Trench (left) AFRL Tank Filled with LN2 During Testing (right)

### Test Results

The first portion of the analysis will go to answer the most crucial of all questions, which sensors are working properly. Looking at the readings from the KSC experiment, the analysis will involve the strain readings from the pressure steps of the experiment. However once the tank was filled with liquid nitrogen, and dropped in temperature to lower than -325 degrees F, UCF's sensors were experiencing difficulties. Due to these extreme conditions, most of the FBG sensors stopped working properly. Gradually with the drop in temperature the wavelength peaks also dropped in magnitude until only one peak was able to be read and therefore was the only sensor properly

working. Furthermore, with nothing to really compare that one sensor with, the analysis of its accuracy and precision will be combined with the analysis of the NASA KSC sensors.

There are a total of four sensors per panel. Each panel will have two levels, one at the middle of the tank and another at the lower portion of the tank. In each level there will be two sensors, one is the axial direction and one in the hoop direction. For this section each subclass will discuss to detail every sensor of the panel and the reasons some are being used for data analysis while others are being discarded.

For the sensor analysis, there will be two key behaviors that will define the validity of the sensor. The first criterion is data consistency with the pressure steps. Since pressure will undoubtedly cause an increase in strain, one would expect any and all strain data to follow the pattern that the pressure step takes. The second criteria will be magnitude. Although a specific number cannot be guessed for the real strain magnitude, comparing the sensors to each other and how large their magnitude is, should serve to better define whether the sensor is giving reasonable data or not.

Ultimately, the following is a simplified diagram of the sensor location of the NASA system. Although not in scale, the figure will be used to convey the information gathered and show the relationship of the sensors with respect to tank location.

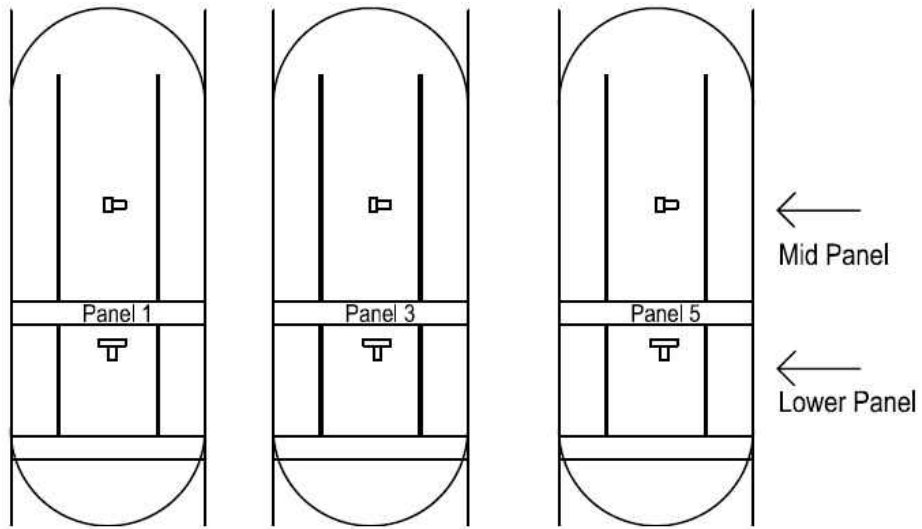


Figure 6:25: KSC Instrumentation Plan

Plotting the whole data at the lower portion of the tank the graphed region will look as follows (Figure 6-26):

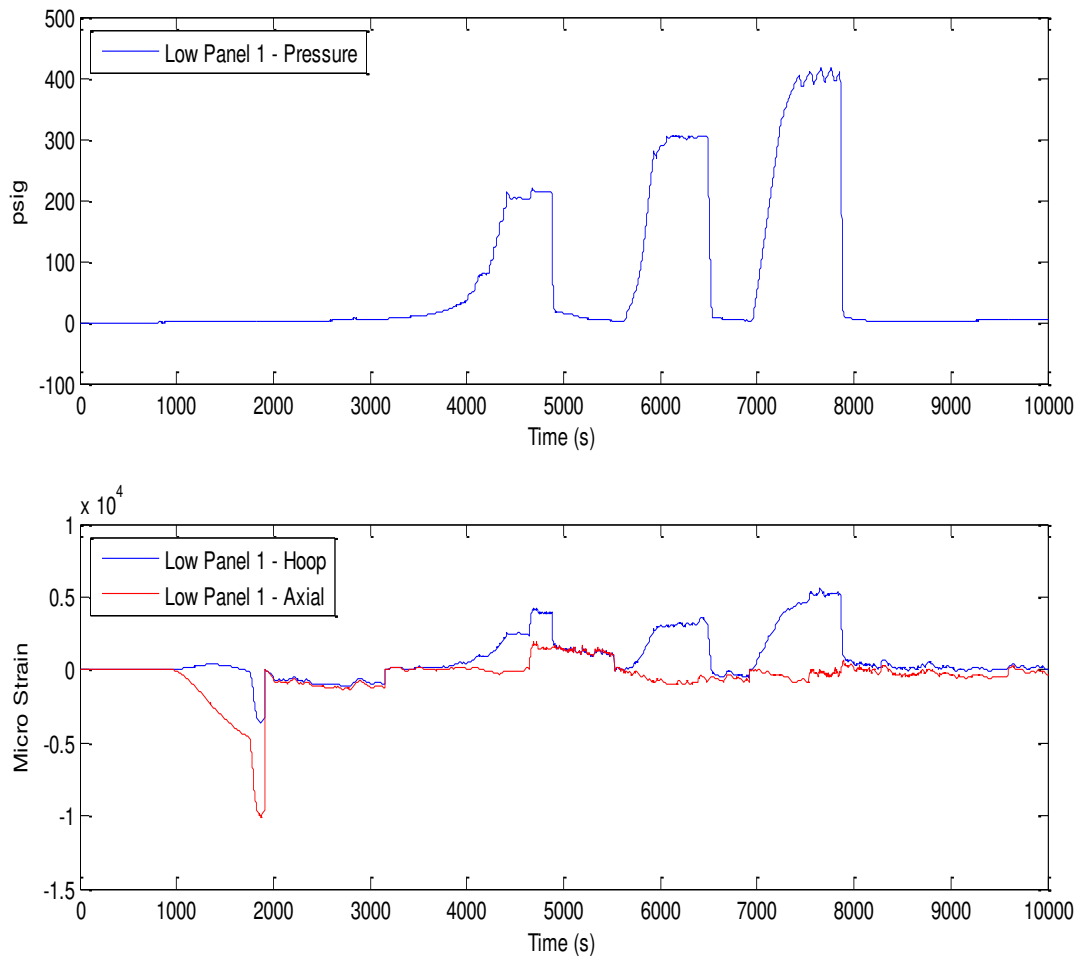


Figure 6:26: Hoop v Axial at the Lower Section of Panel 1

The presented graph (Figure 6-26) shows the overall run of the experiment. Already we can tell some problems with the sensor in the axial direction. In order to better analyze the data, a close-up of the peaks was done. The following picture presents the results:

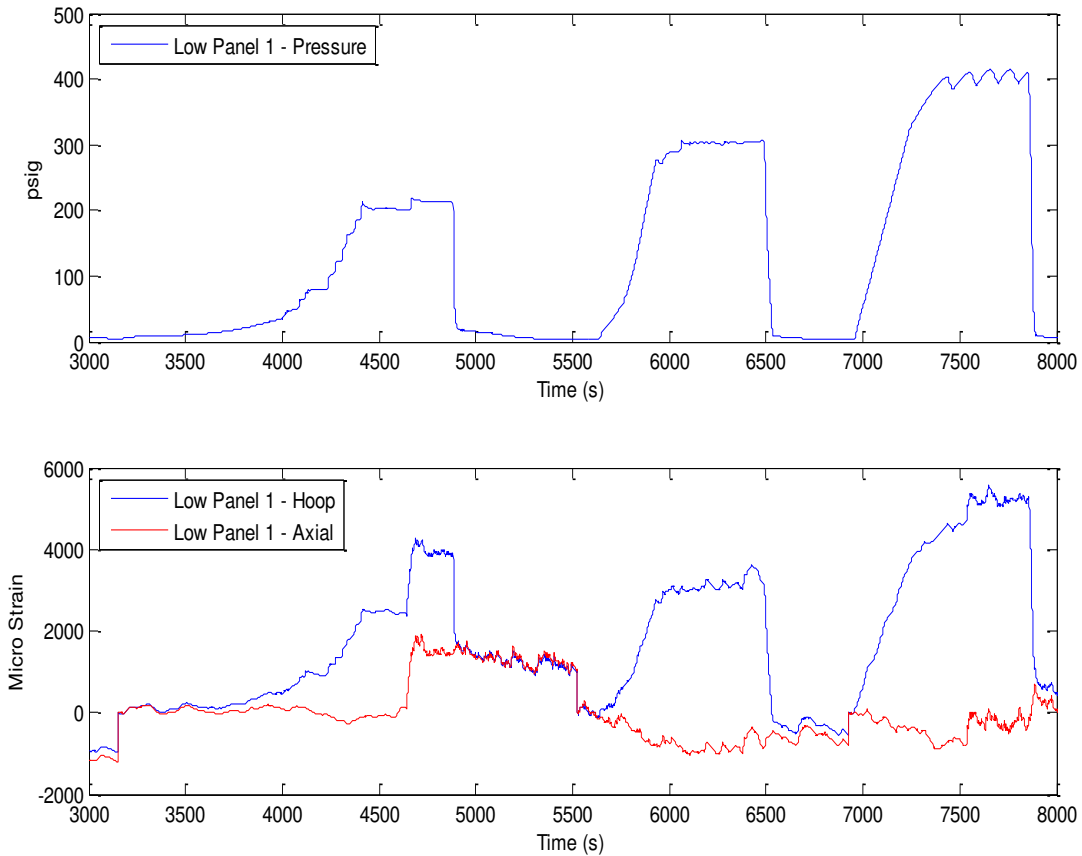


Figure 6:27: Hoop v Axial at the Lower Section of Panel 1

From the previous graph (Figure 6-27) it becomes apparent that the data for the Hoop direction appears correct for the most part except for a portion after “4500sec” where there is a jump in magnitude. Still, the pressure graph shows a spike in that area so further analysis on the sensor is reasonable. In the case of the axial direction however, data is clearly erroneous showing no relationship to the pressure increase and virtually no magnitude for the strain. Ultimately, the useful data for the sensors in the lower panel 1 can best be visually expressed as follows:

Similarly, looking at the plotting of the whole data at the middle portion of the tank the graphed region will look as follows (Figure 6-28):

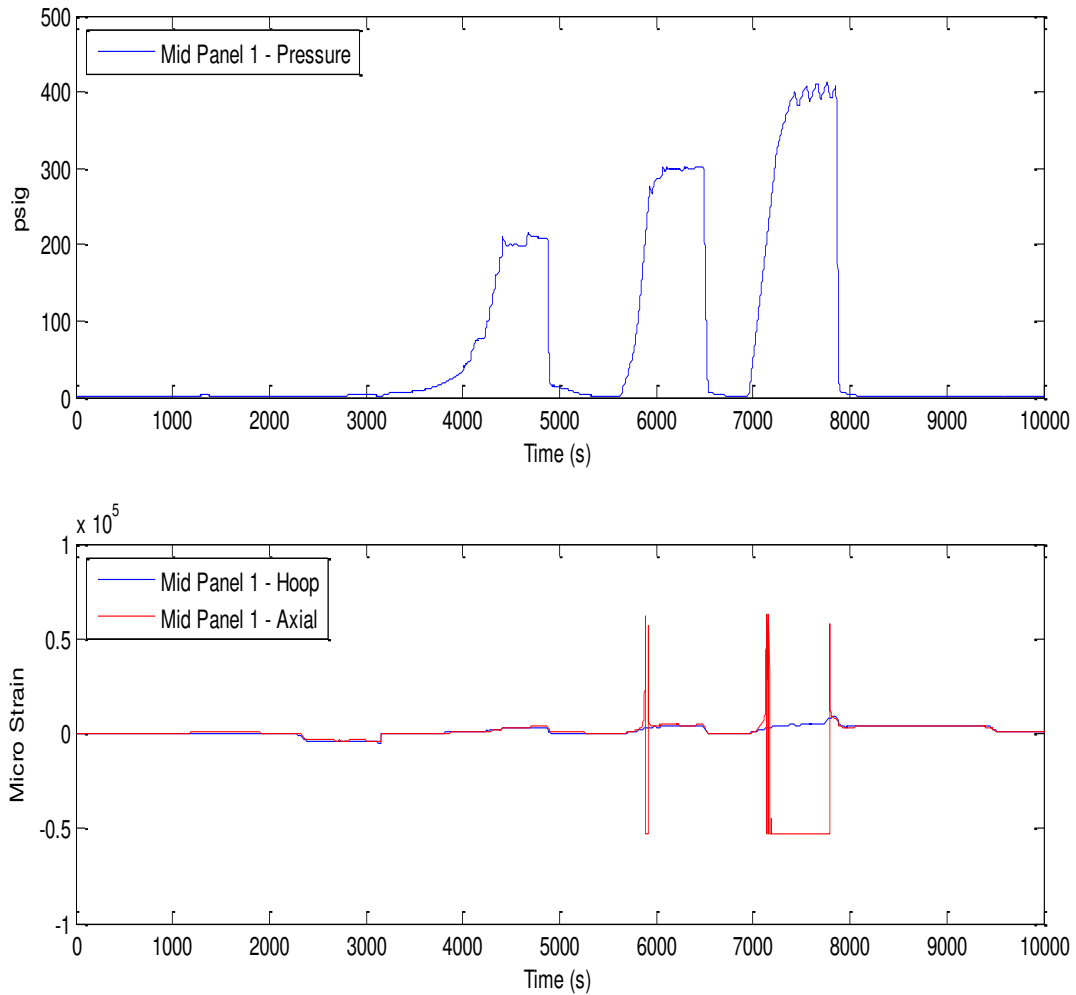


Figure 6:28: Hoop v Axial at the Mid-Section of Panel 1

The presented graph (Figure 6-28) shows the overall run of the experiment. At first glance not much can be discerned. One can see a major issue with the axial sensor at the pressure step of

400psi. As a result, the close-up of the strain data will disregard that portion of the graph in the axial direction. The resulting graph looks as follows (Figure 6-29):

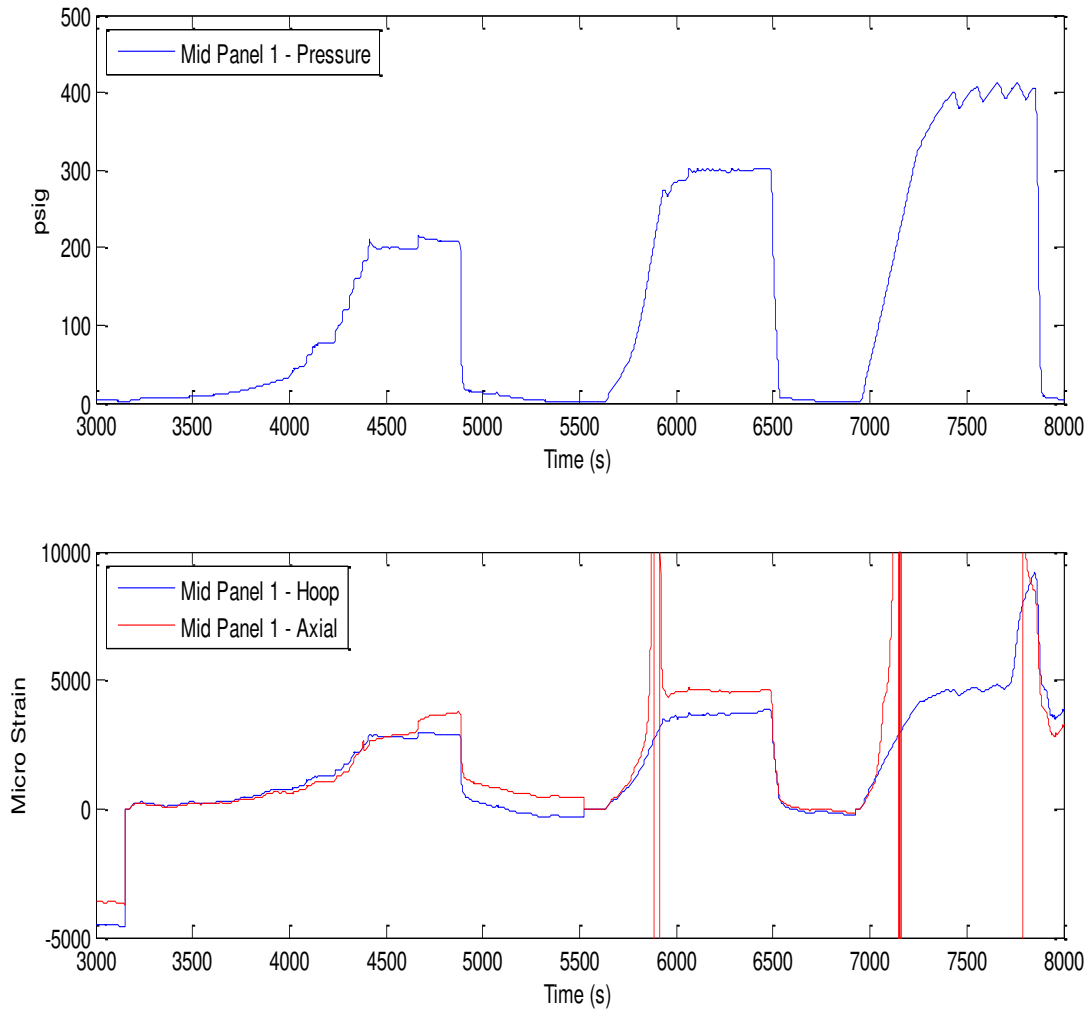


Figure 6:29: Hoop v Axial at the Mid-Section of Panel 1

The previous graph one can discern that overall strain data has reasonable readings. Not only do the peaks match with the pressure steps but similarities in shape between the sensors to

the previous lower panel show great promise. In the end, the only issue of concern for the middle panel is the axial sensor at the 400psi step. Similarly to before, the visual representation suggests the following:

#### UCF and KSC Comparison:

Although the original intent was to analyze the axial and hoop strain in all panels of the tank between the UCF health monitoring group and the NASA KSC group, due to the extreme temperature exposure some of the UCF health monitoring group data was lost or had to be disregarded. Similarly, temperature and or other factors affected the KSC sensors. The resulting analysis will focus on the axial sensor at the dome of panel 1 and how it relates to the different axial readings of the tank. There are three different pressure steps to look at. Sadly data was unsuitable at 400psi. As a result, the analysis will only focus on the pressure steps at 200psi and 300psi. Furthermore, Lower panel readings for the KSC sensors also suffered. As a result, the analysis will limit itself to the mid panel as compared to the dome axial.

For starters, the diagram presented below (Figure 6-30) is the comparison of the axial readings in all panels at a pressure of 200psi. The first behavior to notice is that all graphs share a very similar pattern and shape. The similarity in graph shape suggests precision in data collection. Furthermore, a pattern in sensor magnitude appears to repeat itself. When looking at the 7 psi test the highest level of both axial and hoop readings came from panel 1. Such fact seems to suggest

that overall the tank was the weakest at the mid-section in panel 1.

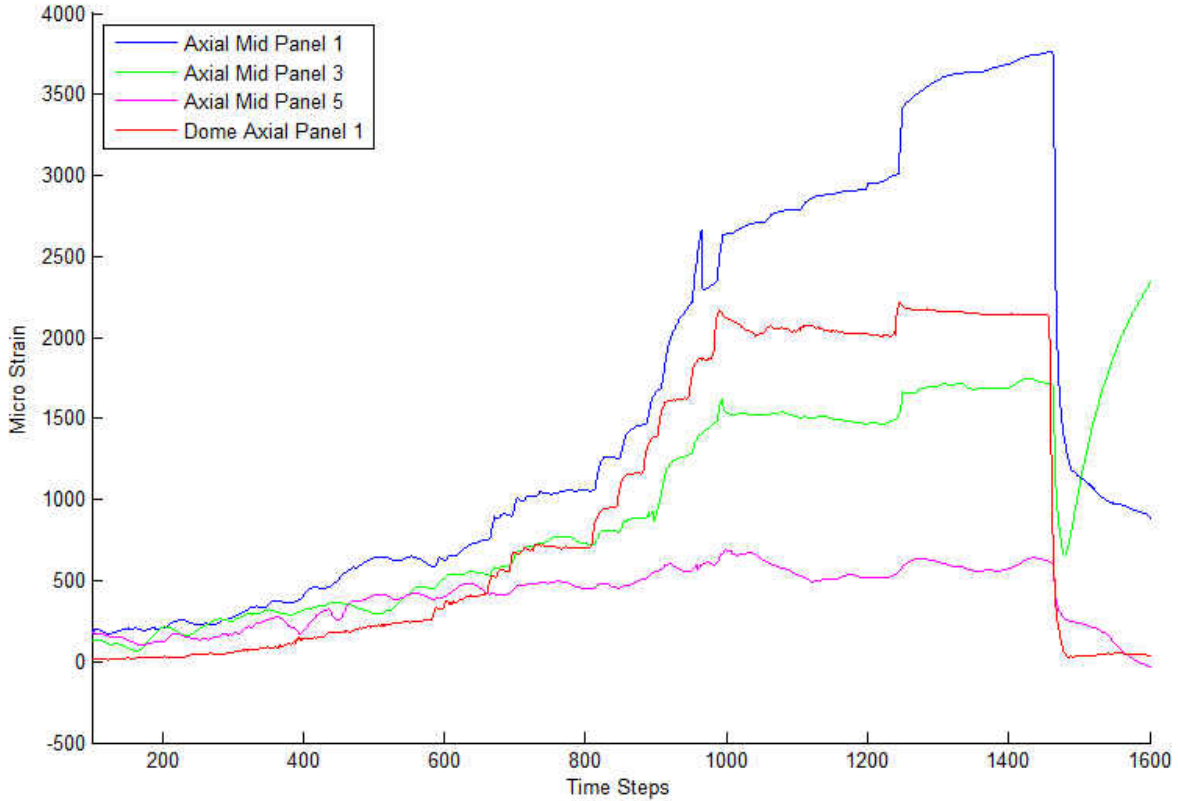


Figure 6:30: Comparison of Axial Strain

The second portion of the analysis is the diagram presented below (Figure 6-31). The diagram, similarly to the previous commentary, is the comparison of the axial readings in all panels at a pressure of 300psi. In the current graph, KSC had major problems in panels 5 and 3. Ultimately, the only relationship available to see is that of the mid panel axial as compared to the dome. Much like before, the similarity in graph shape suggests precision in data collection. Also,

the same pattern mentioned before repeats itself with panel 1 having the highest level of strain.

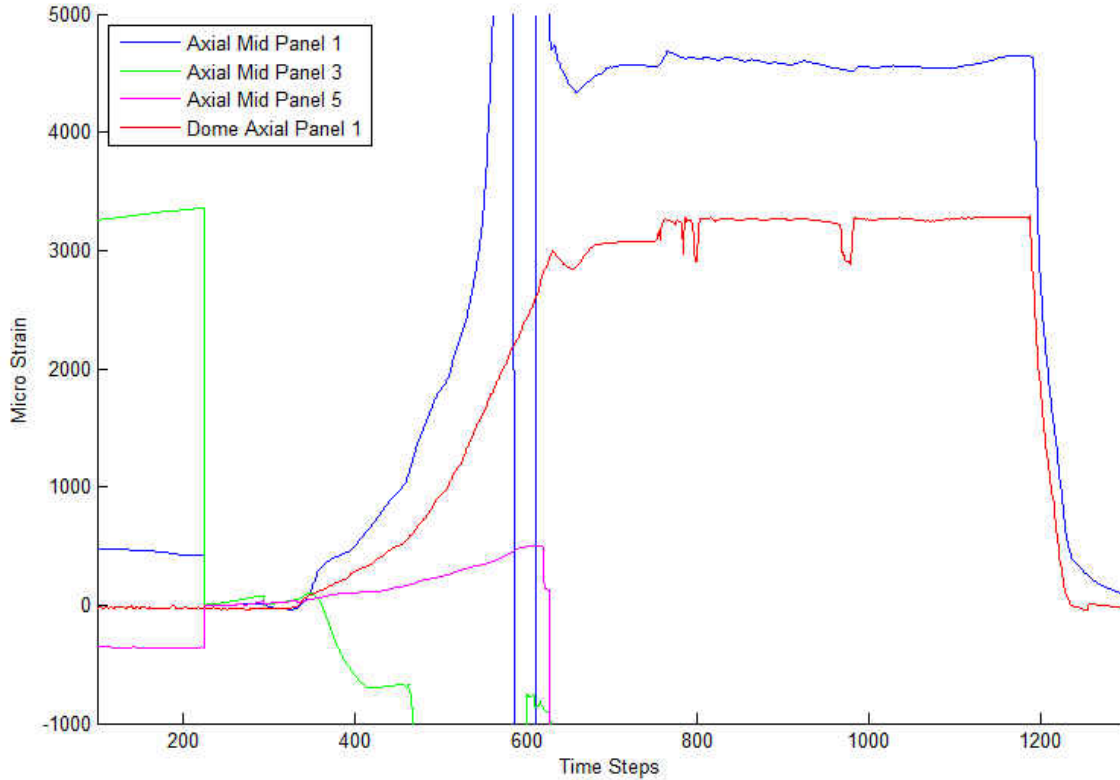


Figure 6:31: Comparison of Axial Strain

In the end, axial reading suggests consistency and precision. Although there were some issues, by combining the collected data along with the 7psi experiment many interpolations can be made. The overall assessment is that enough data was collected to adequately tell the properties and efficacy of the composite tank when exposed to high temperatures. Ultimately though, further analysis should be made in accordance to the recorded information of the report to better represent the tank and its benefits to the NASA program.

## **6.4 Conclusion**

The first step in the analysis of the data comes from defining the accuracy and precision of the system setup. With that in mind, when looking at the data and how both systems fared, one does not have to go further than the 7 psi test to address the issue. The test in itself served to show a great deal of similarities in the readings as well as present the expected behavior of the strain when placed at the failure test. The following (Figure 6-32) shows the mid-section hoop strain readings of both UCF (top) and KSC (bottom) sensors:

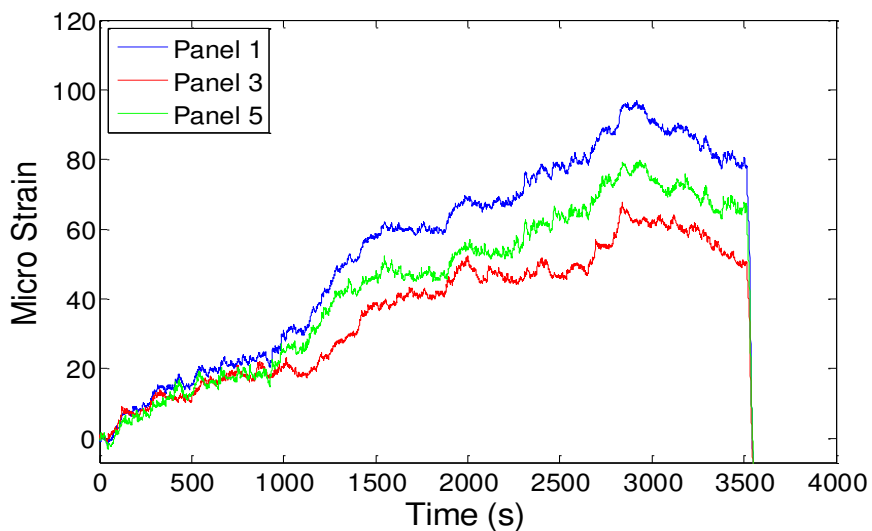
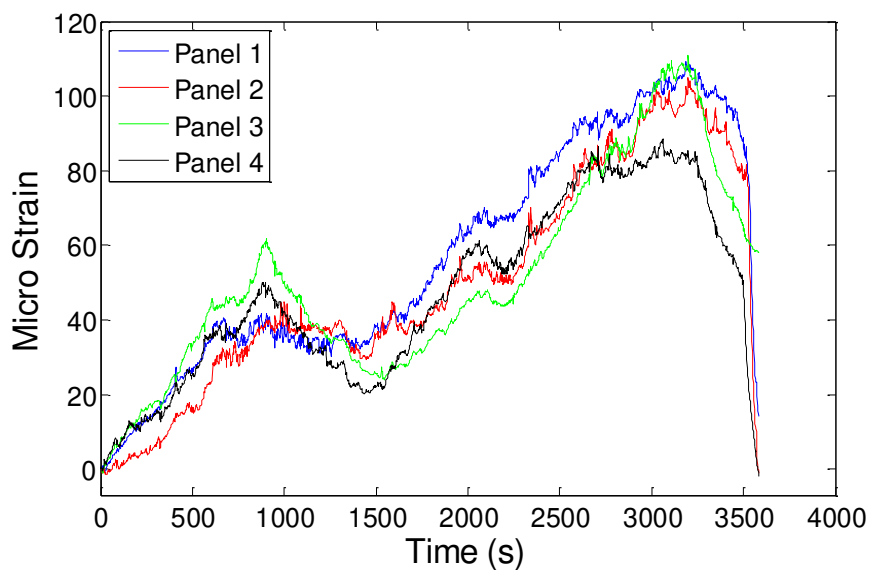


Figure 6:32: Strain in the Hoop Direction at the Mid-Section of the Panels (UCF top and KSC bottom)

The graph comparison shows a similar increase and relatable peaks. As a result, not only can one concur precision from both the KSC and UCF data by graph similarity, but from the resemblance in magnitude of the peaks one can also assume a good degree of accuracy.

Furthermore, individual values of axial and hoops readings suggest great and credible data. It is important to note that in the analysis of the hoop to axial ratio mixed results were found. However most of the inconsistencies are in the dome portion of the tank and can be attributed to the geometry of the vessel. Unlike the side portions of the tank; the dome will not have a 2-1 strain ratio because the hoop strain will be significantly less in magnitude. Ultimately though, the 7psi test served to confirm the validity of the data collection analysis and after viewing the results it is quite clear that interpolation and tank properties can be calculated from the system acquisition placed in the test.

In the case of the final experiment the decreased in temperature played a much more significant role than anticipated. As explained earlier, some data was lost due inadequate sensors/adhesive from all the sensors installed by all parties involved with the failure tests at cryogenic conditions. While this was expected that some sensors would be lost, other situations such as certain mounting and installation procedures were also observed as reasons for failed sensor reading especially with decreasing temperatures. The end result is that the only concrete comparison that can be done is the axial readings at the low portion of the tank in panel 1 for two distinct pressure steps.

In the case of the 200 psi the following graphs shows a comparison of the compared data. It is important to note that the dome reading is equivalent to the UCF sensor recording.

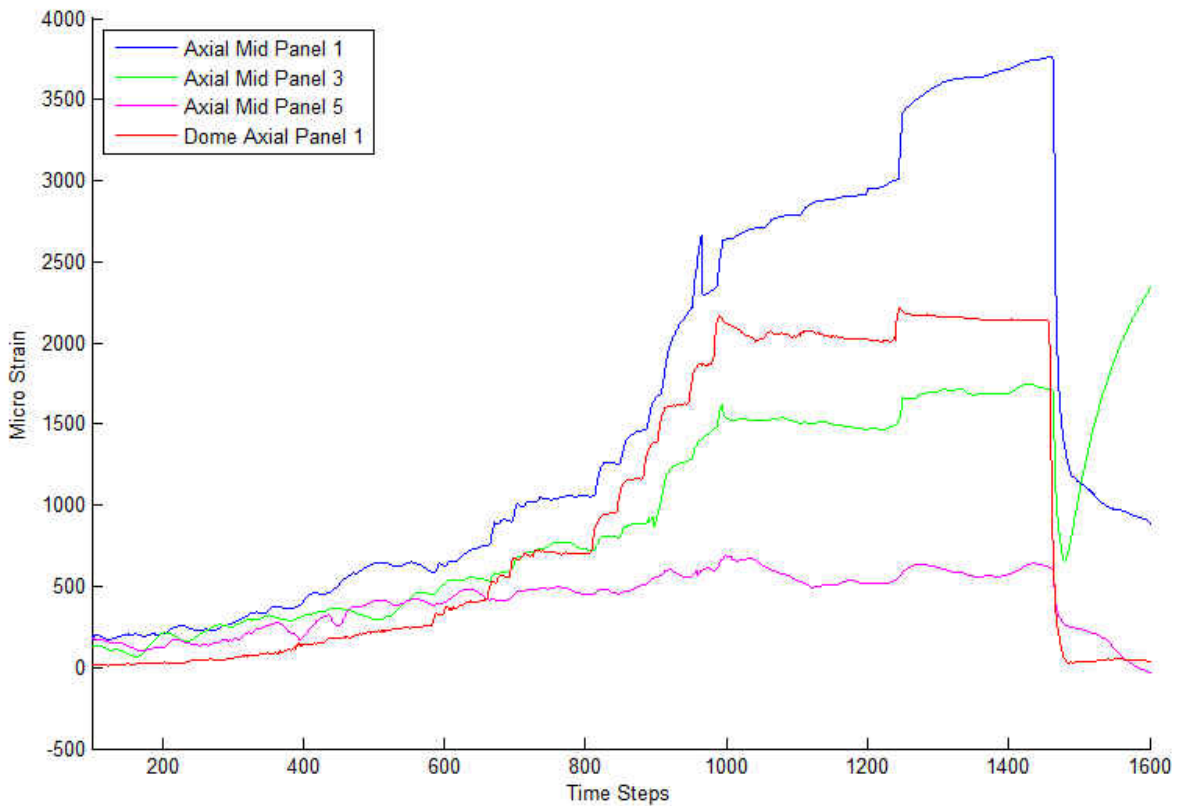


Figure 6:33: Axial strain at mid-panel for KSC vs. UCF dome reading at panel 1 at the 200psi peak

Much like the previous fashion, the first thing to address is the similarity in the graphs. Since the readings show peaks at similar times as well as steady increases in strains it is a fair conclusion that collected data was accurate. Furthermore, when compared to the 7psi test done earlier, the axial pattern of greatest strain to lowest strain in the KSC sensors is exact. Such fact seems to suggest that overall the tank was the weakest at the mid-section in panel 1 and a focused analysis on the differences between panel 1 and the other panels should be conducted.

For the axial analysis at 300 psi KSC had some problems for sensors in panels 5 and 3. Ultimately, the only relationship available to see is that of the mid panel axial as compared to the

dome. Much like before, the similarity in graph (Figure 6-34) shape suggests precision in data collection. The graph does suggest, much like the previous graph (Figure 6-33), that axial at the mid panel is significantly higher than the axial at the dome.

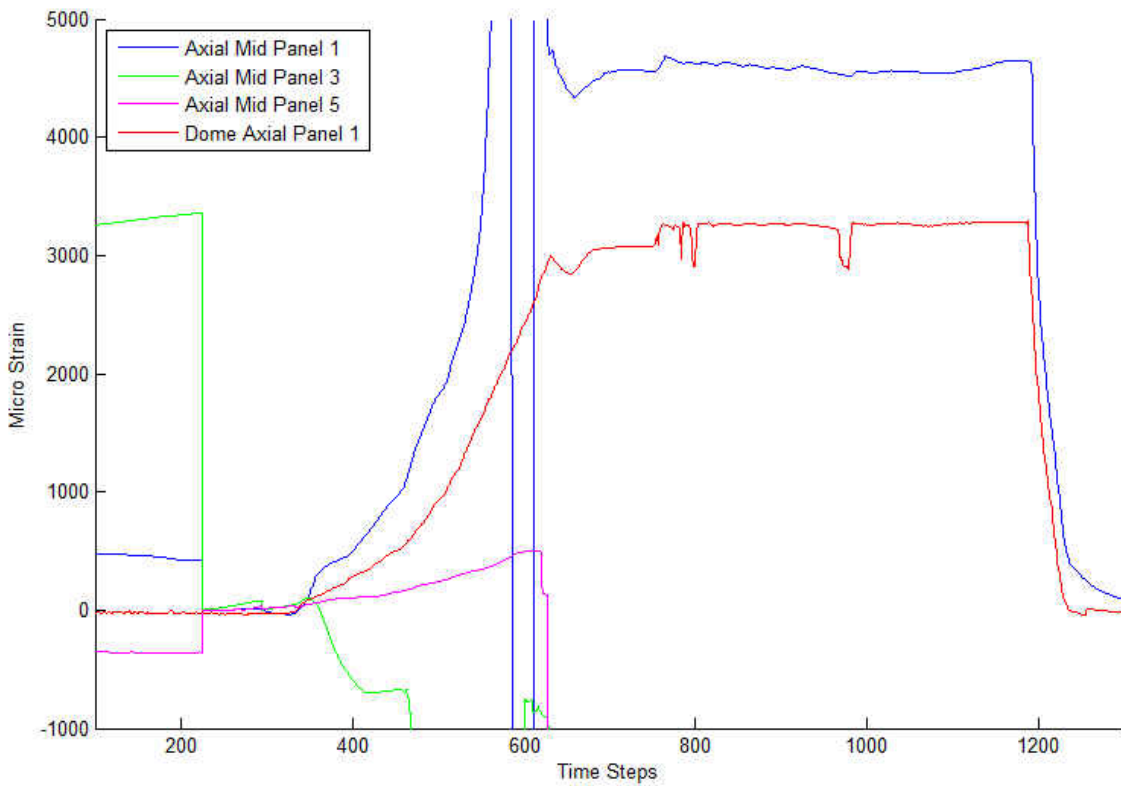


Figure 6:34: Axial strain at mid-panel for KSC vs. UCF dome reading at panel 1 at the 300psi peak

In the end, axial reading suggests accuracy and precision. The 7psi test was very successful and combined with the collected axial data at the failure step can be used to define tank properties and coefficients. Ultimately though, further analysis should be made in accordance to the recorded information of the report to better represent the tank and its benefits to the NASA program.

## **CHAPTER 7: SUMMARY, FINDINGS, CONCLUSIONS AND RECOMMENDATIONS FOR FUTURE WORK**

In this report, structural health monitoring to detect damage is carried out for Composite Overwrapped Pressure Vessels (COPVs) which have historically been used space missions. COPVs have been used to store inert gases like helium (for propulsion) and nitrogen (for life support) under varying degrees of pressure onboard the orbiter since the beginning of the Space Shuttle Program. After the Columbia accident, the COPVs were re-examined and different studies (e.g. Laser profilometry inspection, NDE utilizing Raman Spectroscopy) have been conducted and can be found in the literature. In this study, the UCF researchers collaborated with NASA engineers and received 5 different COPV tanks with 2 of them identified as damaged with thermally hidden delamination or void, and one was identified as a different condition with two materials integrated in helical pattern, and finally 2 of them were defined with normal manufacturing variances.

The instrumented COPVs were tested first under different pressure levels. In this case, both the input (pressure for 50 psi, 100 psi, 150 psi and 200 psi) and response (hoop and axial strains) were recorded. The findings and conclusions are summarized in the following:

- By simple inspection of Tanks 2 and 3 showed variations of hoop strains measured at different measurement locations, while Tanks 1, 4 and 5 indicated consistent (with very slight variations) for hoop strain measurements at different locations under increasing pressures.

- This approach required visual inspection and experience. It can work better when the response is due to well-defined input (pressure) as in this case. It may not require baseline.
- Based on the thin walled pressure vessel theory well-defined in mechanics of materials theory, there is a relationship between the hoop and axial stressed. Hoop-to-axial strain response (also eliminating the need to use input/pressure) data were generated. Histograms of these data sets for each tank were plotted. Theoretically, the ratio should be around 2.00 with slight variations for undamaged and well-manufactured COPVs. It was seen this ratio was very close to 2.00 for Tanks 1, 2 and 5 with 4-6% error with respect to the theoretical 2.00 ratio. For Tanks 3 and 4, the ratio were found to be 2.42 (21% error) and 2.31 (15% error), clearly indicating the damage and variation from an undamaged tank behavior.
  - This approach can be automated and does not require a sophisticated model (may be considered as a data-driven change detection). It also does eliminated the need to know the input data. It may not require baseline. In this particular case of damage with thermally hidden delamination or void, dense spatial sensor layout was not needed. Since this damage can be typical damage, it can be considered as successful detection.
- In addition to hoop-to-axial ratio, hoop 1 -to- hoop 2 response data (for two different locations) were also analyzed (also eliminating the need to use input/pressure). Theoretically, the ratio should be around 1.00 with slight variations for undamaged and well-manufactured COPVs. It was seen this ratio was very close to 1.00 for Tanks 1, 2 and 5 with 1-4 % error with respect to the theoretical 1.00 ratio. For Tanks 3 and 4, the ratio

were found to be 1.44 (44% error) and 1.28 (28% error), clearly indicating the damage and variation from an undamaged tank behavior.

- This approach can be automated and does not require a sophisticated model (may be considered as a data-driven change detection). It also does eliminated the need to know the input data. It may not require baseline. In this particular case of damage with thermally hidden delamination or void, dense spatial sensor layout was not needed. Since this damage can be typical damage, it can be considered as successful detection.
- The cross-correlation of hoop 1 -to- hoop 2 response data were analyzed and compared with respect to the Tank 1 which is showing almost perfect correlation (0.999%) for different sensors. For Tanks 1, 2 and 5, the correlation were found to be between 0.999 to 0.986 with about 1% error with respect to Tank 1's 0.999 correlation. Tanks 3 and 4 correlation was 0.912 and 0.956, which is indicating high correlation, however, less than the other tanks.
  - This approach can be automated and does not require a sophisticated model (may be considered as a data-driven change detection). It also does eliminated the need to know the input data. It may not require baseline. In this case, the correlation was lower for Tanks 3 and 4, it is not very convincing and require more exploration.
- Damage Features using Auto-Regressive models with eXogenous outputs (ARX) Analysis was first implemented using the pressure input and strain responses. ARX models were established and then compared with the measured data. From there, the Damage Feature (DF) was identified based on the established threshold limits. It was observed that the

deviation of the DF from the threshold was much higher for Tanks 3 and 4 while others were below the threshold level.

- This approach can be automated and does require an ARX model (with some experience requirement to determine the model order etc). In this example, it uses the input data. It may not require baseline but a threshold level. In this particular case of damage with thermally hidden delamination or void, dense spatial sensor layout was not needed. Since this damage can be typical damage, it can be considered as successful detection.
- Damage Features using Auto-Regressive models with eXogenous outputs (ARX) Analysis was then implemented using the acceleration responses without using the input data. In this case, the input was considered as all response measurement for a given response data. This approach was well-documented by Dr. Catbas' previous publications. This approach also indicated that the deviation of the DF from the threshold was much higher for Tanks 3 and 4, however, it was also observed that Tank 5 indicated (false positive) values above the threshold level.
  - This approach can be automated and does require an ARX model (with some experience requirement to determine the model order etc), it does not require the use of the input data. It may not require baseline but a threshold level. In this particular case of damage with thermally hidden delamination or void, dense spatial sensor layout was not needed. While damage was successfully identified for Tanks 3 and 4, a false positive for Tank 5 was also observed. The false positive was probably detected due to the difference in material, with the zebra pattern, addition

of zylon material, the mass and stiffness of the COPV is noticeably different and therefore damage was detected.

- A number of experimental technologies, algorithms and damage features were presented building up a collection of various methodologies. A composite index or a table such as the one given in Table 5-8 can be utilized for better decision making.

In chapter six of the report, testing and monitoring Studies of the AFRL Tank in the Field details another experimental study conducted exploring the condition and assessment of the AFRL Tank. This extensive study was conducted along with partners from NASA; Mr. Rudy Werlink (KSC) and Dr. Curtis Banks (MSFC) and the AFRL tank was tested multiple times as well to failure in the field. It provides information on the types of sensing technologies as well as the specification of the DAQs and monitoring system. A unique fiber optic system which was developed at UCF Lab and successfully utilized in several laboratory applications was utilized for cryogenic temperature and failure modes. The design of the tests, instrumentation system, preliminary results are presented.

The first step in the analysis of the data comes from defining the accuracy and precision of the system setup. The 7 psi test in itself served to show a great deal of similarities in the readings as well as present the expected behavior of the strain when placed at the failure test. The results show precision from both the KSC and UCF data by similarity strains, also from the resemblance in magnitude of the peaks one can also assume a good degree of accuracy. Furthermore, individual values of axial and hoops readings suggest great and credible data. It is important to note that in

the analysis of the hoop to axial ratio mixed results were found. However most of the inconsistencies are in the dome portion of the tank and can be attributed to the change in geometry of the vessel. Unlike the side portions of the tank; the dome will not have a 2-1 strain ratio because it does not behave as a cylinder. Ultimately the 7psi test served to confirm the validity of the data collection analysis and after viewing the results it is quite clear that interpolation and tank properties can be calculated from the system acquisition placed in the test.

In the case of the final experiment (failure test) the decrease in temperature due to the cryogenic conditions played a much more significant role than anticipated. As explained in chapter six, some data was lost due inadequate sensors/adhesive from all the sensors installed by all parties involved with the failure tests at cryogenic conditions. While this was expected that some sensors would be lost, other situations such as certain mounting and installation procedures were also observed as reasons for failed sensor reading especially with decreasing temperatures. The end result is that the only concrete comparison that can be done is the axial readings at the low portion of the tank in panel 1 for two distinct pressure steps. Much like the previous fashion, the first thing to address is the similarity in strains. Since the readings show peaks at similar times as well as steady increases in strains it is a fair conclusion that collected data was accurate. Furthermore, when compared to the 7psi test done earlier, the axial pattern of greatest strain to lowest strain in the KSC sensors is exact. Such fact seems to suggest that overall the tank was the weakest at the mid-section in panel 1 and a focused analysis on the differences between panel 1 and the other panels should be conducted. In the end, axial reading suggests accuracy and precision. The 7psi test was very successful and combined with the collected axial data at the failure step can be used to define tank properties and coefficients. Ultimately though, further analysis should be made in

accordance to the recorded information of the report to better represent the tank and its benefits to the NASA program. More information and complete report may be available from NASA KSC.

## **7.1 Recommendations for Future Work**

The most immediate step for future research is the implementation of the cross-correlation and ARX damage detection techniques to the ARFL Tank. With the data already collected and presented in chapter six of this report, it can be analyzed and further interpreted using similar techniques to what was done in chapter five of this report. The results of this new analysis can then be compared to the preliminary results in this study and also the findings concluded by NASA.

Also for future tests high speed data and health monitoring should be turned on at various times to record interesting events such as the acoustic cracking. This will also allow for further analysis, including finding the dynamic properties and characteristics of the structure.

Research into more effective adhesives for composite materials to withstand the high strains and large temperature changes, to -320 F. The cryogenic temperature range and variation, high strains and acoustic stress waves caused some failures of all sensor attachments to the composite surfaces. The sensors were attached using AE-10 epoxy. Past testing reflects experience with failure of attachment adhesives on other high strain and cryogenic tests. New adhesives should be developed under realistic conditions (comparable temperature cycles, high and varying strains) for better performance.

Also related to the adhesives, the type of fiber optic FBG sensors should be further investigated. In the AFRL tank experiment we utilized the os3200 FBG sensors from Micron

Optics; the sensors were manufactured inside a housing to protect the sensor from extremities. However in comparison to the os1100, which was utilized by Dr. Curtis Banks with MSFC, the os3200 did not perform as well in cryogenic conditions. The os1100 is simpler and cheaper (no protective housing) than the os3200 but was able to perform better in cryogenic conditions. Therefore further studies related to housing types on FBG sensors should be investigated, especially in cases dealing with cryogenic conditions.

Another step for future research is to implement more advanced and realistic ways to test the COPVs. For example they could be tested under similar conditions to the AFRL Tank burst test presented in chapter six. The COPVs should be tested under cryogenic conditions as well as to failure. Further and more realistic knowledge would be gained but the scope of this project was limited in funding and resources.

Implantation of various sensor technologies should be used when further testing COPVs. Especially the use of fiber optic sensors; they can sample at incredibly high rates and also be compared to other technologies. Further analysis can be implemented which has already been successfully utilized in previous laboratory experiments.

Placement of the sensors on the COPVs when there are only so many available due to equipment and cost limitations is a compromise when conducting research testing. In this test we only attached sensors on the cylindrical portion of the vessel, based on the common knowledge of cylinder hoop stress being twice the axial stress. We found out in the AFRL Tank test to failure that the dome of the tank is also a critical location because a crack formed in the top being the final

failure area. Therefore, care should be taken to place sensors in more sections, not just the expected failure areas (within cost and equipment limits).

With these areas of research further developed, the next step would implement these sensor technologies and damage detection methodologies on an active pressure vessel being used in a modern aircraft and as a component of a complete SHM system application. In this application, the reliability of these technologies and methodologies can be tested by the environmental factors affecting real-life health monitoring applications.

## REFERENCES

- Aktan, A. E., F. N. Catbas, et al. (2000). "Issues in Infrastructure Health Monitoring for Management." Journal of Engineering Mechanics, ASCE **126**(7): 711-724.
- Box, G. E., Jenkins, G. M. and Reinsel, G. C. (1994). "Time Series Analysis: Forecasting and Control". New Jersey, Prentice-Hall.
- Brownjohn, J. M., S.-C. Tjin, et al. (2004). A Structural Health Monitoring Paradigm for Civil Infrastructure. 1st FIG International Symposium on Engineering Surveys for Construction Works and Structural Engineering, Nottingham, UK.
- Catbas, F. N., D. L. Brown, et al. (2004). "Parameter Estimation for Multiple-Input Multiple-Output Modal Analysis of Large Structures." Journal of Engineering Mechanics ASCE **130**(8): 921-930.
- Catbas, F. N., Gokce, H. B., et al. (2011) "Non-parametric Analysis of Structural Health Monitoring Data for Identification and Localization of Changes: Concept, Lab and Real Life Studies." Structural Health Monitoring, 11(5)- 613-629.
- Catbas, N., Malekzadeh, M., Gul, M., & Kwon, I. B. (2014). "An integrated approach for structural health monitoring using an in-house built fiber optic system and non-parametric data analysis." Smart Structures and Systems, 14(5), 917.)
- Consoli, F. A., Alomari, A. H., Al-Deek, H., Rogers, J., Sandt, A., Noori, M., Hadi, M. (2015). Evaluation of Conditional Transit Signal Priority Technology for Regional Implementation. Press, Transportation Research Record: Journal of the Transportation Research Board, Washington DC.

- Farrar, C. and K. Worden (2007). "An Introduction to Structural Health Monitoring." The Philosophical Transactions of the Royal Society (365): pp. 303-315.
- Goodno, Barry J., and James M. Gere. "Mechanics of Materials". Stamford, Conn: Cengage Learning, 2009. Print.
- Greene, N, Yoder, T, et al. (2007). "Stress Rupture Testing and Analysis of the NASA WSTF-JPL Carbon Overwrapped Pressure Vessels." American Institute of Aeronautics and Astronautics 2007-11613
- Greene, N, Saulsberry, R et al. (2010). "Composite Overwrapped Pressure Vessels (COPV) Stress Rupture Testing." Las Cruces, NM, NASA Johnson Space Center White Sands Test Facility
- Gul, M. (2009). "Investigation of Damage Detection Methodologies for Structural Health Monitoring." Department of Civil, Environmental and Construction Engineering. Orlando, FL, University of Central Florida. **Doctoral Dissertation**.
- Gul, M. and F. N. Catbas (2009). "A Novel Time Series Analysis Methodology for Damage Assessment." The Fifth International Workshop on Advanced Smart Materials and Smart Structures Technology, ANCRISST 2009. Boston, MA.
- Gul, M. and F. N. Catbas (2011). "Structural Health Monitoring and Damage Assessment using a Novel Time Series Analysis Methodology with Sensor Clustering." Journal of Sound and Vibration **330**(6): pp. 1196-1210.
- Instruments, N. (2009). "ARX Model Definitions (Systems Identification Toolkit)." Product Reference Manuals. from <http://zone.ni.com/reference/en-XX/help/372458A-01/lvsysidconcepts/modeldefinitionsarx/>.

- Kersey, A. D., Davis, M. A., Patrick, H. J., LeBlanc, M., Koo, K. P., Askins, C. G., & Friebele, E. J. (1997). Fiber grating sensors. *Journal of light wave technology*, 15(8), 1442-1463.
- Kucukvar, M., Noori, M., Egilmez, G., & Tatari, O. (2014). Stochastic decision modeling for sustainable pavement designs. *The International Journal of Life Cycle Assessment*, 19(6), 1185-1199.
- Kwon, I-B., Malekzadeh, M., Ma, Q., Gokce, B., Terrell, T., Fedatov, A. and Catbas, F.N. (2011), “Fiber Optic Sensor Installation for Monitoring of 4 Span Model Bridge in UCF”, Proceedings of the 29th International Modal Analysis Conference, Jacksonville, FL, January 31 – February 3, 2011.
- Ljung, L. (1999). System Identification: Theory for the User. Upper Saddle River, NJ, Prentice-Hall.
- Lu, Y. and F. Gao (2005). "A Novel Time-domain Auto-regressive Model for Structural Damage Diagnosis." *Journal of Sound and Vibration* **283**: 1031-1049.
- Malekzadeh, M., Gul, M., & Catbas, F. N. (2012). “Use of FBG sensors to detect damage from large amount of dynamic measurements.” In Topics on the Dynamics of Civil Structures, Volume 1 (pp. 273-281). Springer New York.
- Malekzadeh, M., Gul, M., & Catbas, F. N. (2013). “Application of multivariate statistically based algorithms for civil structures anomaly detection.” In Topics in Dynamics of Civil Structures, Volume 4 (pp. 289-298). Springer New York.
- Malekzadeh, M. (2014). “Structural Health Monitoring Using Novel Sensing Technologies and Data Analysis Methods.” Department of Civil, Environmental and Construction Engineering. Orlando, FL, University of Central Florida. **Doctoral Dissertation**.

- Malekzadeh, M., & Catbas, F. N. (2014). "A comparative evaluation of two statistical analysis methods for damage detection using fibre optic sensor data." International Journal of Reliability and Safety, 8(2-4), 135-155.
- Malekzadeh, M., Atia, G., & Catbas, F. N. (2015). "Performance-based structural health monitoring through an innovative hybrid data interpretation framework." Journal of Civil Structural Health Monitoring, 5(3), 287-305.
- Noori, M., Gardner, S., & Tatari, O. (2015). Electric vehicle cost, emissions, and water footprint in the United States: Development of a regional optimization model. *Energy*, 89, 610-625.
- Noori, M., Tatari, O., Nam, B., Golestani, B., & Greene, J. (2014). A stochastic optimization approach for the selection of reflective cracking mitigation techniques. *Transportation Research Part A: Policy and Practice*, 69, 367-378.
- Nam, B., Golestani, B., Noori, M., Tatari, O., & An, J. (2014). Investigation of Reflective Cracking Mitigation Techniques-Final Report, (March 2014).
- Omenzetter, P. and J. M. Brownjohn (2006). "Application of Time Series Analysis for Bridge Monitoring." Smart Material and Structures **15**: pp. 129-138.
- Pandit, S. M. and Wu, S. M. (1993). "Time Series and System Analysis with Applications". Malabar, FL, Krieger Pub. Co.
- Rytter, A. (1993). "Vibration Based Inspection of Civil Engineering Structures." Department of Building Technology and Structural Engineering. Aalborg, Denmark, University of Aalborg. **Doctoral Dissertation**.
- Sohn, H. and C. R. Farrar (2001). "Damage Diagnosis Using Time Series Analysis of Vibration Signals." Smart Materials and Structures 10: 1-6.

Tam, W, Griffin, P (2002). “Design and Manufacture of a Composite Overwrapped Pressure Tank Assembly” American Institute of Aeronautics and Astronautics 2002-4349

Terrell, T. (2011). “Structural Health Monitoring for Damage Detection Using Wired and Wireless Sensor Clusters.” Department of Civil, Environmental and Construction Engineering. Orlando, FL, University of Central Florida. **Master’s Thesis**.

Werlink, R., C. Banks, et al. (2014). “AFRL Composite Tank Pressurization to Failure with Liquid Nitrogen with Structural Health Monitoring Test Report.” Fluid and Cryogenic Development Branch NE-F6. Cape Canaveral, FL, NASA Kennedy Space Center